NASA CR-135032
CASD-NAS-76-026

CENTAUR PROPELLANT THERMAL CONDITIONING STUDY

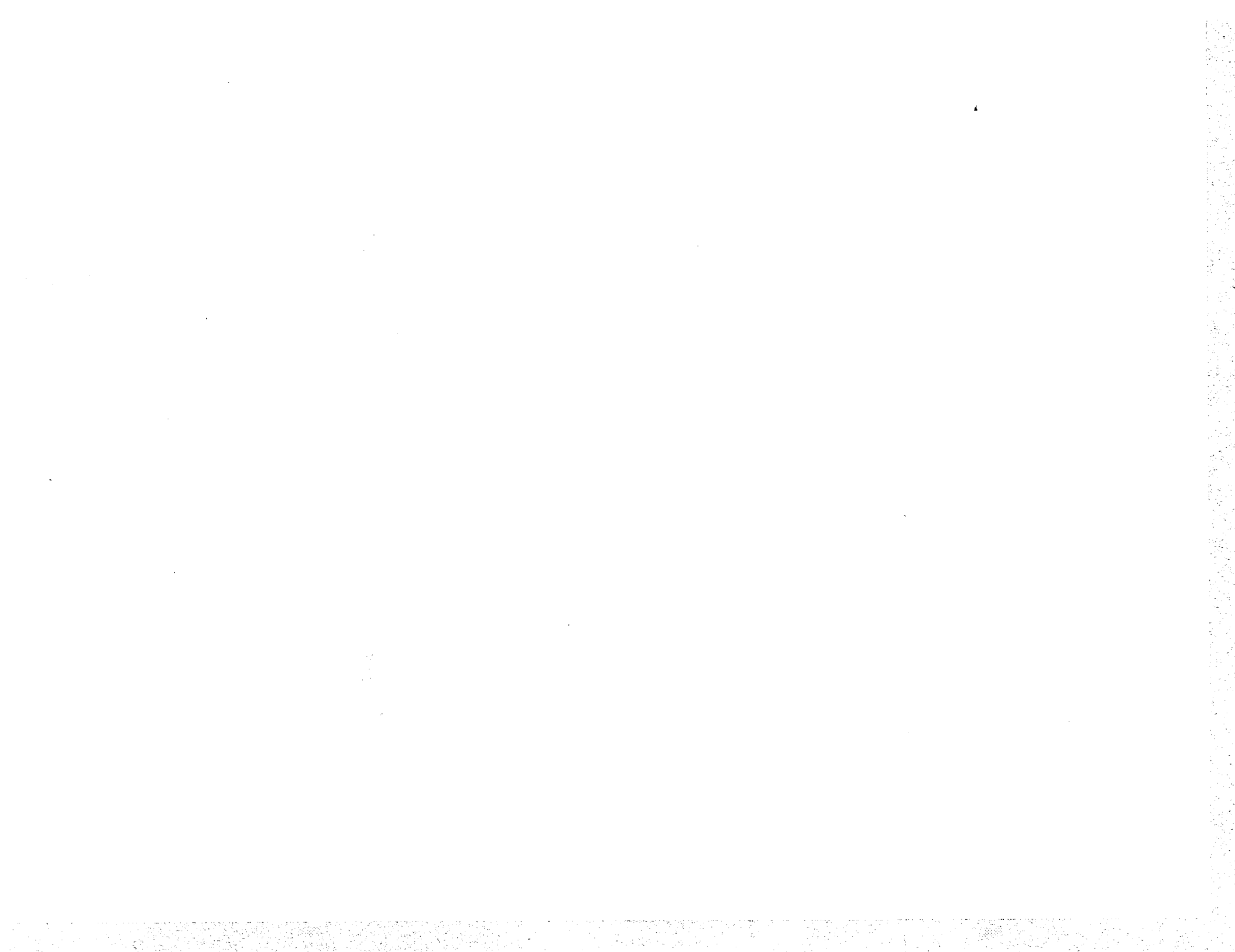July 1976

by
M. H. Blatt
R. L. Pleasant
R. C. Erickson

1. Report No. NASA-CR-135032	2. Government Accession No.	3. Recipient's Catalog No.	
4. Title and Subtitle CENTAUR PROPELLANT THERMAL CONDITIONING STUDY		5. Report Date July 1976	
		6. Performing Organization Code	
7. Author(s) M. H. Blatt, R. L. Pleasant and R. C. Erickson		8. Performing Organization Report No. CASD-NAS-76-026	
		10. Work Unit No.	
9. Performing Organization Name and Address General Dynamics Convair Division P.O. Box 80847 San Diego, CA 92138		11. Contract or Grant No. NAS3-19693	
		13. Type of Report and Period Covered Contractor Report	
12. Sponsoring Agency Name and Address NASA Lewis Research Center Cleveland, OH 44135			
		14. Sponsoring Agency Code	

15. Supplementary Notes

16. Abstract

A study was performed with three objectives: (1) Analytically and experimentally determine the feasibility of using wicking flow to thermally condition cryogenic capillary devices, (2) Determine the feasibility of replacing Centaur D-1S boost pumps with thermal subcoolers and (3) Determine thermodynamic vent/mixer sizing for advanced Centaur.

The wicking investigation revealed that passive thermal conditioning was feasible and provided considerable weight advantage over active systems using throttled vent fluid. Experimental wicking correlations were obtained using empirical revisions to the analytical flow model.

Thermal subcoolers were evaluated parametrically as a function of tank pressure and NPSP. Results showed that the RL10 category I engine was the best candidate for boost pump replacement and the option showing the lowest weight penalty employed passively cooled acquisition devices, thermal subcoolers, dry ducts between burns and pumping of subcooler coolant back into the tank.

A mixing correlation was identified for sizing the thermodynamic vent system mixer. Worst case mixing requirements were determined by surveying Centaur D-1T, D-1S, IUS, and Space Tug vehicles. Vent system sizing was based upon worst case requirements. Thermodynamic vent system/mixer weights were determined for each vehicle.

17. Key Words (Suggested by Author(s)) Acquisition, Capillary Flow, Heat Exchangers, Heat Transfer, Mixing, Screens, Supercooling, Venting, Wicks		18. Distribution Statement Unclassified – Unlimited	
19. Security Classif. (of this report) Unclassified	20. Security Classif. (of this page) Unclassified	21. No. of Pages 121	22. Price*

NASA-C-168 (Rev. 6-71)
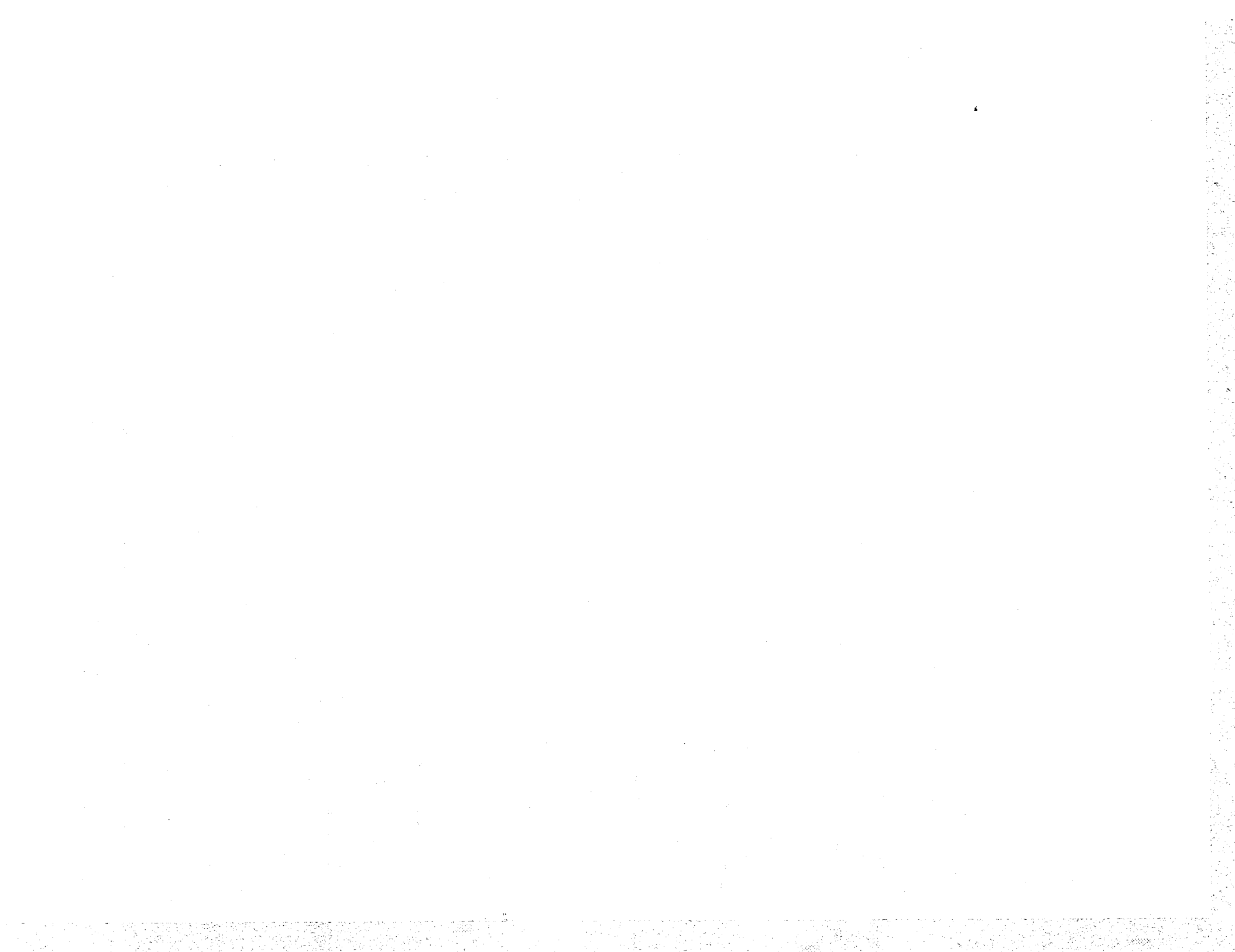
FOREWORD

This report was prepared by General Dynamics Convair Division under Contract NAS3-19693. The contract was administered by the National Aeronautics and Space Administration, Lewis Research Center, Cleveland, Ohio. This is the final report on the contract, summarizing the technical effort from May 5, 1975 to May 28, 1976. Convair program manager was M. H. Blatt. NASA/LeRC program manager was J. C. Aydelott. M. H. Blatt conducted the capillary pumping analysis, prepared the capillary pumping test plan, supervised the fabrication and assembly of the test specimens and test apparatus and correlated the test data with the analytical models. H. G. Brittain was the test conductor. M. D. Walter prepared conceptual capillary device designs and weights for the passively cooled start basket and thermal subcooler hardware. R. L. Pleasant performed the major portion of the thermal subcooling task. R. C. Erickson analyzed the LH_2 thermodynamic vent/mixer system.

All data are presented with the International System of Units as the primary system and English Units as the secondary system. The English system was used for the basic calculations.
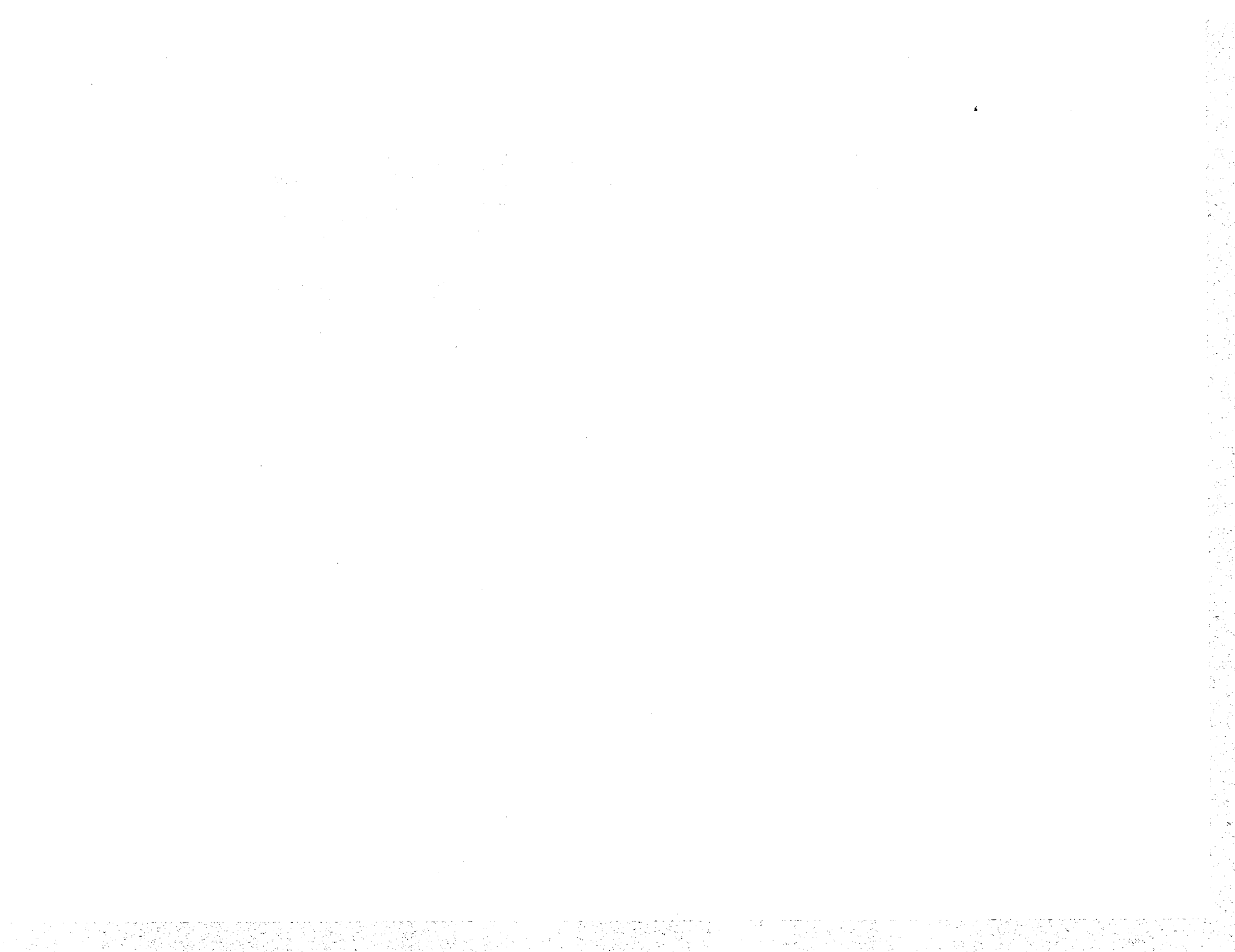
TABLE OF CONTENTS

TABLE OF CONTENTS (Cont'd)

LIST OF FIGURES

LIST OF TABLES

SUMMARY

The study was concerned with three main areas; (1) analytical and experimental investigation of promising capillary pumping concepts for passive cooling of cryogenic capillary acquisition devices, (2) parametric evaluation of thermal subcooler systems for replacing the boost pump and pressurization systems on RL10 engine feed systems (3) developing mixing correlations from available test data and using these correlations to define worst case liquid hydrogen tank vent system requirements

In the passive cooling task, analytical evaluations of 16 capillary pumping configurations were performed using worst case wicking distance, gravity level and heat flux interception requirements based on Centaur D-1S LO_2 and LH_2 start basket cooling requirements. Wick geometries were defined and their manufacturing feasibility was determined. Based on this assessment, four wicking configurations; plate/screen-screen/plate, screen/plate-plate/screen, plate/screen-plate/screen and pleated screen were selected and tested horizontally and at small angles to the horizontal. Ethanol was used as the test fluid in a humidified transparent enclosure. Photographic data was analyzed and analytical predictions were empirically corrected to achieve agreement with the data. The semi-empirical correlations, yielding slower wicking than originally predicted, were applied to the Centaur D-1S conditions. Only the plate/screen-screen/plate and plate/screen-plate/screen could function successfully under worst case conditions.

Weight estimates were developed for the passively cooled configurations. Comparisons were made between passive capillary device cooling system hardware weight and active capillary device cooling system hardware weight and vented fluid payload penalty.

Thermal subcooling comparative analysis related system weight to the NPSP (net positive suction pressure) requirement of the Centaur main engines for both LH_2 and LO_2. The baseline Centaur D-1S engine, the RL10A-3-3 and two other RL10 derivatives, the RL10A-3-3A and RL10 Category I were used to establish the tank pressure and NPSP requirements. Three types of systems were analyzed; (1) The baseline system using propulsive settling, boost pumps and warm gas pressurization, (2) Thermal subcoolers with propulsive settling, and (3) Thermal subcoolers with passively cooled screen acquisition devices and continuously cooled propellant ducts. Analysis and design included both transient and steady state operation. Weight comparisons were made on the basis of equivalent payload penalty using payload partials derived for the Centaur D-1S.

Existing experimental mixing studies to destroy thermal stratification were evaluated to determine the best mixing correlation to fit all available data. This correlation was then incorporated into a computer program that was used to size thermodynamic vent systems for the Centaur D-1T, Centaur D-1S, reusable and expendable Centaur Interim Upper Stage Vehicles and the baseline Space Tug.

1

INTRODUCTION

The objectives of this study were to: (1) analytically and experimentally evaluate the feasibility and weight penalty of passive capillary acquisition system cooling; (2) perform a parametric evaluation of thermal subcooler requirements for replacing the boost pumps on the Centaur D-1S for realistic engine turbopump inlet pressure and NPSP requirements, and (3) develop mixing correlations from available test data and use these correlations to define liquid hydrogen tank vent system requirements.

Work performed in NAS3-17802, "Centaur Propellant Acquisition System," Reference 1-1, forms the basis for this study. In Reference 1-1, Sections 6 and 7, the use of passive capillary acquisition device cooling was advocated because of the complexity and weight associated with the use of an active system with cooling coils designed to prevent screen dryout between burns. Thermal subcooling was found to be an attractive alternative to pressurization for supplying feed system net positive suction pressure (NPSP). Thermal subcooling uses a compact heat exchanger to remove heat from the liquid leaving the main propellant tanks during main engine startup and firing. Thermodynamic vent system development was identified as being a critical technology item in evolution of the current Centaur D-1T to a Shuttle based Centaur.

Passive means of thermal conditioning, such as using capillary pumping is a light-weight and simple approach to keeping screens wet and maintaining capillary device retention when subjected to incident heating. Work performed in this study analytically and experimentally demonstrated the fundamental feasibility of this concept.

Thermal subcoolers were examined for replacing the boost pumps with the existing RL10A-3-3, the RL10A-3-3A engine and the Category I engine inlet pressure and NPSP requirements. Weight penalties and conceptual designs were generated for each of these engines. Several options were considered including; (1) the baseline Centaur D-1S system using peroxide settling rockets, ambient pressurization and boost pumps, (2) thermal subcooling with peroxide settling rockets, and (3) thermal subcooling with capillary acquisition and wet feedlines. Based on weight comparisons for these options for the three engines, two additional options were evaluated for the RL10 Category I engine. These options were (4) thermal subcooling with coolant pumped back into the tank and settling rockets, and (5) thermal subcooling with coolant pumped back into the tank, capillary acquisition and a dry feedline.

Centaur/Shuttle integration studies have indicated the importance of using a thermo-dynamic vent system for controlling tank pressure while in the Shuttle cargo bay and in

low gravity, particularly when the tanks are relatively full. Centaur/Tug derivatives require the use of thermodynamic vent systems. The thermodynamic vent/mixer analysis was the initial effort required to bring the vent system to a fully operational flight status. This work is preparatory to the procurement of hardware, flight qualification,and flight of a noninterference LH_2 vent system on a future Centaur flight.

1.1 GROUND RULES

The baseline vehicle configuration for this study is the Centaur D-1S as defined in Contract NAS3-16786 and reported in NASA CR-134488, Reference 1-2. The Centaur D-1S is a nonreusable minimum modification Centaur D-1T designed to be compatible with Shuttle. The major changes, cited in Reference 1-2, that affected this contract are shown in Figure 1-1.
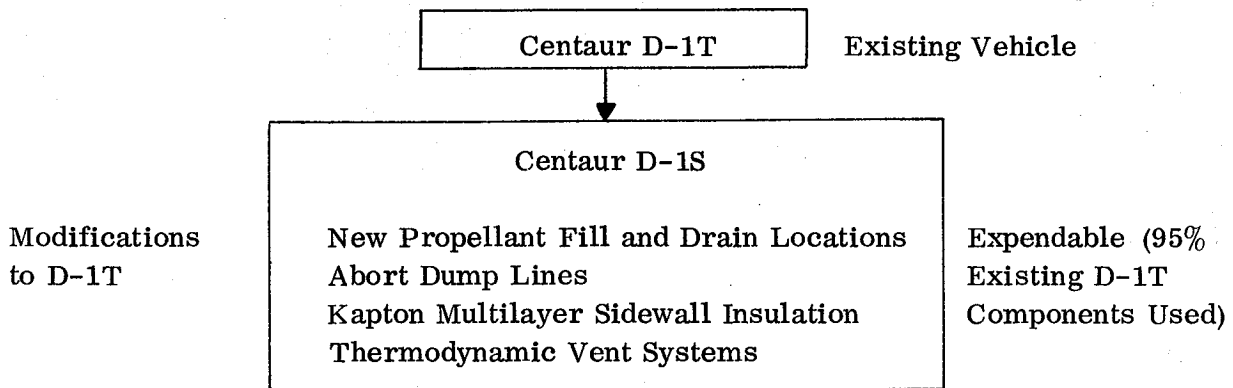
Figure 1-1.   Evolution of Centaur D-1T to Future Centaur D-1S

For the passive acquisition device cooling and thermal subcooler work, mission profiles (from Reference 1-2) as given in Tables 1-1, 1-2 and 1-3 were used. Payload sensitivity factors used for thermal subcooler weight comparisons are shown in Table 1-4 for the three missions. Heating rates and nominal tank pressure levels were obtained either from Reference 1-2 or from engine specifications for the three engines considered in Task II. The systems designed in the study did not impose constraints on the operation of the Shuttle nor affect the Centaur/Shuttle abort capability.

To determine the worst case thermodynamic vent/mixer design requirements, all current versions of Shuttle based Centaur were considered. Both reusable and expendable Centaur Interim Upper Stage vehicles have been studied at Convair. Three tank sizes were investigated for each expendable and reusable version (a total of six vehicles). The expendable versions are similar to the Centaur D-1S relative to thermal protection, fill and drain and propulsion. The reusable versions have Superfloc insulation. Vehicle conditions affecting thermodynamic vent system sizing were determined based on information developed in F04701-75-C-0035, "Centaur Interim Upper Stage Systems Study." The baseline Space Tug configuration, Ref. 1-3,thermodynamic vent system design conditions were also evaluated.

Table 1-1. Planetary Mission Profile

Event/Time (min.)	Initial Mass kg_m (lb_m)	Burn Time, sec	Propellant Burned, kg_m (lb_m)	Final Mass kg_m (lb_m)	Initial Percent Full*	Initial Acceleration g
Loading	11554 (25,450) LO_2					
(T = 0)	2397 (5,279) LH_2					
MES1	11488 (25,304) LO_2	441.4	11302 (24,894) LO_2	186 (410) LO_2	96	0.61
(T = 67)	2344 (5,164) LH_2		2243 (4,941) LH_2	101 (223) LH_2	95	
	22434 (49,413) Vehicle			8888 (19,578) Vehicle		

Main engine thrust 13620 kg_f (30,000 lb_f), *Assumes 11946 kg_m (26,313 lb_m), LO_2, 2478 kg_m (5,459 lb_m), LH_2 for full tank, Maximum ACS thrust = 10.9 kg_f (24 lb_f), Maximum ACS acceleration before last burn = 4.86×10^{-4} g's, Main engine flow rates - LO_2 = 25.6 kg/sec (56.4 lb/sec), LH_2 = 5.1 kg/sec (11.2 lb/sec), ISP = 443.82 sec, Payload = 6567 kg_m, (14,465 lb_m). Dry weight = 2015 kg_m (4,439 lb_m), Burnout acceleration = 1.53 g's.

Table 1-2. Synchronous Equatorial Mission Profile

Event/Time (min.)	Initial Mass, kg_m (lb_m)	Burn Time, sec	Propellant Burned, kg_m(lb_m)	Final Mass kg_m (lb_m)	Initial Percent Full*	Initial Acceleration g
Loading	11554 (25,450) LO_2					
(T = 0)	2397 (5,279) LH_2					
MES1	11488 (25,304) LO_2	305.4	7854 (17,299) LO_2	3634 (8,005) LO_2	96	0.63
(T = 67)	2344 (5,164) LH_2		1525 (3,360) LH_2	819 (1,804) LH_2	95	
	21541 (47,447)			12100 (26,653)		
MES2	3621 (7,975) LO_2	132.3	3403 (7,496) LO_2	190 (419) LO_2	30.3	1.12
(T = 384)	782 (1,723)LH_2		665 (1,465)LH_2	117 (258) LH_2	31.6	
	12162 (26,788) Vehicle			7956 (17,525) Vehicle		

Main engine thrust 13620 kg_f (30,000 lb_f), *Assumes 11946 kg_m (26,313 lb_m), LO_2, 2478 kg_m(5,459 lb_m), LH_2 for full tank, Maximum ACS thrust = 10.9 kg_f (24 lb_f), Maximum ACS acceleration before last burn = 8.96×10^{-4} g's, Mixture ratio = 5.0, Main engine flow rates - LO_2 = 25.7 kg/sec (56.65 lb/sec), LH_2 = 5.01 kg/sec (11.03 lb/sec), ISP = 443.35 sec, Payload = 5538 kg_m (12,199 lb_m), Dry weight = 2090 kg_m (4,604 lb_m), Burnout acceleration = 1.71 g's.

1-3

Table 1-3. Low Earth Orbit Mission Profile

Event/Time (min.)	Initial Mass kg_m (lb_m)	Burn Time, Sec	Propellant Burned, kg_m (lb_m)	Final Mass kg_m (lb_m)	Initial Percent Full *	Initial Accel. g
Loading (T = 0)	11554 (25450) LO_2 2397 (5279) LH_2					
MES1 (T = 67)	11488 (25304) LO_2 2344 (5164) LH_2 19090 (42048) Vehicle	88.6	2294 (5052) LO_2 434 (955) LH_2	9194 (20252) LO_2 1911 (4209) LH_2 16363 (36042) Vehicle	96 95	0.71
MES2 (T = 118)	9155 (20165) LO_2 1885 (4153) LH_2 16264 (35824) Vehicle	191.32	4955 (10915) 935 (2060) LH_2	4200 (9250) LO_2 950 (2093) LH_2 10373 (22849) Vehicle	77 76	0.84
MES3 (T = 408)	4162 (9167) LO_2 913 (2010) LH_2 10246 (22568) Vehicle	120.51	3121 (6875) LO_2 587 (1294) LH_2	1038 (2286) LO_2 325 (716) LH_2 6536 (14397) Vehicle	35 37	1.33
MES4 (T = 459)	998 (2198) LO_2 295 (650) LH_2 6443 (14192) Vehicle	18.90	489 (1078) LO_2 93 (204) LH_2	509 (1121) LO_2 207 (456) LH_2 5861 (12910) Vehicle	8.4 11.9	2.11
MES5 (T = 553)	468 (1031) LO_2 178 (393) LH_2 5765 (12698) Vehicle	10.8	279 (614) LO_2 53 (116) LH_2	189 (417) LO_2 126 (277) LH_2 5433 (11967) Vehicle	3.9 7.2	2.36

Main engine thrust = 13620 kg_f (30000 lb_f), *Assumes 11946 kg_m (26313 lb_m), LO_2, 2478 kg_m (5459 lb_m), LH_2 for full tank, Maximum ACS thrust = 10.9 kg_f (24 lb_f), Maximum ACS acceleration before 5th burn = 1.89×10^{-3} g's, Mixture ratio = 5.298, Main engine flow rates - LO_2 = 25.9 kg/sec (57.05 lb/sec), LH_2 4.89 kg/sec (10.77 lb/sec), ISP = 443.8 sec. Payload = 2842 kg_m (6260 lb_m), Dry weight = 2225 kg_m (4901 lb_m), Burnout acceleration = 2.51 g's.

Table 1-4. Centaur D-1S Payload Sensitivity Factors

Criteria		Mission		
		Planetary	Sync. Equatorial	Low Altitude
Jettison Weight		-1.000	-1.000	-1.000
Propellant Weight		+0.646	+0.587	+0.420
LH_2 and LO_2 Loss Before Burn (Without I_{SP} Effect)	No. 1	-0.646	-0.587	-0.420
	No. 2		-0.946	-0.510
	No. 3			-0.771
	No. 4			-1.215
	No. 5			-1.337
LH_2 and LO_2 Lost After Last Burn (Residual or RFP)		-1.646	-1.587	-1.419
Auxiliary Propellant Used Prior to Burn	No. 1	0	0	0
	No. 2		-0.459	-0.072
	No. 3			-0.352
	No. 4			-0.796
	No. 5			-0.917
Auxiliary Propellant Used After Last Burn (Residual)		-1.000	-1.000	-1.000
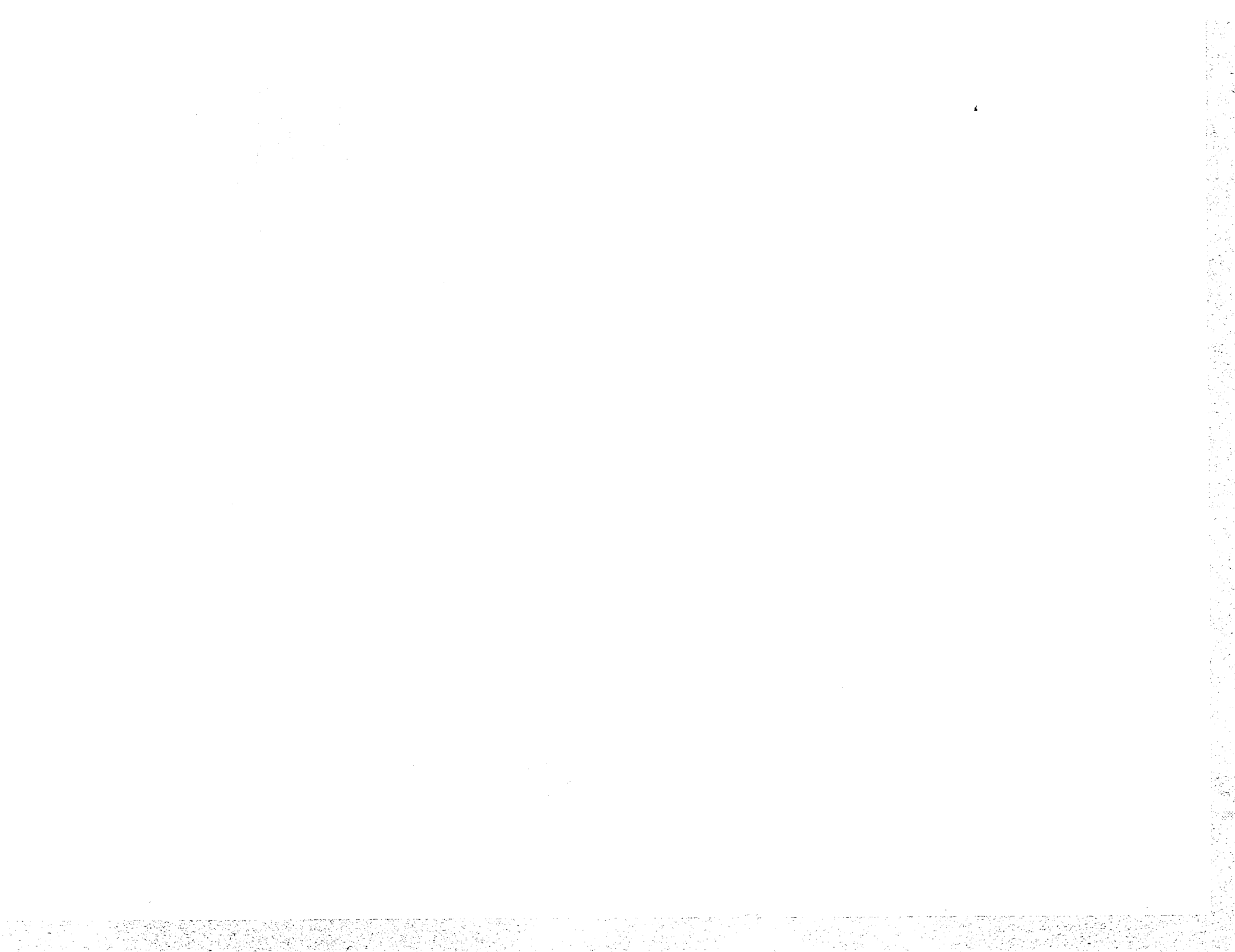
2

PASSIVE CAPILLARY ACQUISITION SYSTEM COOLING

Under contract NAS3-17802, Reference 2-1, passive thermal conditioning of start baskets for the Centaur D-1S was found to be the preferred approach for capillary acquisition. Based on this assessment, work was initiated on NAS-19683 to investigate possible methods of accomplishing passive thermal conditioning. Passive thermal conditioning consists basically of using wicking flow to keep retention barriers wet and allow liquid to be retained within the basket. Heat input causes liquid to be evaporated from the screen surface. The heat input must not cause screen drying since screen retention systems operate by keeping vapor out rather than keeping liquid in.

Passive thermal conditioning (wicking) of capillary devices was evaluated by establishing the ground rules of the study, the method of analysis, and selecting the most promising wicking concepts for both LO_2 and LH_2. This was followed by development of a test plan for evaluating the most promising wicks using ethanol as the test fluid. After written approval of the test plan (Reference 2-2), design and fabrication of the apparatus and wicking samples was accomplished. Reference and candidate wicking samples were then tested and data was correlated with the analytical and semi-empirical models developed in this study and in Reference 2-3.

2.1 COMPARATIVE ANALYSIS OF WICKING CONFIGURATIONS

Initially, ground rules were determined for wicking rate requirements and compared to the capability of sixteen different wicking configurations to intercept worst case heat flux requirements. Wick sizes and heat flux interception capability were determined for each configuration. Fabricability of each wick for LO_2 and LH_2 Centaur D-1S start basket cooling requirements were assessed. Weight estimates were made for fabricable passive cooling configurations.

2.1.1 GROUND RULES. Heat transfer conditions that could cause screen drying were examined for all start basket screened surfaces for Centaur D-1S mission conditions. Local heat transfer coefficients as well as average heat transfer coefficients were established for forced convection, free convection and conduction with vapor adjacent to the start basket screened surfaces. Total fluid vaporized, assuming interception of heat by wicking was determined for each portion of the mission for both

the oxygen and hydrogen capillary device. Only mission conditions were considered where there was a possibility that the entire basket could be surrounded by vapor. Vapor volumes generated were translated into wicking distances for each basket surface as shown in Figure 2-1, assuming worst case vapor location in the start baskets. Start basket volumetric requirements were reduced from those of Reference 2-1 to 1.14 m^3 (40.4 ft^3) for LH$_2$ and 0.21 m^3 (7.3 ft^3) for LO$_2$. The LH$_2$ basket is identical to the Reference 2-1 LH$_2$ basket except for the angle the basket subtends around the intermediate bulkhead. This is reduced from 5.74 radians (330 degrees) to 4.785 radians (275 degrees). The LO$_2$ basket cylindrical section is reduced in size. In addition, the LO$_2$ basket must be spaced off the aft bulkhead in order to prevent heat from entering the basket directly and displacing large quantities of liquid. In Reference 2-1 basket volumes for active cooling, where condensation heat transfer had to be intercepted, were 1.38 m^3 (48.6 ft^3) for LH$_2$ and 0.24 m^3 (8.5 ft^3) for LO$_2$. Table 2-1 gives maximum and local heat fluxes and maximum wicking distance and g level during periods when the basket could be surrounded by vapor.

For each time period and basket surface the maximum wicking distance was determined by computing the maximum volume of vapor that could be generated by incident heating. A vapor bubble of this volume was placed adjacent to the surface of interest so that the maximum distance between the midpoint of the vapor bubble, on the basket surface, and the liquid pool in the basket would occur. This distance is the maximum wicking distance for that surface.

Table 2-1 represents the matrix of possible worst case wicking rate requirements. and was used to determine wicking geometry for each specimen of interest.

2.1.2 <u>HEAT FLUX INTERCEPTION ANALYSIS OF WICKING CONCEPTS.</u> Flow analysis of capillary pumping for providing capillary device passive thermal conditioning was initiated. A literature review was performed to assess the available information on wicking flow. The pressure differentials of interest are those dependent upon surface tension (ΔP_σ), gravity (ΔP_g) and viscosity (ΔP_f) (laminar frictional pressure loss). Momentum losses can normally be neglected for the low flow rates that occur during wicking. The pressure differentials are related by

$$\Delta P_\sigma = \Delta P_g + \Delta P_f \tag{2-1}$$

Expressions were derived for the surface tension pressure differential

$$\Delta P_\sigma = \sigma \, (1/R_1 + 1/R_2) \approx F/A_F \tag{2-2}$$

where

σ is the liquid surface tension

R_1 and R_2 are principal radii of curvature of the liquid wicking front

F is the surface force

A_F is the cross sectional area of the wicking front

The surface force $F = \sigma$ (WP), where WP is the wetted perimeter of the wicking front.

TOP

SIDE

BOTTOM

LO$_2$ BASKET

TOP

SIDEWALL

SIDE PANEL

BOTTOM

LH$_2$ BASKET
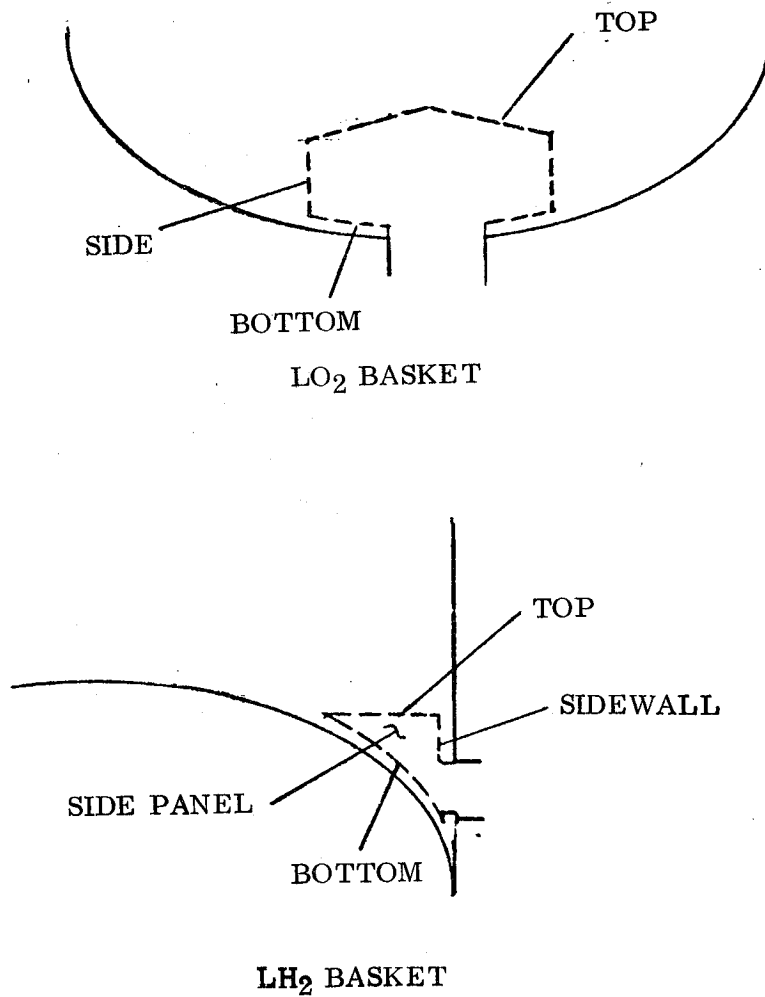
Figure 2-1. Schematic of Start Basket Passive Cooling Surfaces

Table 2-1. **Passive Cooling Requirements**

Basket	Location*	Maximum Average Heat Flux		Maximum Local Heat Flux		Time Period	Maximum Wicking Distance from Pool To Heat Source		Acceleration Level
		Watts/m^2	(Btu/hr-ft^2)	Watts/m^2	(Btu/hr-ft^2)		m	(ft)	g's
LO$_2$	Bottom	35.3	(11.2)	35.3	(11.2)	Shuttle ACS	0.09	(0.31)	0.0085
		9.8	(3.1)	9.8	(3.1)	Centaur ACS – Low Earth Orbit	0.09	(0.31)	0.00189
		9.8	(3.1)	9.8	(3.1)	Centaur ACS – Synchronous Eq.	0.09	(0.31)	0.0009
	Top	1.9	(0.6)	4.4	(1.4)	Shuttle ACS	0.04	(0.14)	0.0085
		1.9	(0.6)	4.4	(1.4)	Centaur ACS – Low Earth Orbit	0.15	(0.48)	0.00189
		1.9	(0.6)	4.4	(1.4)	Centaur ACS – Synchronous Eq.	0.19	(0.63)	0.0009
	Side	1.6	(0.5)	4.4	(1.4)	Shuttle ACS	0.11	(0.36)	0.0085
		1.6	(0.5)	4.4	(1.4)	Centaur ACS – Low Earth Orbit	0.14	(0.45)	0.00189
		1.6	(0.5)	4.4	(1.4)	Centaur ACS – Synchronous Eq.	0.14	(0.47)	0.0009
LH$_2$	Bottom	30.3	(9.6)	30.3	(9.6)	Shuttle ACS	0.16	(0.51)	0.0085
		30.3	(9.6)	30.3	(9.6)	Centaur ACS – Low Earth Orbit	0.32	(1.05)	0.00189
		30.3	(9.6)	30.3	(9.6)	Centaur ACS – Synchronous Eq.	0.34	(1.11)	0.0009
	Sidewall	31.5	(10)	31.5	(10)	Shuttle ACS – Insulation Outgassing – t = 480 sec	0	(0)	0.0085
		5.7	(1.8)	5.7	(1.8)	OMS ACS – Avg. Heat Trans.	0.43	(1.4)	0.0085
		2.5	(0.8)	2.5	(0.8)	OMS ACS – Before Deployment	0.56	(1.85)	0.0085
		2.5	(0.8)	2.5	(0.8)	Centaur ACS – Low Earth Orbit	0.63	(2.06)	0.00189
		2.5	(0.8)	2.5	(0.8)	Centaur ACS – Synchronous Eq.	0.65	(2.13)	0.0009
	Top	2.5	(0.8)	2.5	(0.8)	Shuttle ACS	0.38	(1.25)	0.0085
		2.5	(0.8)	2.5	(0.8)	Centaur ACS – Low Earth Orbit	0.41	(1.33)	0.00189
		2.5	(0.8)	2.5	(0.8)	Centaur ACS – Synchronous Eq.	0.41	(1.35)	0.0009
	Side Panel	.9	(0.3)	2.2	(0.7)	Shuttle ACS	0.73	(2.41)	0.0085
		.9	(0.3)	2.2	(0.7)	Centaur ACS – Low Earth Orbit	0.73	(2.41)	0.00189
		.9	(0.3)	2.2	(0.7)	Centaur ACS – Synchronous Eq.	0.73	(2.41)	0.0009

* See Figure 2-1 for a schematic of cooling surfaces

Surface tension pressure differentials were derived for each of the configurations of interest as shown in Table 2-2, using Equation 2-2. For open channels, the results of Bressler and Wyatt, Reference 2-4, were also used to compute the surface tension pressure. They found that an expression

$$\Delta P_\sigma = \frac{2\sigma}{R_E} \cos \phi, \text{ successfully correlated their data}$$

where

R_E is the effective capillary radius device by $R_E = \dfrac{2A_F}{WP-Width}$

ϕ is the contact angle, which is equal to zero for LH_2 and LO_2.

The frictional pressure drop was computed using

$$\Delta P_f = \frac{2fL}{D_H} \frac{\rho V^2}{g_c}$$

where

f = the Fanning friction factor (Blasius friction factor = 4 × Fanning friction factor)

L = the distance between the liquid pool and the wicking front

D_H = the hydraulic diameter of the wicking cross section

ρ = the fluid density

V = the liquid wicking velocity

g_c = a dimensional constant

The friction factor is normally expressed as a function of Reynolds number

$$f = C/Re$$

where

C is a constant depending upon the cross section shape

Re is the Reynolds number defined as $(\rho V D_H)/\mu$

Table 2-2. Candidate Wicking Configurations

Config.	Sketch	D_H	A_F	C	ΔP_f	ΔP_σ	$\Delta P_{\sigma R_E}$ [1]	$\Sigma \dot{Q}_T/W$ [5]	Notes
Circle	(circle, radius R)	$2R$	πR^2	16^2	$\dfrac{8 \dot{m} \mu L}{\rho \pi R^4 g_c}$	$\dfrac{2\sigma}{R}$		$\dfrac{\rho \lambda \pi R^3 g_c}{8 \mu L}\left[\dfrac{2\sigma}{R} - \dfrac{\rho g}{g_c} L \sin\theta\right]$	$N = W/R$ = number of wicks per surface of width W
Closed Semicircle	(closed semicircle, R)	$\dfrac{2\pi R}{(\pi+2)}$	$\dfrac{\pi R^2}{2}$	16^6	$\dfrac{16 \dot{m}\mu L (\pi+2)^2}{\rho \pi^3 R^4 g_c}$	$\dfrac{2(\pi+2)\sigma}{\pi R}$		$\dfrac{\rho\lambda R^3 g_c \pi^3}{32\mu L (\pi+2)^2}\left[2\dfrac{(\pi+2)\sigma}{\pi R} - \dfrac{\rho g}{g_c} L \sin\theta\right]$	$N = W/R$ Impractical to fabricate. Welding, forming difficult. CRES weight = 6.6 kg/m^2 (1.35#/ft^2)
Open Semicircle	(open semicircle, R)	$2R$	$\dfrac{\pi R^2}{2}$	16^6	$\dfrac{16 \dot{m}\mu L}{\rho \pi R^4 g_c}$	$\dfrac{2\sigma}{R}$	$\dfrac{2(\pi-2)\sigma}{\pi R}$	$\dfrac{\rho\lambda R^3 g_c \pi}{32\mu L}\left[\dfrac{2\sigma}{R} - \dfrac{\rho g}{g_c} L \sin\theta\right]$ $\dfrac{\rho\lambda R^3 \pi g_c}{32\mu L}\left[\dfrac{2(\pi-2)\sigma}{\pi R} - \dfrac{\rho g}{g_c} L \sin\theta\right]$	$N = W/R$ Circles too small, impractical to fabricate. Weight is less than pleated screen.
Parallel Plates	(sketch a, b) Plate/Screen-Screen	$2b$	ba	24^3	$\dfrac{12 \dot{m}\mu L}{\rho a b^3 g_c}$	$\dfrac{2\sigma}{b}$		$\dfrac{\rho\lambda b^3 g_c}{12\mu L}\left[\dfrac{2\sigma}{b} - \dfrac{\rho g}{g_c} L \sin\theta\right]$	$N = 1$, Straight forward if thin perforated plates are used for backup. 5.4 kg/m^2 (1.1#/ft^2)
Parallel Plates	n = no. of holes, e, b, z, x; x = z, 50% Open Area, e ~ 0.064 cm (0.025")	$\dfrac{8(b+e)a}{3a+8ne}$	$(b+e)a$	24^3	$\dfrac{3\dot{m}\mu L(3a+8ne)^2}{4\rho(b+e)^3 a^3 g_c}$	$\dfrac{(3a+8ne)\sigma}{2(b+e)a}$		$\dfrac{4\rho\lambda(b+e)^3 a^2 g_c}{3\mu L(3a+8ne)^2}\left[\dfrac{\sigma(3a+8ne)}{2(b+e)(a)} - \dfrac{\rho g}{g_c} L \sin\theta\right]$	$N = 1$, Easiest to maintain uniform spacing. 5.9 kg/m^2 (1.2#/ft^2) Screen/Plate-Plate
Parallel Plates	Plate/Screen-Plate, b+e, b, x, z; x = z	$\dfrac{4(2b+e)a}{3a+4ne}$	$\left[\dfrac{2b+e}{2}\right]a$	24^3	$\dfrac{6\dot{m}\mu L(3a+4ne)^2}{\rho(2b+e)^3 a^3 g_c}$	$\dfrac{(3a+4ne)\sigma}{(2b+e)a}$		$\dfrac{\rho\lambda(2b+e)^3 a^2 g_c}{6\mu L(3a+4ne)^2}\left[\dfrac{(3a+4ne)\sigma}{(2b-e)a} - \dfrac{\rho g}{g_c} L \sin\theta\right]$	$N = 1$, Similar to the parallel screens if thin perforated plates are used. 5.9 kg/m^2 (1.2 /ft^2)
Parallel Plates	Plate/Screen-Plate/Screen	$\dfrac{(2b+e)a}{a+ne}$	$\left[\dfrac{2b+e}{2}\right]a$	24^3	$\dfrac{96\dot{m}\mu L(a+ne)^2}{a^3(2b+e)^3}$	$\dfrac{4(a+ne)\sigma}{a(2b+e)}$		$\dfrac{\rho\lambda(2b+e)^3 a^2 g_c}{96\mu L(a+ne)^2}\left[\dfrac{2\sigma(2a+2ne)}{a(2b+e)} - \dfrac{\rho g}{g_c} L \sin\theta\right]$	$N=1$, Similar to Screen/Plate-Plate/Screen 7.3 kg/m^2 (1.5#/ft^2)
Parallel Plates	Screen/Plate-Plate/Screen 50% Open Area	$\dfrac{2(b+e)a}{a+2ne}$	$(b+e)a$	24^3	$\dfrac{12(a+2ne)^2 \dot{m}\mu L}{(b+e)^3 a^3 \rho g_c}$	$\dfrac{2(a+2ne)\sigma}{(b+e)a}$		$\dfrac{\rho\lambda g_c (b+e)^3 a^2}{12\mu L(a+2ne^2)}\left[\dfrac{2\sigma(a+2ne)}{(b+e)a} - \dfrac{\rho g}{g_c} L \sin\theta\right]$	$N=1$ 7.3 kg/m^2 (1.5#/ft^2) 50 × 250 screen used for all weight data
Annuli	(annulus, r_i, r_o, ϕ)	$2(r_o - r_i)$	$\pi(r_o^2 - r_i^2)$	18 to 24^2	$\dfrac{C\dot{m}\mu L}{2\rho\pi(r_o-r_i)^4 g_c}$	$\dfrac{2\sigma}{r_o-r_i}$		$\dfrac{\rho\lambda g_c b^3}{12\mu L}\left[\dfrac{2\sigma}{b} - \dfrac{\rho g}{g_c} L \sin\theta\right]$, $b = r_o - r_i$	Reduces to parallel plate equation when $r_o \gg b$.

Table 2-2. Candidate Wicking Configurations (Continued)

Config.	Sketch	D_H	A_F	C	ΔP_f	ΔP_σ	$\Delta P_\sigma \frac{1}{R_E}$	$\Sigma \dot{Q}_T/W^5$	Notes
Rectangular Channels Closed	a, b	$\dfrac{2ab}{(a-b)}$	ab	$\begin{array}{c}2\\14\text{ to }24\end{array}$	$\dfrac{2C\,\dot{m}\mu L\,(a-b)^2}{\rho\,4(ab)^3 g_c}$	$\dfrac{2(a-b)}{ab}\sigma$		Square $a=b$, $C=14.23$ $\dfrac{\rho\lambda g_c\,a^3}{28.6\,\mu L}\left[\dfrac{4\sigma}{a}-\dfrac{\rho g}{g_c}L\sin\theta\right]$	$N=W/a$, $7.0\,kg/m^2(1.44\#/ft^2)$ Separation barriers will probably have to be solid sheet stock. Channel width sensitive to depth.
Rectangular Channels Open	a, b	$\dfrac{4ab}{(2a+b)}$	ab	24^4	$\dfrac{3\,\dot{m}\mu L\,(2b+a)^2}{\rho\,(ab)^3 g_c}$	$\dfrac{(2b+a)}{ab}\sigma$	$\dfrac{2\sigma}{b}$	$\dfrac{\rho\lambda a^2 b^3 g_c}{3\mu L\,(2b+a)^2}\left[\dfrac{(2b+a)\sigma}{ab}-\dfrac{\rho g}{g_c}L\sin\theta\right]$ $\dfrac{\rho\lambda a^2 b^3 g_c}{3\mu L\,(2b+a)^2}\left[\dfrac{2\sigma}{b}-\dfrac{\rho g}{g_c}L\sin\theta\right]$	$N=W/A$ Same comments as closed channels. 5.4 to 5.9 kg/m² (1.1 to 1.2#/ft²)
V Grooves Isosceles Closed	b, α, b, A	$\dfrac{A/(\tan\frac{\alpha}{2}+\sec\frac{\alpha}{2})}{}$; $\dfrac{A^2}{4\tan\frac{\alpha}{2}}$	$\dfrac{A^2}{4\tan\frac{\alpha}{2}}$	$\begin{array}{c}2\\12\text{ to }14\end{array}$	$\dfrac{8C\dot{m}\mu L\tan\frac{\alpha}{2}\left[\tan\frac{\alpha}{2}+\sec\frac{\alpha}{2}\right]^2}{\rho A^4 g_c}$	$\left[4\sigma(\tan\frac{\alpha}{2}+\sec\frac{\alpha}{2})\right]/A$		$60°$ (Equilateral Triangle), $C=13.33$ $\dfrac{\rho\lambda g_c A^3\left[\frac{4\sigma}{A}\left(\tan\frac{\alpha}{2}+\sec\frac{\alpha}{2}\right)-\frac{\rho g}{g_c}L\sin\theta\right]}{106.64\mu L\,\tan\frac{\alpha}{2}\left(\tan\frac{\alpha}{2}+\sec\frac{\alpha}{2}\right)^2}$	$N=W/A$ Difficult to fabricate except for large angles [2.44 rad (140°) for example]. 5.9 kg/m² (1.2 #/ft²)
V Grooves Isosceles Open	b, α, b, A	$\dfrac{A}{\sec\frac{\alpha}{2}}$; $\dfrac{A^2}{4\tan\frac{\alpha}{2}}$	$\dfrac{A^2}{4\tan\frac{\alpha}{2}}$	14^4	$\dfrac{112\,\dot{m}\mu L\,\sin\frac{\alpha}{2}}{\rho A^4\,(\cos\frac{\alpha}{2})^2 g_c}$	$\left[4\sec\frac{\alpha}{2}\right]\sigma /A$	$\left[4\tan\frac{\alpha}{2}\right]\sigma /A$	$\dfrac{\rho\lambda A^3(\cos^2\frac{\alpha}{2})g_c}{112\mu L\,(\sin\frac{\alpha}{2})}\left[\dfrac{4(\sec\frac{\alpha}{2})\sigma}{A}-\dfrac{\rho g}{g_c}L\sin\theta\right]$ $\dfrac{\rho\lambda A^3(\cos^2\frac{\alpha}{2})g_c}{112\mu L\,(\sin\frac{\alpha}{2})}\left[\dfrac{4\tan\frac{\alpha}{2}}{A}-\dfrac{\rho g}{g_c}L\sin\theta\right]$	$N=W/A$, Weight is less than pleats. Larger angles can be fabricated but maintaining the free edge and providing stiffness are difficult.
Pleated Screens Open	p, w, r, t ; p = pitch; t = depth of pleat	$\dfrac{4r(w+2r)}{w+\pi r}$	$2r(w+2r)$	$\begin{array}{c}C=16\\ \text{circles}\\ C=24\\ \text{plates}\end{array}$	$\dfrac{C\dot{m}\mu L\,(w+\pi r)^2}{16\,r^3\rho\,(w+2r)^3 g_c}$	$\dfrac{(\pi r-w)\sigma}{r(w+2r)}$	$\dfrac{[r(\pi-2)-w]\sigma}{r(w+2r)}$	$\dfrac{4r^2(w+2r)^3}{C(w+\pi r)^2}\dfrac{\rho\lambda g_c}{\mu L}\left[\dfrac{(\pi r+w)\sigma}{r(w+2r)}-\dfrac{\rho g}{g_c}L\sin\theta\right]$ $\dfrac{4\,r^2(w+2r)^3\rho\lambda g_c}{C(w+\pi r)^2\mu L}\left[\dfrac{[r(\pi-2)+w]\sigma}{r(w+2r)}-\dfrac{\rho g}{g_c}L\sin\theta\right]$	$N=W/2r$ Requires small pleats that may be difficult to manufacture. 6.5 kg/m² (1.32#/ft²)
Pleated Screens Closed	w	$\dfrac{4r(w+2r)}{w+(\pi+2)r}$	$2r(w+2r)$	$\begin{array}{c}C=16\\ \text{circles}\\ C=24\\ \text{plates}\end{array}$	$\dfrac{C\dot{m}\mu L\,(w+(\pi+2)r)^2}{16\,r^3\rho(w+2r)^3 g_c}$	$\dfrac{(w+(\pi-2)r)\sigma}{r(w+2r)}$		$\dfrac{4r^2(w+2r)^3}{C[w+(\pi+2)r]^2}\dfrac{\rho\lambda g_c}{\mu L}\left[\dfrac{(w+(\pi+2)r)\sigma}{r(w+2r)}-\dfrac{\rho g}{g_c}L\sin\theta\right]$	$N=W/2r$ Same as above only diffusion bonding will probably be required to attach screens. 7.4 kg/m² (1.52/ft²)
Screen	Perforated Plate Backup	D_s Bubble Point	$\phi t W$ $\phi=$ porosity $t=$ thickness		$\dfrac{V_W A_F\mu L}{K_1 A_T g_c}$ $A_F=$ flow area $A_T=$ total cross sectional area $K_1=$ permeability $B=$ an empirical constant	$\dfrac{\sigma\sigma}{D_s}$	$\dfrac{\sigma}{D_s}$	$\dfrac{\rho\lambda g_c}{\mu L}B\,pt\left[\sigma-\dfrac{\rho g}{g_c}\dfrac{D_s}{\sigma}L\sin\theta\right]$	$N=W/2r$ Simple to fabricate. Use 50×250 screen as the baseline screen material. 4.9 kg/m² (1.0#/ft²)

NOTES:

1. Uses $\Delta P_\sigma = (2\sigma/R_E)$, where $R_E = (2AF)/(WP-width)$ from Bressler, R. G. and Wyatt, P. W., "Surface Wetting Through Capillary Grooves," Transactions of the ASME, Journal of Heat Transfer, February 1970.

2. Lundgren, T. S., Sparrow, E. M., and Starr, J. B., "Pressure Drop Due to the Entrance Region in Ducts of Arbitrary Cross Section," Transactions of the ASME, Journal of Basic Engineering, September 1964. All C's used in the table are based on $C = f$ Re where Re is $\rho V D_H/\mu$.

3. Knudsen, J. G. and Katz, D. L., Fluid Dynamics and Heat Transfer, McGraw-Hill; New York: 1958.

4. Chow, V. T., Open Channel Hydraulics, McGraw-Hill, New York: 1959.

5. $\dot{Q}_T/W = (\dot{m}_T\lambda)/W$, where $\dot{m}_T$ is the total mass flow rate.

   $\dot{m}_T = \dot{m}_c N$, where $\dot{m}_c$ is the mass flow rate in one capillary and N is the number of capillaries.

6. Straub, L. G., Silberman, E. and Nelson, H. C., "Open Channel Flow at Small Reynolds Number," ASCE Transactions 1958, Vol. 123, pp 685 - 706.

where

μ is the liquid viscosity,

Thus,

$$\Delta P_f = \frac{2\,C\,\dot{m}\,\mu\,L}{\rho\,D_h^{\,2}\,A_F\,g_c} \qquad (2\text{-}3)$$

where $\dot{m}$ is the wicking mass flow rate

Values for C were determined for each configuration of interest as shown in Tables 2-2, 2-3, 2-4 and 2-5. For the pleated screens, the value of C was determined based on the weighted average of wetted perimeters (C = 16 for semicircles, C = 24 for parallel plates).

The hydrostatic pressure differential, $\Delta P_g = \rho g/g_c\ L \sin \theta$

where

g = the ambient acceleration level

θ = angle of the wicking direction with the horizontal

Equation 2-1 and 2-3 were combined and manipulated to yield the heat rate interception capability of a wicking barrier for a single capillary.

$$\dot{Q} = \frac{\rho\,\lambda\,g_c\,D_h^{\,2}\,A_F}{2\,C\mu\,L}\left[\Delta P_\sigma - \Delta P_g\right] \qquad (2\text{-}4)$$

where

$\dot{Q} = \dot{m}\,\lambda$

λ is the heat of vaporization

For thermal conditioning purposes it is more efficient to express the wicking capability in terms of heat rate per unit width, $\dot{Q}/W$. For a heat source acting along a line at distance L from the liquid pool this is

$$\frac{\dot{Q}}{W} = \frac{\rho\,\lambda\,g_c\,D_h^{\,2}\,A_F}{2\,C\,\mu\,L\,w}\left[\Delta P_\sigma - \Delta P_g\right] \qquad (2\text{-}5)$$

where

w is the width of a single capillary
W is the width of the capillary device surface

Equation 2-4, the heat rate interception capability for a single capillary, is transformed into Equation 2-5, the heat rate interception capability for a capillary device surface by multiplying Equation 2-4 by the number of capillaries (W/w) in that surface.

For a distributed heat source, $\dot{Q}/A = \dot{Q}/(WL)$ which is equivalent to evaluating Equation 2-5 for $\dot{Q}/W$ at a distance L from the liquid pool. All heat interception can thus be expressed in terms of $\dot{Q}/W$. Formulas for computing the $\dot{Q}/W$ capability of each candidate wicking configuration are given in Table 2-2.

Table 2-3. Rectangular Duct Friction Factors

b/a Aspect Ratio	$f\,Re_{D_H}$
0	24
1/20	22.48
1/10	21.17
1/8	20.58
1/6	19.70
1/4	18.23
2/5	16.37
1/2	15.55
3/4	14.47
1	14.23

Table 2-4. Isosceles Triangular Duct Friction Factors

α Subtended Angle	$f\,Re$
10	12.48
20	12.82
30	13.07
40	13.22
50	13.31
60	13.33
70	13.31
80	13.25

Table 2-5. Annular Duct Friction Factors

r_i/r_o Inner Radius/Outer Radius	$f\,Re$
0.0001	17.95
0.001	18.67
0.01	20.03
0.05	21.57
0.10	22.34
0.15	22.79
0.20	23.09
0.30	23.46
0.40	23.68
0.60	23.90
0.80	23.98
0.90	24
1.0	24

Heat interception requirements were determined using data from Table 2-1. Table 2-6 indicates the type of calculations performed. The basket surfaces noted in Table 2-6 are shown schematically in Figure 2-1. A programmable desktop computer was used to generate data, similar to Table 2-6, for the 16 configurations shown in Table 2-2. Those specific conditions that would obviously be less severe than the others, were not included in the calculations. For LO_2 this occurred on the bottom surface where the Shuttle ACS condition had higher heat flux and g level requirements than the Centaur ACS condition at equal wicking distances. For LH_2 this occurred for the side panel where the Shuttle ACS had higher g levels than the Centaur ACS conditions at equal heat flux and wicking distance. For the LH_2 sidewall Shuttle ACS case where the wicking distance is zero, no wicking is required. Thus, this condition was excluded.

The $\dot{Q}/W$ requirement for each surface was generated and used to compute configuration geometry for each possible worst case LO_2 and LH_2 condition. Minimum and maximum allowable spacing was computed to satisfy each $\dot{Q}/W$ for each acceleration level and distance from the wicking pool. These spacings were found by solving the heat flux interception equations of Table 2-2 for real, positive roots. Optimum spacing for each condition was computed by differentiating the heat interception equation with respect to the spacing and setting it equal to zero. This gave the spacing that produced the maximum heat flux interception capability.

The results were sorted in terms of the highest minimum spacing, the lowest maximum spacing and the lowest optimum spacing. The minimum and maximum spacing establish manufacturing limits. The lowest optimum spacing was used to determine the design point safety factor of each configuration. Using this optimum spacing for each configuration, the heat interception capability for each configuration was computed at all acceleration and wicking conditions and compared to the required heat interception of Table 2-1. These results are shown in Table 2-6 for a typical configuration.

Flow optimization of rectangular and triangular wick geometry was restricted to square and equilateral triangle dimensions since these would be easiest to manufacture. To obtain higher heat interception capability, higher aspect ratio rectangles (b>a) and smaller vertex angles ($\alpha < 1.05$ radians (60°)) could be used. (See Table 2-2 for definitions.)

Optimum pleated screen, r, (see Table 2-2) was computed as a function of surface area to projected area ratio for both LO_2 and LH_2. The area ratios and radii were compared to pleat pitch and depth forming capability obtained from local filter manufacturers and suppliers. Pleated screen configurations selected from an evaluation similar to that shown in Table 2-6 were those that gave maximum heat interception capability (maximum area ratio) and had pleat pitch (4r) within manufacturable limits. (For pleat lengths needed for LO_2 and LH_2 start baskets, special tooling, not currently in use, would be required.)

Comparisons of heat interception capability for all configurations were determined, at the lowest optimum spacing, in Reference 2-5, (Table 6). The heat interception

Table 2-6. Typical Hea

Basket* Location	Maximum Average Heat Flux watts/ (Btu/ m^2 hr-ft^2)	Maximum Local Heat Flux watts/ (Btu/ m^2 hr-ft^2)	Time Period	Max. Wicking Distance From Pool to Heat Source m (ft)	Accel- eration Level g's	Sur Ar m
LO$_2$ Bottom	35.3 (11.2) 9.8 (3.1) 9.8 (3.1)	35.3 (11.2) 9.8 (3.1) 9.8 (3.1)	Shuttle ACS Centaur ACS-Low Earth Orbit Centaur ACS - Synchronous Eq.	.09 (.31) .09 (.31) .09 (.31)	.0085 .00189 .0009	.7 ↓
LO$_2$ Top	1.9 (.6) 1.9 (.6) 1.9 (.6)	4.4 (1.4) 4.4 (1.4) 4.4 (1.4	Shuttle ACS Centaur ACS- Low Earth Orbit Centaur ACS - Synchronous Eq.	.04 (.14) .15 (.48) .19 (.63)	.0085 .00189 .0009	1. ↓
LO$_2$ Side	1.6 (.5) 1.6 (.5) 1.6 (.5)	4.4 (1.4) 4.4 (1.4) 4.4 (1.4)	Shuttle ACS Centaur ACS - Low Earth Orbit Centaur ACS - Synchronous Eq.	.11 (.36) .14 (.45) .14 (.47)	.0085 .00189 .0009	.7 ↓
LH$_2$ Bottom	30.3 (9.6) 30.3 (9.6) 30.3 (9.6)	30.3 (9.6) 30.3 (9.6) 30.3 (9.6)	Shuttle ACS Centaur ACS - Low Earth Orbit Centaur ACS - Synchronous Eq.	.16 (.51) .32 (1.05) .34 (1.11)	.0085 .00189 .0009	6 ↓
LH$_2$ Sidewall	31.5 (10) 5.7 (1.8) 2.5 (.8) 2.5 (.8) 2.5 (.8)	31.5 (10) 5.7 (1.8) 2.5 (.8) 2.5 (.8) 2.5 (.8)	Shuttle ACS - Insul. Outgassing - t = 480 sec Shuttle ACS - Avg. Heat Transfer Shuttle ACS - Before Deployment Centaur ACS - Low Earth Orbit Centaur ACS - Synchronous Eq.	0 (0) .43 (1.4) .56 (1.85) .63 (2.06) .65 (2.13)	.0085 .0085 .0085 .00189 .0009	5.1 ↓
LH$_2$ Top	2.5 (.8) 2.5 (.8) 2.5 (.8)	2.5 (.8) 2.5 (.8) 2.5 (.8)	Shuttle ACS Centaur ACS - Low Earth Orbit Centaur ACS - Synchronous Eq.	.38 (1.25) .41 (1.33) .41 (1.35)	.0085 .00189 .0009	4 ↓
LH$_2$ Side Panel	.9 (.3) .9 (.3) .9 (.3)	2.2 (.7) 2.2 (.7) 2.2 (.7)	Shuttle ACS Centaur ACS - Low Earth Orbit Centaur ACS - Synchronous Eq.	.73 (2.41) .73 (2.41) .73 (2.41)	.0085 .00189 .0009	.4 ↓

* See Figure 2-1.

LO$_2$ Minimum R   = 0.0061 cm (0.00
** "Optimum" R = 0.25 cm (0.0081
Maximum R   = 0.37 cm (0.012

FOLDOUT FRAME /

Flux Interception Calculations (Closed Semicircular Channels)

	Maximum Average Heat Rate $\dot{Q}$ (Btu/ watts hr)	Maximum Local Heat Rate $\dot{Q}_p$ (Btu/ watts hr)	Total Heat Rate $\dot{Q}_T$ (Btu/ watts hr)	W Minimum m (ft)	$\dot{Q}_T/W$ Required watts/(Btu/ m sec ft)	$R_{maximum}$ cm (ft)	$R_{minimum}$ cm (ft)	R_{opt} cm (ft)	$\dot{Q}/W'_{opt}$ at R_{opt} watts/m (Btu/sec ft)	$\dot{Q}/W$ at R_{design}** watts/m (Btu/sec ft)
5)	24.6 (84)	0 (0)	24.6 (84)	1.2 (3.9)	20.5 (.006)	.43 (.014)	.003 (.00011)	.29 (.0094)	5.6×10^4 (16.3)	5.3×10^4 (15.4)
	6.8 (23.3)	↓	6.8 (23.3)	↓	5.7 (.002)	– –	– –	– –	– –	– –
	6.8 (23.3)	↓	6.8 (23.3)	↓↓	5.7 (.002)	– –	– –	– –	– –	– –
0.5)	4.3 (14.7)	.4 (1.4)	4.7 (16.1)	.2 (0.5)	23.5 (.009)	.94 (.031)	.0028(.000095)	.67 (.022)	6.1×10^5 (17.7)	2.0×10^5 (59.2)
	↓	↓	↓	↓	↓	1.25 (.041)	.0061(.0002)	.82 (.029)	3.1×10^5 (88.9)	6.5×10^4 (18.7)
	↓	↓	↓	↓	↓	1.98 (.065)	.0058(.00019)	1.34 (.044)	6.0×10^5 (17.3)	5.4×10^4 (15.6)
.2)	3.0 (10.0)	.5 (1.6)	3.5 (11.7)	.2 (.63)	17.5 (.005)	.37 (.012)	.0034(.00011)	.25 (.0081)	3.6×10^4 (10.4)	3.6×10^4 (10.4)
	↓	↓	↓	↓	↓	1.31 (.043)	.0037(.00012)	.88 (.029)	3.7×10^5 (10.8)	7×10^4 (20.2)
	↓	↓	↓	↓	↓	2.68 (.083)	.0037(.00012)	1.80 (.059)	1.4×10^6 (41.8)	7.5×10^4 (21.6)
/)	182 (621)	0 (0)	182 (621)	1.1 (3.62)	166 (.048)	.64 (.021)	.0023(.00074)	.46 (.015)	2.3×10^4 (6.7)	2768 (0.8)
	↓	↓	↓	↓	↓	1.46 (.048)	.034 (.0011)	.98 (.032)	5.53×10^4 (16)	1384 (0.4)
	↓	↓	↓	↓	↓	2.87 (.094)	.034 (.0011)	1.92 (.063)	2.0×10^5 (58)	1384 (0.4)
3)	–	–	–	–	–	– –	– –	– –	– –	– –
	29.2 (99.5)	0 (0)	29.2 (99.5)	.7 (2.32)	41.7(.012)	.24(.0079)	.021 (.0007)	.16 (.0053)	1038 (.3)	692 (0.2)
	13.0(44.2)	↓	13 (44.2)	↓	18.6(.005)	.18(.0059)	.014 (.00046)	.12 (.004)	346 (.1)	346 (0.1)
	↓	↓	↓	↓	↓	.91(.030)	.014 (.00047)	.49 (.016)	7267 (2.1)	692 (0.2)
	↓	↓	↓	↓	↓	1.49(.049)	.015 (.00048)	.10 (.033)	692 (0.2)	692 (0.2)
2)	10.1(34.6)	0 (0)	10 (34.6)	.73 (2.41)	13.8(.004)	.27(.0087)	.01 (.00033)	.18 (.005)	1730 (.5)	692 (0.2)
	↓	↓	↓	↓	↓	1.13(.037)	.01 (.00034)	.76 (.025)	2.6×10^4 (7.6)	1038 (0.3)
	↓	↓	↓	↓	↓	2.35(.077)	.01 (.00034)	1.58 (.052)	1.1×10^5 (32.2)	1038 (0.3)
	.4 (1.2)	0 (0)	.4 (1.2)	.71 (2.32)	.6 (.0001)	.14(.0046)	.0024(.00008)	.094 (.0031)	346 (0.1)	208 (0.06)
	↓	↓	↓	↓	↓	– –	– –	– –	– –	– –
	↓	↓	↓	↓	↓	– –	– –	– –	– –	– –

LH_2 Minimum R = .034 cm (.0011 ft)
**"Optimum" R = 0.094 cm (0.0031 ft) = R design
  Maximum R = 0.14 cm (0.0046 ft)

R design

capabilities are not shown here because, as seen in Section 2.1.3 many of the configurations considered were not fabricable within the dimensional tolerances shown in Table 2-7. Thus the values shown in Reference 2-5 are only theoretically attainable. The worst case design point for LO_2 was $g/g_o = 0.0085$ and $L = 0.11$ m (0.36 ft). For LH_2 the worst case was $g/g_o = 0.0085$ and $L = 0.73$ m (2.41 ft). (See Table 2-1.) The screens and parallel plates are the most isotropic in terms of capillary pumping. Other configurations show a decided directional preference and would require two orthogonal layers of wicking configuration to satisfy all heat flux interception conditions.

2.1.3   <u>WICKING CONFIGURATION SELECTION.</u>   Configurations specified in Table 2-2 were evaluated for capillary pumping capability, fabricability and weight. An evaluation similar to that of Table 2-6 was made for each of the configurations in Table 2-2. Table 2-7 lists all configurations, with three dimensions shown for each configuration. The minimum and maximum dimensions are, respectively, the smallest and largest wick dimensions that will provide enough flow to intercept all heat flux incident on the screen. The optimum dimension of Table 2-7 is the spacing that gives maximum wicking flow at the worst case condition of acceleration and wicking distance specified in the previous paragraph. For several configurations (screen/plate-plate and open squares with LH_2) no optimum existed; i.e. the optimum condition as defined above yielded a dimension which was greater than the maximum dimension for other conditions listed in Table 2-1 (or Table 2-6). Open semicircles for LH_2 using Reference 2-4 surface tension pressure relations could not be designed to satisfy all heat flux conditions because of the weak capillary pumping predicted. No minimum dimensions are noted for the configurations using perforated plate as a primary barrier. This is due to the method of analysis which includes the perforated plate thickness in the flow area and wetted perimeter incorporated in the heat flux interception equation. The perforated plate analysis essentially assumes maximum stagger between adjacent plates. (Even when the plates are touching there is a path for flow between the plates because holes on the bottom plate are connected to holes on the top plate.)

Only five configurations were found to be fabricable for both LO_2 and LH_2. The pleated screen configuration could only be fabricated with special tooling. The heat interception capability of the configurations employing screen/plate combinations ranged from 500 to 1000 times the required heat interception for LO_2. Pleated screens, if fabricable have even greater potential than the plate/screen combinations. For LO_2, screen alone could supply the required heat interception capability with wicking in the warp direction but only 40% of the required capability in the shute direction. For LH_2, safety factors were approximately 3 to 10 for the plate/screen combination and the pleated screen. For screen alone only 1% to 3% of the required heat could be intercepted. (Screen alone was the 50×250 screen used for the entire LO_2 start basket surface and the bottom portion of the LH_2 basket in Reference 2-1.)

Table 2-8 shows a comparison between actively cooled start basket weights and passively cooled baskets using the five fabricable configurations. The passively cooled weights are based upon the reduced basket volumes previously given in

2-12

Table 2-7. Manufacturability of Configurations

| Configuration | Geometric Variable | LH_2 cm (inches) | | | | LO_2 cm (inches) | | | |
		Minimum	Optimum	Maximum	Manufact-urability	Minimum	Optimum	Maximum	Manufact-urability
Plate/Screen-Screen	b	0.03 (0.012)	0.058 (0.023)	0.086 (0.034)	Yes	0.0048 (0.0019)	0.152 (0.06)	0.23 (0.089)	Yes
Plate/Screen-Plate/Screen	b	–	0.028 (0.011)	0.056 (0.022)	Yes	–	0.124 (0.049)	0.20 (0.080)	Yes
Screen/Plate-Plate/Screen	b	–	0.015 (0.0061)	0.028 (0.011)	Yes	–	0.099 (0.039)	0.18 (0.071)	Yes
Plate/Screen-Plate	b	–	0.013 (0.00528)	0.032 (0.132)	Yes	–	0.088 (0.0348)	0.15 (0.058)	Yes
Screen/Plate-Plate	b	–	–	0.0070 (0.0028)	No	–	0.061 (0.024)	0.12 (0.048)	Yes
Closed Semicircles	R	0.022 (0.0089)	0.094 (0.0372)	0.14 (0.0552)	No	0.034 (0.013)	0.25 (0.0972)	0.37 (0.144)	No
Open Semicircles	R	0.025 (0.01)	0.058 (0.0228)	0.086 (0.034)	No	0.0025 (0.00098)	0.15 (0.059)	0.22 (0.0888)	No
Open Semicircles**	R	–	–	–	No	0.043 (0.017)	0.056 (0.022)	0.08 (0.032)	No
Closed Squares	a	0.028 (0.011)	0.11 (0.045)	0.17 (0.067)	No	0.0046 (0.0018)	0.30 (0.119)	0.43 (0.168)	No
Open Squares**	a	0.061 (0.024)	–	0.086 (0.034)	No	0.01 (0.0041)	0.15 (0.060)	0.22 (0.089)	No
Open Squares	a	0.048 (0.019)	0.086 (0.034)	0.13 (0.050)	No	0.081 (0.032)	0.23 (0.090)	0.34 (0.132)	No
Closed Equilateral Triangles	A	0.055 (0.022)	0.23 (0.09)	0.34 (0.132)	No	0.010 (0.004)	0.61 (0.24)	0.89 (0.35)	Yes
Open Equilateral Triangles	A	0.046 (0.018)	0.16 (0.064)	0.198 (0.078)	No	0.0076 (0.003)	0.36 (0.14)	0.53 (0.21)	No
Open Equilateral Triangles**	A	0.064 (0.025)	0.066 (0.026)	0.096 (0.038)	No	0.011 (0.0044)	0.18 (0.069)	0.254 (0.10)	No
Pleated Screen	N = 2	t=0.05 (0.02)	t=0.094 (0.037)	t=0.13 (0.051)	Yes	t=0.01 (0.004)	t=0.025 (0.097)	t=0.35 (0.138)	Yes
		p=0.05 (0.02)	p=0.132 (0.052)	p=0.183 (0.072)		p=0.0147 (0.0058)	p=0.35 (0.136)	p=0.49 (0.192)	

** Using surface tension pressure defined by Bressler, R.G. and Wyatt, P.W.,
"Surface Wetting Through Capillary Grooves," Transactions of the ASME,
Journal of Heat Transfer, February 1970.

Table 2-8. Passively Cooled Start Basket Weight Penalties (Aluminum Screen
and Plate) (Based on Pretest Analysis)

Actively Cooled Start Baskets, kg (lb_m)			Total LH_2 + LO_2 kg (lb_m)	
LH_2 Start Basket Wt = 62.8 (138.3)	LO_2 Start Basket Wt = 17.6 (38.8)	Start Basket Weight = 80.4 (177.1)
Cooling Coil Weight = 59.8 (131.6)	Cooling Coil Weight = 8.5 (18.8)	Cooling Coil Weight = 68.3 (150.4)
Total Weight = 122.6 (269.9)	Total Weight = 26.1 (57.6)	Total Weight = 148.7 (327.5)

Passively Cooled Start Baskets

	LH_2 Start Basket Weight, kg (lb_m)		LO_2 Start Basket Weight, kg (lb_m)		LO_2 + LH_2 kg (lb_m)	
Plate/Screen-Screen	55	(121.2)	14.8	(32.5)	69.8	(153.7)
Plate/Screen-Plate/Screen	71.8	(158.2)	17.2	(37.8)	89	(196)
Screen/Plate-Plate/Screen	71.8	(158.2)	17.2	(37.8)	89	(196)
Screen/Plate-Plate	66.4	(146.2)	16.4	(36.1)	82.8	(182.3)
Pleated Screen	69.9	(154.0)	17.0	(37.4)	86.9	(191.4)

Section 2.1.1, corresponding support requirements for the start baskets, and provisions for wicking around the corners. This required conceptual corner joints to be designed for the plate/screen configurations. The pleated screen consists of two layers of pleated screen with adjacent pleats orthogonal.

Analysis of the wicking configurations revealed the desirability of using plate/screen combinations and pleated screen because of their low weight and good heat flux interception capability. The plate/screen combinations selected for testing were plate/screen-screen, plate/screen-plate/screen, and screen/plate-plate/screen. During the fabrication phase it was found that spacing between screens could not be controlled due to sagging of the screens between spacers. The plate/screen-screen configurations were thus altered to plate/screen-screen/plate, increasing passively cooled system weight, but providing accurate dimensional control. Pleated screen was also selected as a unique concept. As indicated in Table 2-8 the passively cooled start basket concept shows a substantial weight advantage over the actively cooled basket concept. In fact the weight advantage is more than that shown in Table 6-3 of Reference 2-1. (This is because passively cooled start basket volume is less than actively cooled start basket volume). Based on this comparison, a test plan was developed.

2.2 EXPERIMENT PROGRAM

2.2.1 SPECIMENS. Based upon the discussion of Section 2.1, four configurations were selected for experimental evaluation. Plate/screen-screen/plate, plate/screen-plate/screen and screen/plate-plate/screen configurations were selected because of their ease of fabricability. Pleated screen was selected because it offers design flexibility in permitting increased screen area (and thus low pressure drop transverse to the capillary barrier) as the ratio of screen flow area to projected area is increased.

The four wicking configurations were sized for normal gravity operation in ethanol. Optimum wick dimensions were determined by expressing the wicking velocity as a function of wick geometry. Differentiating with respect to spacing and setting the resulting expression equal to zero yielded the optimum spacing for a given specimen angle with the horizontal. The lower limit of wick spacing was the manufacturable limit (e.g., 0.025 cm (0.010 in) for parallel plate or screen spacing). The upper limit of wick spacing was the point at which the capillary pumping height equalled the wick spacing. A more practical limit was set at the wick being completely full of liquid at a distance from the wicking pool of one half the total wick length. This limit was set to assure that a reasonable amount of the wick would be used in the test. Using optimum spacing plotted as a function of specimen angle, as shown for example in Figure 2-2, three specimen angles were selected for design purposes that would allow the upper limit (a full wick at an equilibrium distance of one half the total wick length) and the lower limit (minimum manufacturing tolerance) of wick geometry to be met for all three configurations. These three specimen angles were found to be 0.007 radians

SCREEN/PLATE - PLATE/SCREEN

LENGTH = 0.46 m, (1.5 ft), ETHANOL, NORMAL GRAVITY
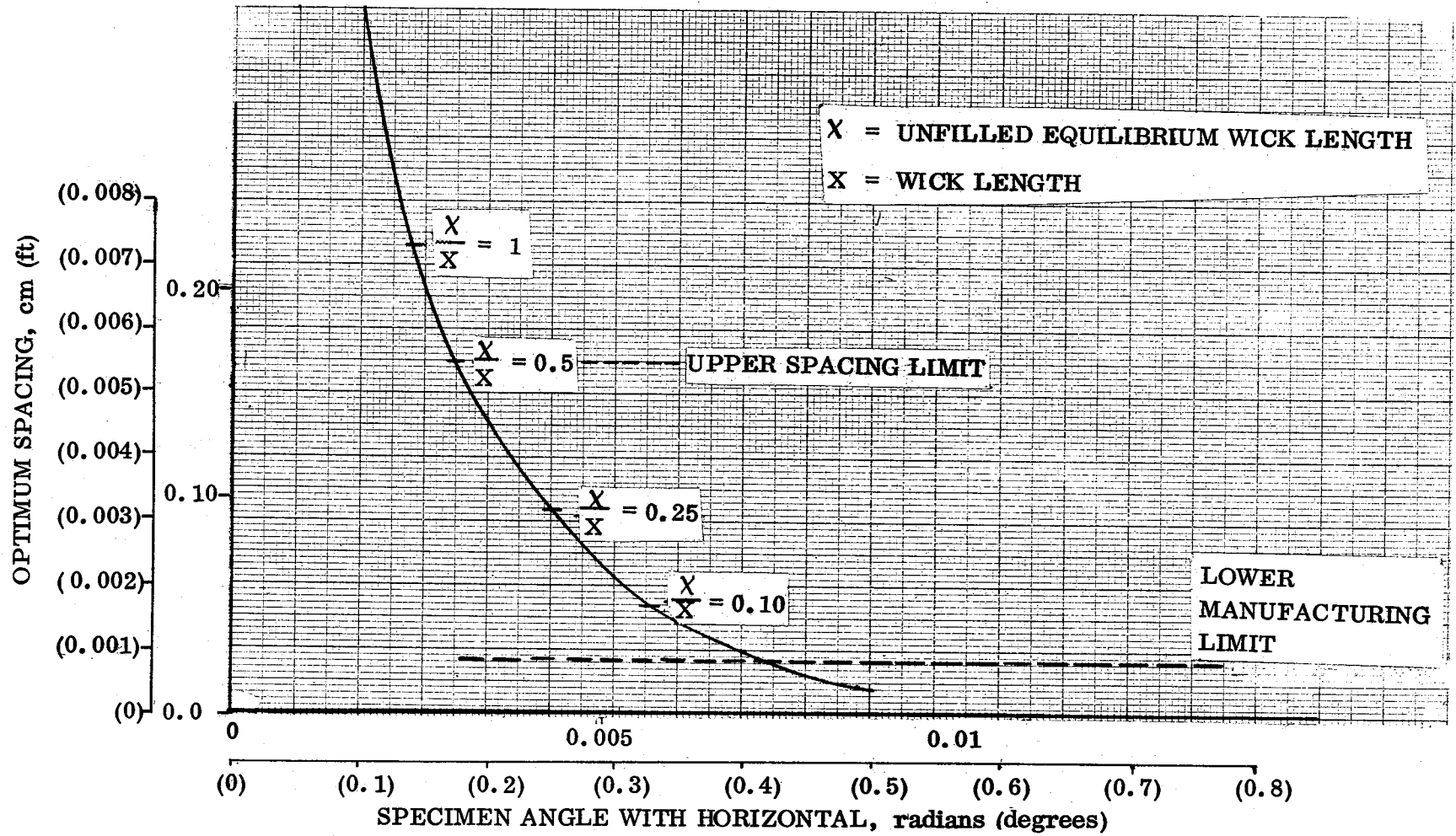
Figure 2-2. Typical Plot of Optimum Spacing Versus Specimen Angle

(0.4°), 0.005 radians (0.3°) and 0.004 radians (0.25°) with the horizontal. To simplify fabrication, minimum spacing for the experimental specimens was taken to be .051 cm (.020 inches).

Based upon the analysis of heat flux interception capability and fabricability of wicking configurations described above, four configurations were selected for testing:
1. Plate/screen-screen/plate, 2. Plate/screen-plate/screen, 3. Screen/plate-plate/screen, and 4. Pleated screen. Three geometries were selected for each type of configuration based upon the criteria of providing maximum wicking velocity at specimen angles of 0.007 radians (0.4°), 0.005 radians (0.3°) and 0.004 radians (0.25°) with the horizontal. The geometries selected are shown below in Table 2-9.

Table 2-9. Selected Specimen Geometries

Plate/screen-screen/plate, Specimen #1	b = 0.089 cm (0.035 in), e = 0.057 cm (0.0225 in)
Plate/screen-screen/plate, Specimen #2	b = 0.111 cm (0.004 in), e = 0.057 cm (0.0225 in)
Plate/screen-screen/plate, Specimen #3	b = 0.14 cm (0.056 in), e = 0.057 cm (0.0225 in)
Screen/plate-plate/screen, Specimen #1	b = 0.05 cm (0.020 in), e = 0.057 cm (0.0225 in)
Screen/plate-plate/screen, Specimen #2	b = 0.06 cm (0.025 in), e = 0.057 cm (0.0225 in)
Screen/plate-plate/screen, Specimen #3	b = 0.10 cm (0.038 in), e = 0.057 cm (0.0225 in)
Pleated screen, Specimen #1*	p = 0.22 cm (0.087 in), t = 0.38 cm (0.150 in), N = 4
Plate/screen-plate/screen, Specimen #1	b = 0.0635 cm (0.025 in), e = 0.057 cm (0.0225 in)
Plate/screen-plate/screen, Specimen #2	b = 0.11 cm (0.044 in), e = 0.057 cm (0.0225 in)

Where b is the distance between inner barriers, e is the perforated plate thickness, p is the pleat pitch (distance between corresponding points on adjacent pleats), t is the pleat depth, and N is the screen surface area divided by the projected area.

* Minimum pleat pitch and depth for 46 cm (18 in) long pleat

All screens consisted of 50 × 250 (1WP) screen. Perforated plate had 0.95 cm (3/8 in) holes on 1.27 cm (1/2 in) centers for 51% open area. These are typical of Centaur D-1S LO_2 and LH_2 start basket materials identified in Reference 2-1, NAS3-17802. Stainless steel material was used for the test specimens in order to facilitate fabrication. This did not affect test results (compared to the baseline aluminum screen and perforated plate specified in Reference 2-1) since the test fluid will completely wet both aluminum and stainless steel.

Actual specimen geometries, as measured after fabrication, are given in Table 2-10 along with the dimensional tolerance for each specimen. Actual measured perforated plate thickness was 0.058 cm (0.0229 in). Initially, a test setup was made using reference specimens specifically fabricated for checking out the apparatus. The reference specimens consisted of 50 × 250 mesh screen tested in both the warp and shute direction and a 50 × 250 mesh screen with perforated plate, tested in the warp direction. Screen test results were compared to those of Reference 2-3.

Table 2-10. Actual Specimen Geometry

Configuration	Nominal Spacing
Plate/screen-screen/plate	0.086 ± 0.001 cm, (0.034 ± 0.0005")
Plate/screen-screen/plate	0.113 + 0.001 cm, (0.0445 + 0.0005")
Plate/screen-screen/plate	0.142 cm, (0.056")
Plate/screen-plate/screen	0.086 ± 0.001 cm, (0.034 ± 0.0005")
Plate/screen-plate/screen	0.113 + 0.001 cm, (0.0445 + 0.0005")
Screen/plate-plate/screen	0.051 cm, (0.020")
Screen/plate-plate/screen	0.065 cm, (0.0255")
Screen/plate-plate/screen	0.086 ± 0.001 cm, (0.034 ± 0.0005")
Pleated screen	p = 0.22 cm, (0.088") t = 0.38 cm, (0.15")

In addition to these specimens, some runs were made with the apparatus in a horizontal position using 200 × 1400 screen specimens, plate/screen-screen/plate configurations and 0.113 + 0.001 cm (0.0445 + 0.0005") and 0.142 cm, (0.056") spacers. These runs were made to checkout specimen wicking using screens that would typically be used for a start basket ground test article.

2-18

Consideration was given to making the wicking specimens out of transparent screen and perforated plate materials. (Plain reverse Dutch weaves are available in micron ratings similar to the 50×250 screen). This would have eased visualizing the wicking front between the screens but would have complicated scaling of the results to a plain Dutch specimen. A simple bench test was run to determine how fast the screen would be wetted by the wicking front in a stainless steel sample. Essentially instantaneous wetting was seen to occur. This allowed all metallic wicking screen/plate specimens to be used with appropriate correction made for the screen volume in the wicking rate calculations.

The test specimens were 7.6 cm (3 in) wide by 46 cm (18 in) long. Isometric sketches of typical test specimens are shown in Figure 2-3. All of these test specimens were tested with the screen aligned so that wicking occurred in the warp direction. Screens backed up by perforated plate were spotwelded to the perforated plate. The plate/screen-screen/plate, screen/plate-plate/screen, and plate/screen-plate/screen pre-test specimen designs used 3 spacers to maintain the correct distance between the inner wicking barriers. The spacers were manufactured of aluminum shim stock. Overall spacer size was 1.27 cm (1/2 in) square in order to span the holes in the perforated sheets that were employed. This made the test specimen conform more closely to the analysis, i.e., non zero wicking velocity at zero plate spacing. This required that the center of the holes in one sheet be opposite the center of the lands in the opposite sheet. The sheets were attached with screws through the plate/screen combinations and through the spacers. The attachment screws spanned the 0.95 cm (3/8 in) hole on the upper perforated sheet.

All screens and plates were sheared to size and were resistance welded using a micro-welder. Several dozen spot welds were used to join each screen and perforated plate. The microwelder was used to minimize distortion in the weld area and to thus impede screen wicking as little as possible.

During the initial test runs with the bolted configurations shown in Figure 2-3, considerable dripping occurred from the attaching screws nearest the knife edges. This reduced the liquid in the wick and impaired test results. To eliminate dripping, all surfaces protruding from the bottom surface of the wick were removed. Spacers were fabricated of 0.64 cm (1/4 in.) × 2.54 cm (1 in.) aluminum material of the thicknesses indicated in Table 2-10. As shown in Figure 2-4, spacers were placed in six locations between specimen halves. These locations were adjacent to the knife edges, approximately one third in from the edge in the direction perpendicular to the wicking front. These spacers eliminated any protrusions and minimized dripping from the lower specimen surface. Small weights were used to keep the specimen halves in contact with the spacers.

As indicated previously, several runs were also successfully completed with 200 × 1400 mesh, plate/screen-screen/plate sandwiches.

2-19

ATTACHING
SCREW

PERFORATED
PLATE

SCREEN

SPACER

SCREEN

PERFORATED PLATE

PLATE/SCREEN – SCREEN/PLATE CONFIGURATION

ATTACHING
SCREW

SCREEN

PERFORATED PLATE

PERFORATED PLATE

SPACER

SCREEN

SCREEN/PLATE-PLATE/SCREEN CONFIGURATION

ATTACHING
SCREW

SCREEN

PERFORATED PLATE

SCREEN

SPACER

PERFORATED PLATE

PLATE/SCREEN-PLATE/SCREEN CONFIGURATION

PLEATED SCREEN

PLEATED SCREEN CONFIGURATION

Figure 2-3. Isometric Sketch of Planned Wicking Specimens

Figure 2-4. Isometric Sketch of Actual Wicking Test Specimens

PLEATED SCREEN CONFIGURATION

PLEATED SCREEN

PLATE/SCREEN - PLATE/SCREEN CONFIGURATION

PERFORATED PLATE

SCREEN

PERFORATED PLATE

SCREEN

SPACERS

SCREEN/PLATE - PLATE/SCREEN CONFIGURATION

SCREEN

PERFORATED PLATE

PERFORATED PLATE

SCREEN

SPACERS

PLATE/SCREEN - SCREEN/PLATE CONFIGURATION

PERFORATED PLATE

SCREEN

SCREEN

PERFORATED PLATE
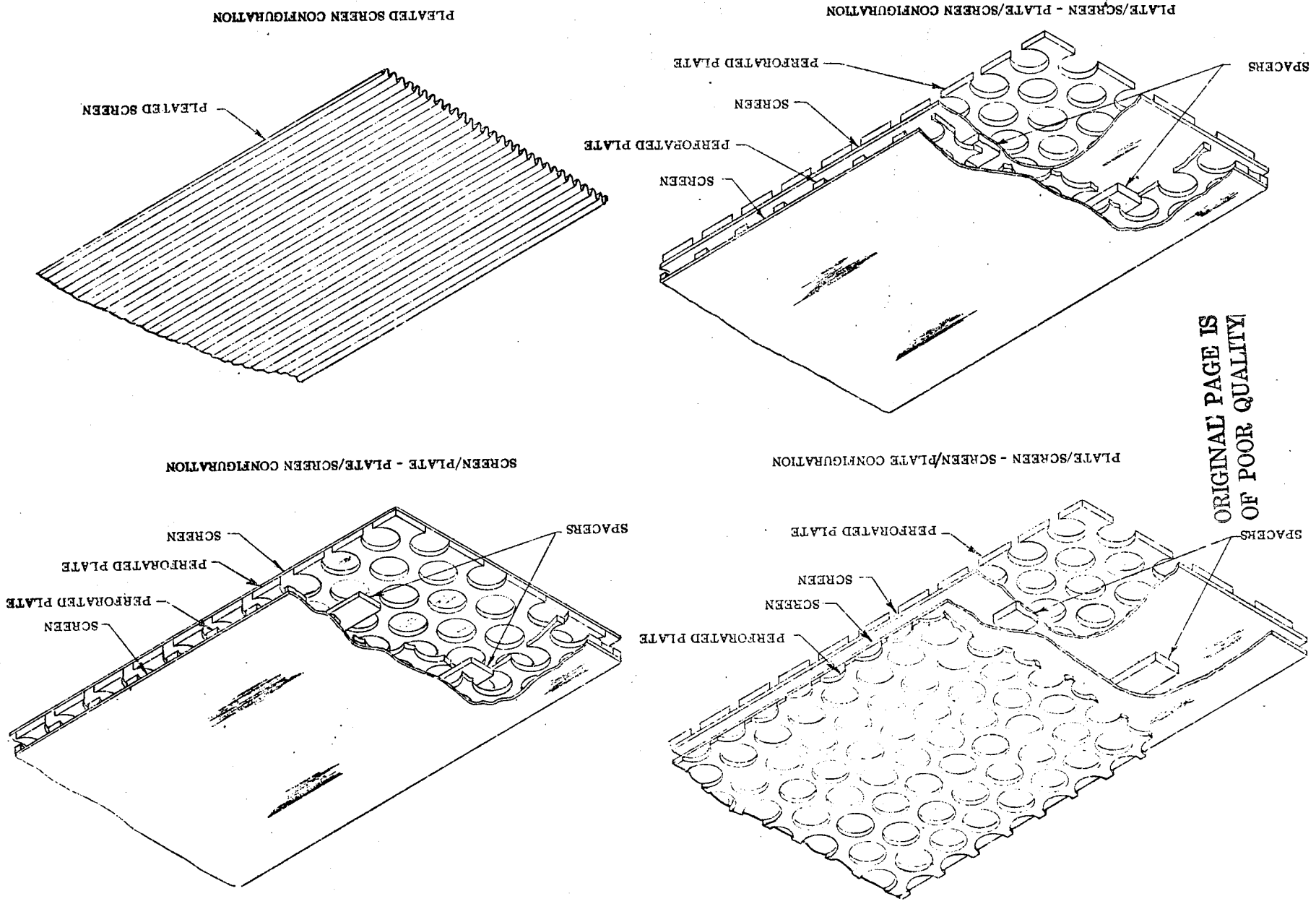
SPACERS

ORIGINAL PAGE IS
OF POOR QUALITY

2-21

A single run was made with a 50 × 250 screen, plate/screen-screen/plate configuration using 0.090 cm (0.0355 in.) spacers and countersunk screw holes on the plate lands. Using #2-56 UNC thread flat head screws allowed spacers to be used to make a configuration that did not protrude from the bottom of the specimen. A subsequent test showed that no dripping occurred from the bottom of the specimen (screw head down) and wicking results were in the range anticipated. This test indicated that a configuration of this type can be successfully used in a capillary device ground test article.

2.2.2 CONFIGURATION DESIGN AND FABRICATION. An apparatus was designed to test the wicking capability of the specimens described in Section 2.2.1. This apparatus was approved by NASA/LeRC and with slight modifications was fabricated and assembled as shown in Figure 2-5. This photograph was taken in the test area after cleaning, checkout and testing of the apparatus.

Figure 2-6 shows the apparatus with the reference specimens (and thermocouples installed). Figure 2-7 is a test setup showing typical wicking sandwich specimens. In the design shown in Figure 2-5, the test specimens were mounted on an aluminum base plate which was enclosed in a transparent box. A glass plate was used for the top cover of the box for viewing and photographically recording data. Glass was used because it is clearer than plastic and less susceptible to scratching or crazing. The sides of the enclosure, the fluid reservoir, reservoir refill and leveling devices were Lexan polycarbonate. This material was chosen over glass because of its machinability. Joints were cemented leak tight and reinforced with screws as required. The transparent glass cover was not cemented to the test enclosure. The cover could thus be removed without disturbing the test specimens, base plate or test enclosure. Base plate orientation was controlled by adjusting three pointed screws.

Fixtures were fabricated for clamping and holding the reference screen specimens during testing. Three coplanar knife edges were used for supporting the more rigid sandwich configurations and pleated screen. For some of the tests the reservoir edge replaced the knife edge nearest the reservoir in order to minimize dripping from the specimens.

Two levelers, consisting of plastic troughs filled with test fluid, were mounted at right angles to each other on the base plate. These were used in conjunction with a tooling transit to control specimen orientation. With this arrangement, the end of the specimen, approximately 43.2 cm (17 inches) from the source could be positioned within ± 0.00254 cm (0.001 inch).

In order to supply liquid to the test specimen, the upstream side of the specimen was bent down below the edge of the reservoir. The reservoir was kept full to the top of the wick by adjusting the needle valve on the reservoir refill. A fast drain was also provided for initially filling the reservoir or draining the reservoir refill.

Evaporation of liquid within the test enclosure was minimized by maintaining a high partial pressure in the experiment enclosure. This was accomplished with a
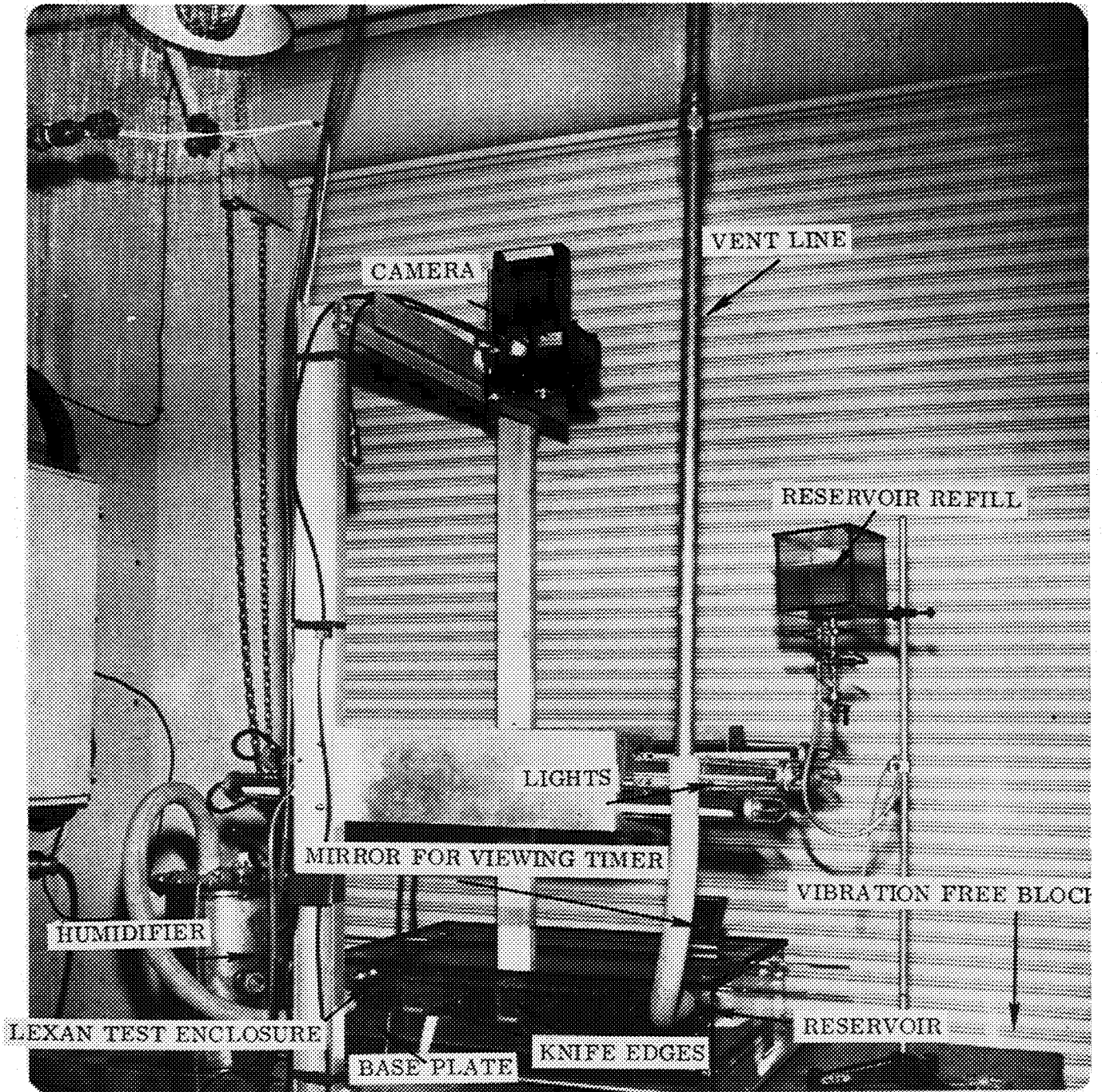
Figure 2-5. Wicking Test Apparatus in Environmentally Controlled Room

Figure 2-6. Reference Test Specimens
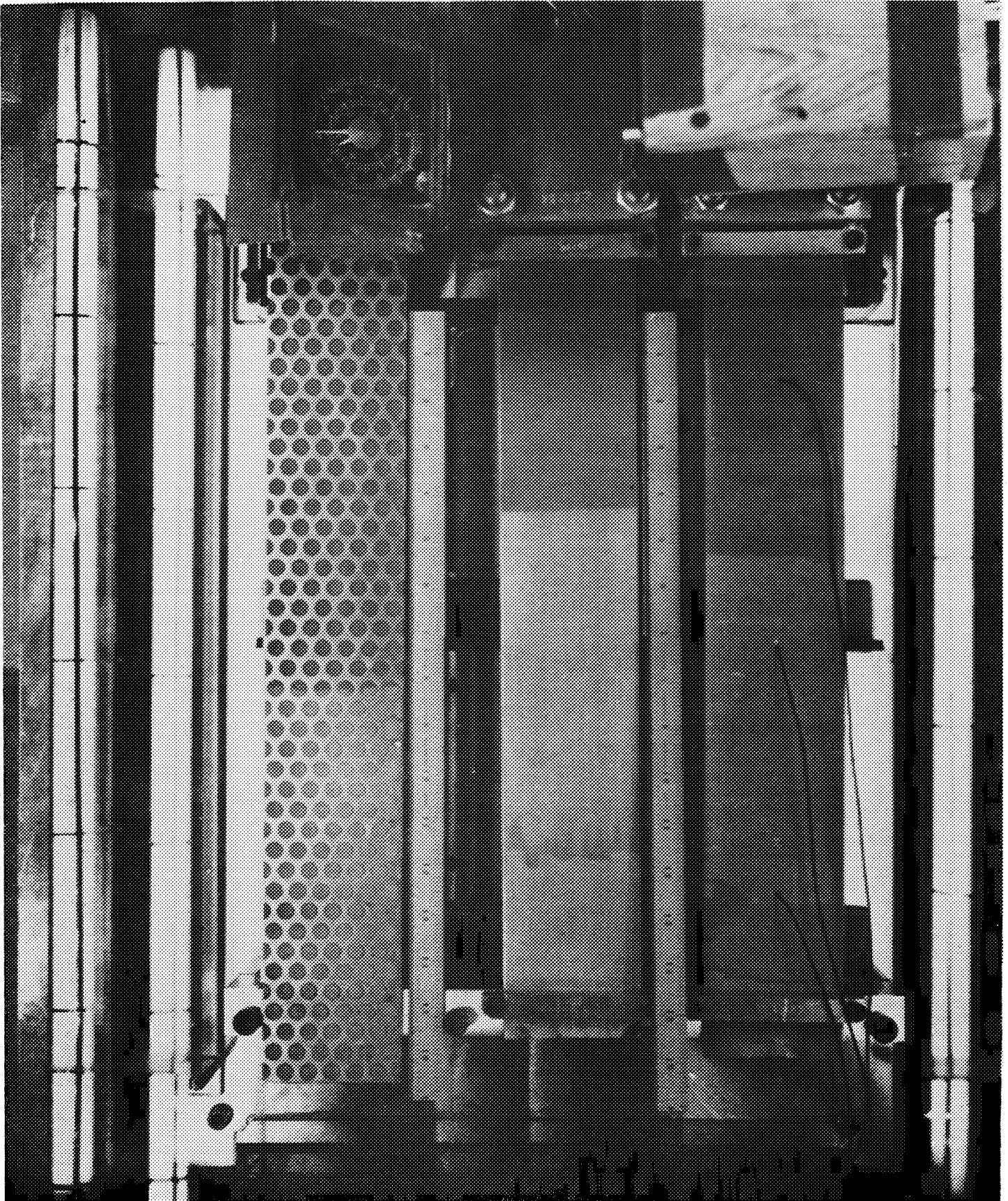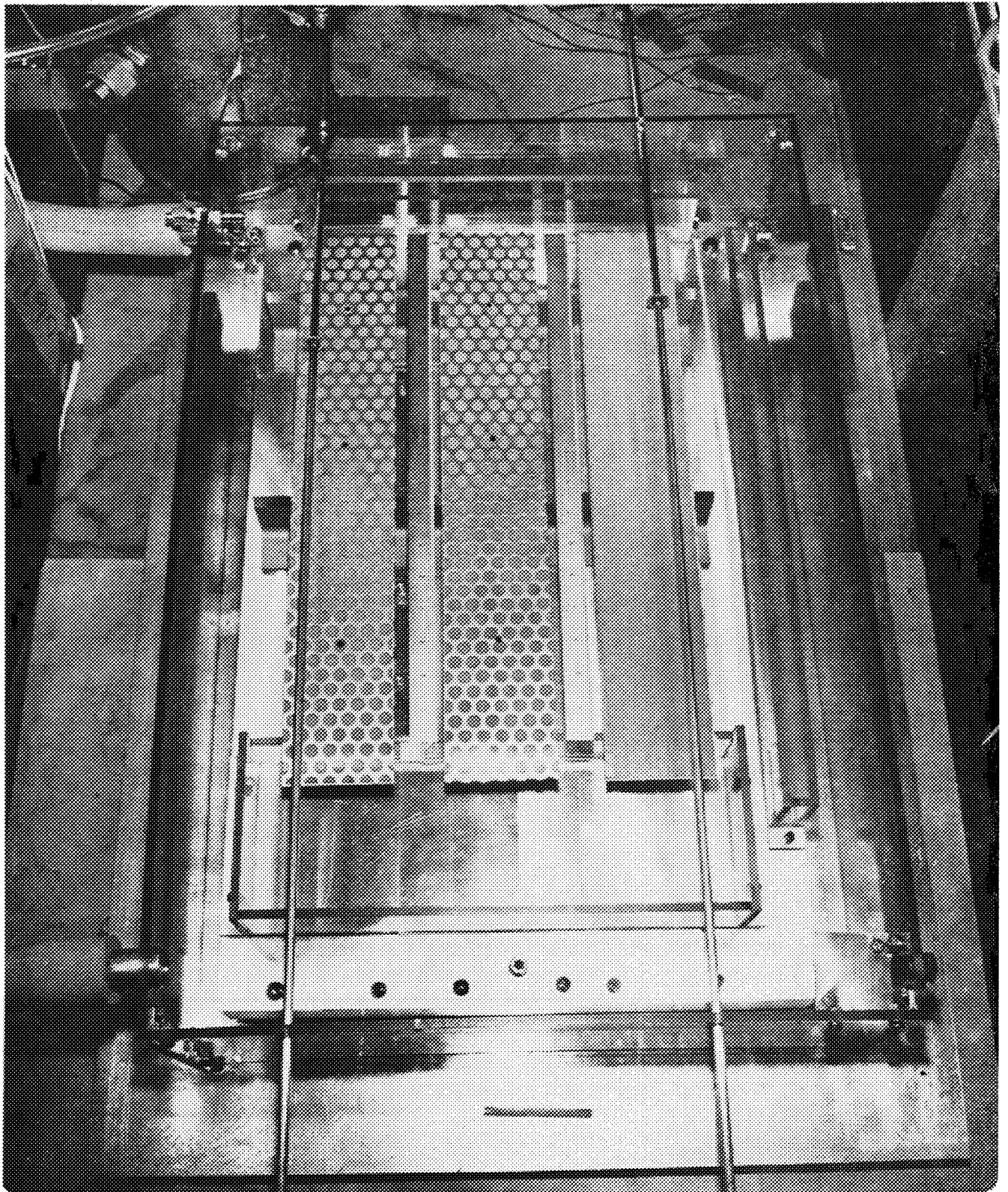
Figure 2-7.   Setup With "Sandwich" Wicking Specimens

2-25

pressurized humidifier, containing a 25 watt aquarium heater, partially filled with test fluid through which gaseous nitrogen (boiled off from liquid nitrogen) was bubbled. An aquarium air stone was used to disperse the GN_2 bubbles and the heater was used to replace the heat lost in vaporizing the test fluid. The humidifier was kept several degrees below the test enclosure temperature to prevent liquid condensation on the enclosure surfaces and possible degradation in viewing the wicking. A qualitative humidity indicator was wetted prior to each run and examined periodically to note any drying out of the screen due to ethanol evaporation.

The test enclosure was vented out of the environmentally controlled room to reduce fire potential and to protect test personnel from respiratory hazards. A timer, mounted in the field of view of the camera, as shown in Figure 2-6, was used to measure wicking time. Rulers aligned on the side of wicking specimens measured the distance travelled by the wicking fluid. Thermocouples on the apparatus and reference test specimen measured the absolute temperature of the enclosure and specimens and the differential between the humidifier and the enclosure. Checkout of the apparatus with the reference specimens showed that temperature differences along the wicking front were negligible. Because of this, thermocouples were not attached to the other wicking test specimens. The humidifier heater was controlled according to the temperature differential between the humidifier and enclosure.

Originally it was thought that screen wetting would be instantaneous and recording of the wicking front could be made by photographing the wetting of the top screen. This proved to be an inaccurate method of recording the position of the wicking front inside the specimen since, in many cases, the top screen wicked ahead of the liquid inside the wick. An indirect method was therefore used to photograph the wicking front. The washers, shown in Figure 2-7, were aligned with the wicking front by sliding a metal rod along as the fluid wicking progressed. With this observation method, only the two end specimens could be recorded simultaneously unless the middle specimen was the pleated screen. The pleated screen wicking was directly photographed.

Lexan components were cut using a band saw and joined using methylene dichloride (dichloromethane) solvent. The aluminum knife edges and base plate were machined and fitted to achieve coplanar knife edges. The base plate was drilled and tapped to accommodate the reservoirs, levels, knife edges and ruler holders. Mounting clamps, for holding the reference specimens flat during tests were machined, tapped and fitted to the base plate. Reservoir refill valving was assembled using standard fittings, and needle and shutoff valves that were thoroughly rinsed in ethanol prior to assembly.

During apparatus assembly, all parts were rinsed in 200 proof reagent grade ethanol and dried using GN2 boiled off from LN_2.

Wicking distances were measured photographically using a long focal length 70 mm still camera mounted above the specimen. The camera allowed clear photographs to be taken at discrete time intervals (noted by the clock in the field of view) during the testing.

2.2.3 TEST PROCEDURE. The test fluid used was reagent grade 200 proof ethanol. This fluid was selected because of its good wettability, low toxicity and low vapor pressure at room temperature. The properties of ethanol allowed wicks to be designed and tested in reasonable time periods at small positive specimen angles with the horizontal. As indicated previously, the humidity of the chamber was kept near 100% (completely saturated with ethanol) by bubbling GN_2 through an ethanol container into the test chamber.

After spot welding, each specimen was cleaned according to the following procedure.

1. Slosh specimen in trichlorethane (to remove grease).

2. Put specimen in solution of 26-36 wt-oz/gal nitric acid, 1.5-3 wt-oz/gal sodium dichromate at room temperature for 15 minutes (to dissolve particulates).

3. Rinse three times with distilled water.

4. Put vertically for 5 minutes in ultrasonic cleaner. (Repeat for a total of four cycles, changing the distilled water each time.)

5. Allow specimens to dry overnight in a protected, dust free environment.

6. Individually seal each specimen in a clear plastic wrapper and microscopically examine for particulate content.

Prior to each test the specimens were removed from their sealed bags and placed on the knife edges with the spacers in place and the base plate at the correct angle. Since it was considerably more time consuming to change the specimen angle compared to changing the specimen, all specimens were run at a given angle before the angle was changed.

Initially the reference specimens were tested using the clamping fixture shown in Section 2.2.2. After apparatus checkout, runs were made with bolted configurations. As indicated, spacers that did not protrude from the specimens were then run to minimize dripping. A series of 26 test runs were completed before data analysis indicated that several runs should be repeated to check data reproducibility. Six runs were made for this purpose. An additional run was made with a countersunk bolted specimen which demonstrated a dripless configuration that could realistically be used in a prototype capillary acquisition device. After this test run, 200 × 1400 P/S-P/S sandwiches were tested to demonstrate the capability of a typical wicking barrier for a ground test article. Including these runs, a total of 36 runs were made.

Test runs performed are listed in Table 2-11.

Table 2-11. Wicking Tests Performed (50 × 250 Screen)

Test Run No.	Specimen Angle, Radians (degrees)	Specimen Spacing, cm	Specimen Spacing, cm	Specimen Spacing, cm
1	0 radians (0°)	Plate/Screen, Warp	Screen, Warp	Screen, Shute
2	"	"	"	"
3	"	"	"	"
4	"	"	"	"
5	"	"	"	"
6	0.007 radians (0.4°)	S/P-P/S, .051, bolted	S/P-P/S, .086, bolted	S/P-P/S, .142, bolted
7	"	P/S-S/P, .051 bolted	P/S-S/P, .086 bolted	P/S-S/P, .142, bolted
8	"	P/S-P/S, .051 bolted	P/S-P/S, .086 bolted	P/S-P/S, .142, bolted
9	"	S/P-P/S, .051	Plate/Screen, Warp	P/S-P/S, .086
10	"	S/P-P/S, .065	Plate/Screen, Warp	P/S-S/P, .086
11	"	S/P-P/S, .086	Lexan-P/S, .065	P/S-S/P, .113
12	"	P/S-P/S, .113	Lexan-S/P, .065	P/S-S/P, .142
13	"	P/S-P/S, .113	Pleated Screen	P/S-S/P, .142
14	"	P/S-P/S, .113	Pleated Screen	P/S-S/P, .142
15	.004 radians (0.25°)	S/P-P/S, .051	Pleated Screen	P/S-P/S, .086
16	"	S/P-P/S, .065	Lexan/Plate-P/S, .113	P/S-S/P, .086
17	"	S/P-P/S, .065	P/Pleated Screen/P	P/S-S/P, .086
18	"	S/P-P/S, .085	Lexan-S/P, .065	P/S-S/P, .113
19	"	S/P-P/S, .113	–	P/S-S/P, .142
20	0 radians (0°)	S/P-P/S, .051	Pleated Screen	P/S-P/S, .086
21	"	S/P-P/S, .065	Lexan-S/P, .113	P/S-S/P, .086
22	"	S/P-P/S, .086	Lexan-P, .065	P/S-S/P, .113
23	"	S/P-P/S, .086	Lexan-P, .065	P/S-S/P, .113
24	"	P/S-P/S, .113	Screen, Warp	P/S-S/P, .142
25	"	P/S-P/S, .065	Screen, Shute	S/P-S/P, .086
26	.004 radians (0.25°)	P/S-P/S, .113	–	S/P-S/P, .086
27	"	P/S-S/P, .086	–	P/S-S/P, .113
28	"	P/S-S/P, .086	–	P/S-S/P, .113
29	"	P/S-S/P, .086	–	P/S-S/P, .113
30	"	S/P-P/S, .051	–	S/P-P/S, .086
31	0 radians (0°)	S/P-P/S, .051	–	S/P-P/S, .086
32	0.007 radians (0.4°)	P/S-S/P, .065	–	P/S-S/P, .113
33	0.007 radians (0.4°)	P/S-S/P, .093 flathead screws	–	
34	0 radians (0°)	*P/S-S/P, .113	–	*P/S-S/P, .142
35	0 radians (0°)	*P/S-S/P, .113	–	*P/S-S/P, .142
36	0 radians (0°)	*P/S-S/P, .113	–	*P/S-S/P, .142

* 200 × 1400 screen

2.3 DATA CORRELATION

Data was obtained using a timer and 70 mm stop action camera. For the reference specimens and the pleated screen, direct observation of the wicking front was made. For the "sandwich" configurations, pointers were moved concurrently with the wicking front. Data obtained was reduced and analyzed. Horizontal data yielded correction factors that were applied to the nonhorizontal data. The conservative correlations were then used to predict Centaur D-1S LO_2 and LH_2 start basket heat interception capability. Acceptable wicking configurations were selected. Revised weight estimates were performed and candidate conceptual configurations for wicking around start basket corners were designed.

2.3.1 DATA REDUCTION AND CORRELATION. The 70 mm film was analyzed using a light table, magnifying lenses and an orthogonal grid. Wicking distance versus time was determined for each test run, specimen and specimen angle. Results were initially plotted on Cartesian coordinates to determine data trends and comparisons with test predictions. Wicking with the 50×250 screens was compared to the results of Reference 2-3. These comparisons are shown in Figures 2-8 and 2-9 for the warp and shute direction respectively. Better wicking was obtained in the current testing. This was probably due to better apparatus humidification and specimen cleaning procedures compared to Reference 2-3. Specimen variability could account for some of the difference, as well. These runs were felt to properly check out the apparatus and allow the remainder of the test program to be initiated.

Data from several runs were evaluated using a least squares linear regression analysis to determine the effect of evaporation. The wicking velocity, obtained by differencing the wicking distance and time, was plotted against the reciprocal of the wicking distance in a manner similar to that of Reference 2-3. A typical plot of 50×250 ethanol wicking in the warp direction is shown in Figure 2-10. The linear regression line has an intercept of essentially zero and a correlation coefficient of 0.996. Figure 2-11 shows data for plate/screen wicking that has a correlation coefficient of 0.975. These plots indicate that the effect of evaporation on test results was negligible.

Prior to testing, wicking predictions were made of wicking distance vs time by equating ΔP_F to $\Delta P_\sigma - \Delta P_g$ where ΔP_f is the frictional pressure loss, ΔP_σ is the surface tension driving pressure and ΔP_g is the pressure loss due to hydrostatic head. Expressing ΔP_f in terms of the wicking velocity and solving for the wicking velocity V_W yielded an expression

$$V_W = \frac{g_c \, D_H^2}{2C\mu L} \, (\Delta P_\sigma - \Delta P_g)$$

where

g_c is a dimensional constant

D_H is the hydraulic diameter of the wicking constant
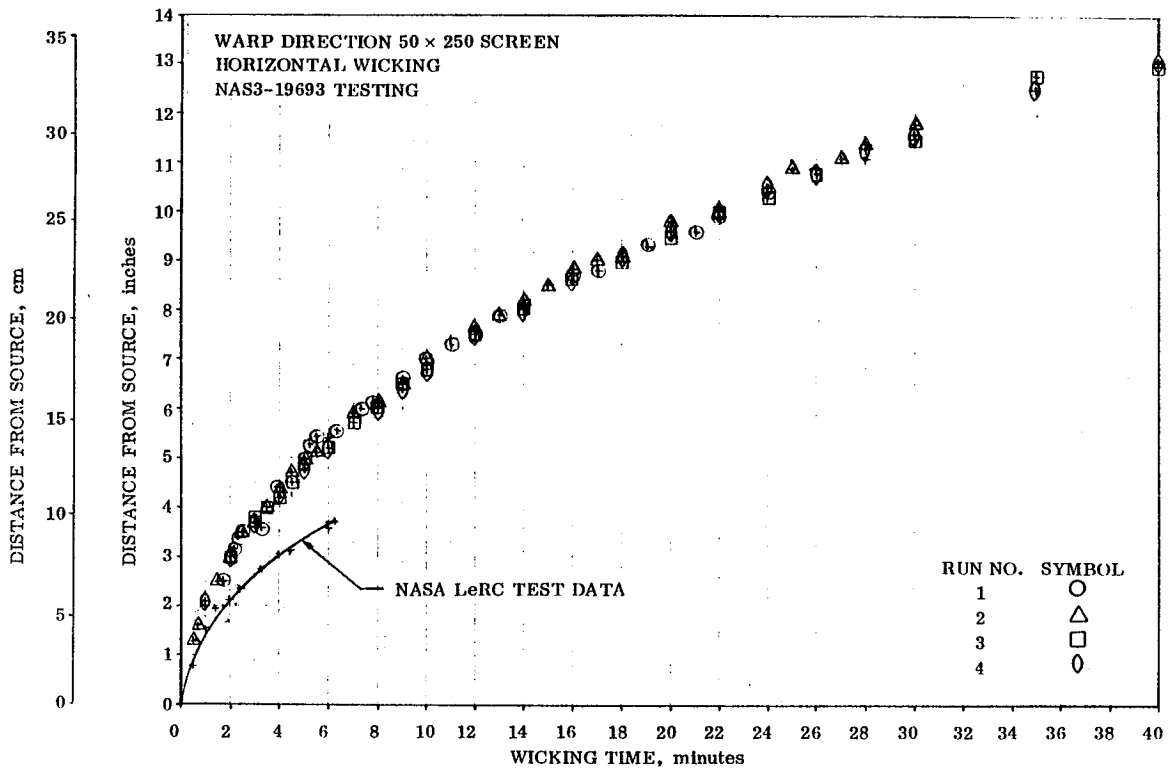
Figure 2-8. 50 × 250 Warp Direction Horizontal Ethanol Wicking
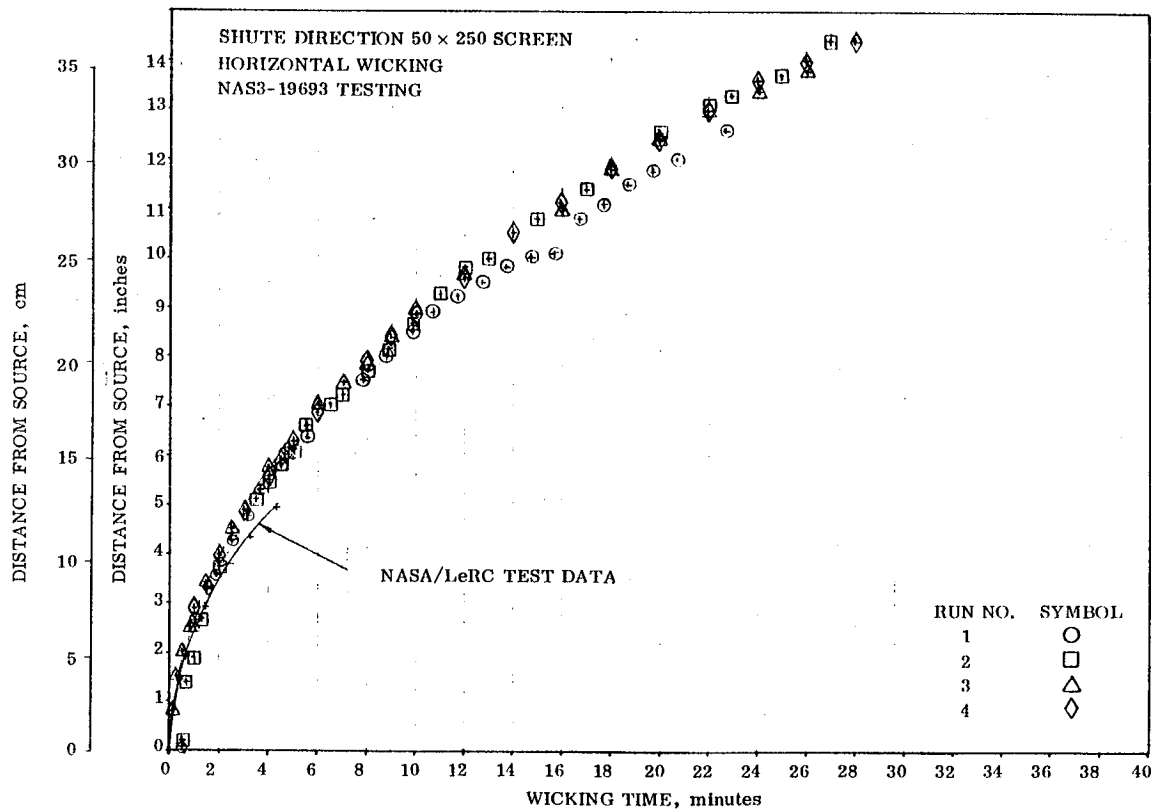
Figure 2-9. 50 × 250 Shute Direction Horizontal Ethanol Wicking

LEAST SQUARES
REGRESSION LINE

RUN NO. 3
DATA FROM 300 TO
1500 CM/SEC NOT
SHOWN (4 PTS)

VELOCITY, cm/sec

VELOCITY, in/min

1/WICKING DISTANCE, 1/inch

1/WICKING DISTANCE, 1/cm

LEAST SQUARES
REGRESSION LINE

RUN NO. 4

VELOCITY, cm/sec

VELOCITY, in/min

1/WICKING DISTANCE, 1/inch

1/WICKING DISTANCE, 1/cm
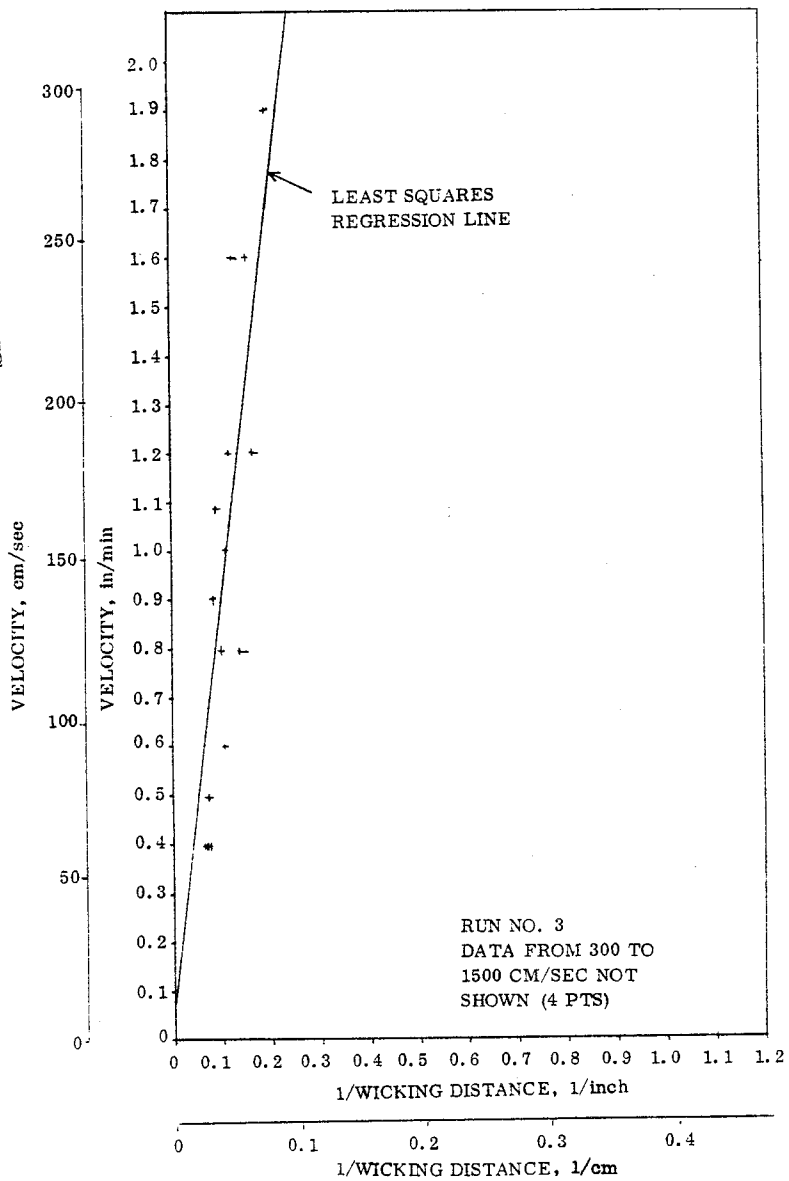
Figure 2-10. 50 × 250 Screen Wicking (Warp Direction)   Figure 2-11. 50 × 250 Screen/Plate Wicking (Warp Direction)
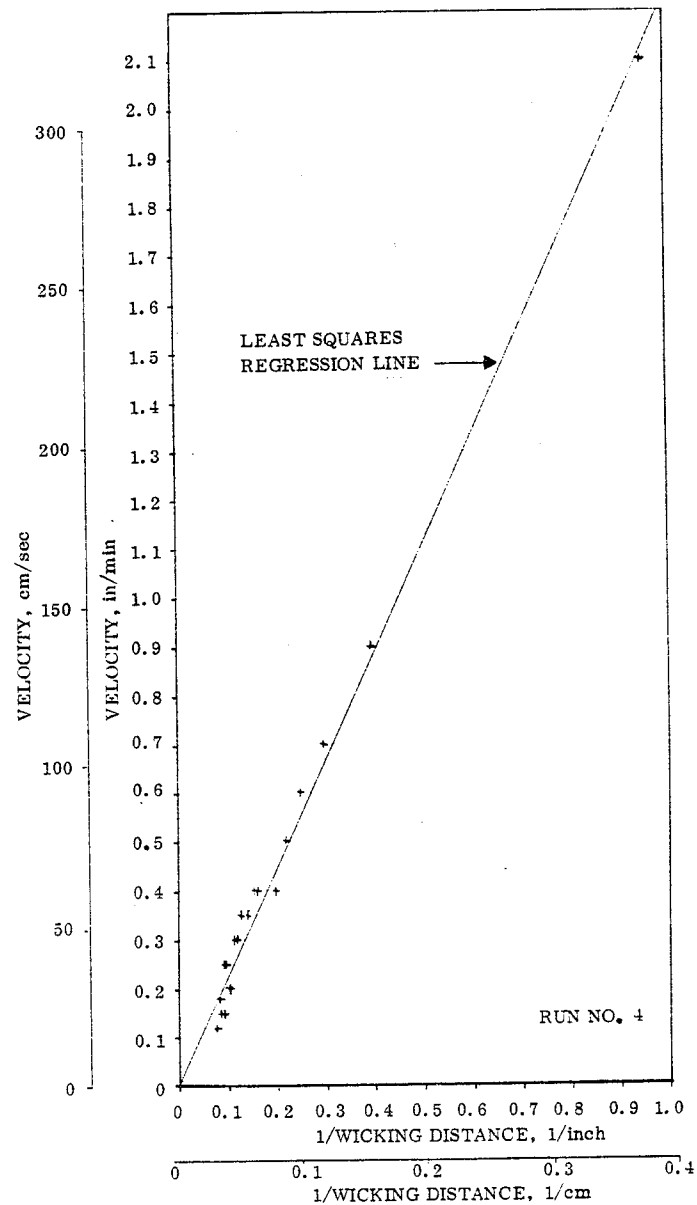
C is a constant used to determine the friction factor, $C = f \, Re$, where Re is the Reynolds number

μ is the liquid viscosity

L is the distance from the liquid pool to the wicking front

A correction factor was introduced to account for screen filling such that;

$$V_W = \frac{g_c \, D_H^2 \, (\Delta P_\sigma - \Delta P_g) / A_c}{2 \, C \mu \, L}$$

where A_C is a correction factor for screen filling $= A_F/(A_F - A_S)$ where A_F is the wicking cross sectional flow area in the channel and A_S is the screen open area perpendicular to flow. $(A_F/(A_F - A_S - A_p))$, where A_p is the plate cross sectional flow area that must be filled by wicking fluid was also used to correlate the data but yielded results that were less consistent than the A_c correction factor).

The wicking velocity

$$V_W = \frac{dL}{dt} = f(L)$$

therefore

$$t = \int_{L_1}^{L_2} \frac{dL}{f(L)}$$

This equation was solved for each of the four wicks tested as a function of spacing, specimen angle and wicking distance. For nonhorizontal wicking, the expression is fairly complicated. The following equations represent theoretical wicking for horizontal and nonhorizontal specimens.

Table 2-12.   Theoretical Wicking Time Equations

Configuration: Plate/screen-screen/plate

Angle: Nonhorizontal

Equation:

$$\Delta t = \frac{A_F}{A_F - A_S} \left[\frac{24 \, \mu \, \sigma}{\rho^2 b^3 g^2 / g_c \, \sin^2 \theta} \right] \left[- \frac{\rho g / g_c \, b \, L \sin \theta}{2 \, \sigma} - \ell n \left(1 - \frac{\rho g / g_c \, b \, L \sin \theta}{2 \, \sigma} \right) \right]$$

Configuration: Plate/screen-screen/plate

Angle: Horizontal

Table 2-12. Theoretical Wicking Time Equations (Continued)

Equation:

$$\Delta t = \frac{A_F}{A_F - A_S} \quad \frac{3 \mu L^2}{\sigma b \, g_c}$$

Configuration: Screen/plate-plate/screen

Angle: Nonhorizontal

Equation:

$$\Delta t = \frac{A_F}{A_F - A_S} \left[\frac{24 \, \mu \sigma \, (a+2ne)^3}{a^3 (b+e)^3 \rho^2 g^2 / g_c \, \sin^2 \theta} \right] \left[- \frac{a(b+e) \, \rho g / g_c \, L \sin \theta}{2\sigma \, (a+2ne)} \right.$$

$$\left. - \ell n \left(1 - \frac{a(b+e) \, \rho g / g_c \, L \sin \theta}{2\sigma \, (a+2ne)} \right) \right]$$

Configuration: Screen/plate-plate/screen

Angle: Horizontal

Equation:

$$\Delta t = \frac{A_F}{A_F - A_S} \left[\frac{3 \mu L^2 (a+2ne)}{(b+e) \, \sigma \, g_c \, a} \right]$$

Configuration: Plate/screen-plate/screen

Angle: Nonhorizontal

Equation:

$$\Delta t = \frac{A_F}{A_F - A_S} \left[\frac{192 \, \mu \sigma \, (a+ne)^3}{a^3 (2b+e)^3 \rho^2 g^2 / g_c \, \sin^2 \theta} \right] \left[- \frac{\rho g / g_c \, (2b+e) \, a \, L \sin \theta}{4\sigma \, (a+ne)} \right.$$

$$\left. - \ell n \left(1 - \frac{\rho g / g_c \, (2b+e) \, a \, L \sin \theta}{4\sigma \, (a+ne)} \right) \right]$$

Configuration: Plate/screen-plate/screen

Angle: Horizontal

Equation:

$$\Delta t = \frac{A_F}{A_F - A_S} \left[\frac{6 \, \mu L^2 (a+ne)}{\sigma \, a \, (2b+e) \, g_c} \right]$$

2-33

Table 2-12. Theoretical Wicking Time Equations (Continued)

Configuration: Pleated screen

Angle: Nonhorizontal

Equation:

$$\Delta t = \left[\frac{A_F}{A_F - A_S}\right] \frac{2C\mu\sigma(2t + 0.571p)^3}{(pt)^3 \rho^2 g^2/g_c \sin^2\theta} \left[-\frac{\rho g/g_c (pt) L \sin\theta}{2\sigma(2t + 0.571p)} - \ell n\left(1 - \frac{\rho g/g_c (pt) L \sin\theta}{2\sigma(2t + 0.571p)}\right)\right]$$

Configuration: Pleated Screen

Angle: Horizontal

Equation:

$$\Delta t = \left[\frac{A_F}{A_F - A_S}\right] \frac{C\mu L^2 (2t + 0.571p)}{4\sigma(tp) g_c}$$

where

A_F is the wick cross sectional area in the direction of flow

A_S is the screen open cross sectional area in the direction of flow

μ is the liquid viscosity

σ is the liquid surface tension

ρ is the liquid density

b is the spacing between wicking barriers

g is the gravitational acceleration

g_c is a dimensional constant

θ is the angle between the wicking path and the horizontal

a is the width of the wick

n is the number of holes per unit width

e is the perforated plate thickness

C is a constant used to determine the friction factor (17.3 for the pleated screen tested)

t is the depth of pleat

p is the pleat pitch

2-34

Plots were made using the equations of Table 2-12 and the test variables for each of the wicks tested. An example of one of these plots is shown in Figure 2-12 for pleated screen. Figure 2-12 also shows the test data obtained for the configuration.

Figure 2-13 shows the improvement in horizontal wicking obtained using plate/screen-screen/plate wicks compared to plate/screen and to screen alone. Screen/plate gives better wicking than screen alone, because spot welding of the screen to the plate was done on only a few dozen lands on the perforated plate. This leaves a path between the screen and plate where they are not in intimate contact.

Initially, a least squares analysis of all the data was attempted but this proved to be too complicated because of the complex form of the nonhorizontal wicking equations. (A least squares analysis of L on Δt or vice versa requires formulation of the equation believed to fit the data and then solving a set of simultaneous equations derived by taking the partial derivatives of the formulated equation with respect to each constant and setting each expression equal to zero.) A simpler approach was taken in determining correlation constants using the horizontal equations for each configuration.

Data obtained was fitted to several possible correlating equations. The equation that best fit the data was one of the form

$$\Delta P_\sigma = \Delta P_f + \Delta P_x \qquad\qquad (2\text{-}6)$$

where

ΔP_σ is the surface tension driving pressure

ΔP_f is the frictional pressure loss

ΔP_x is the correction term

$$\Delta P_f = \frac{KL^2}{\Delta t}$$

where

K is a constant determined analytically for each configuration

L is the distance from the liquid pool to the wicking front

Δt is the time from initiation of wicking

Equation 2-6 was evaluated using measured geometry to evaluate ΔP_σ and measured values of L and Δt, over the entire range of L and Δt.

Values of ΔP_x obtained for each configuration are given in Table 2-13. Note the close agreement between the ΔP_x terms found for the 50×250 and 200×1400 screens. Graphs showing
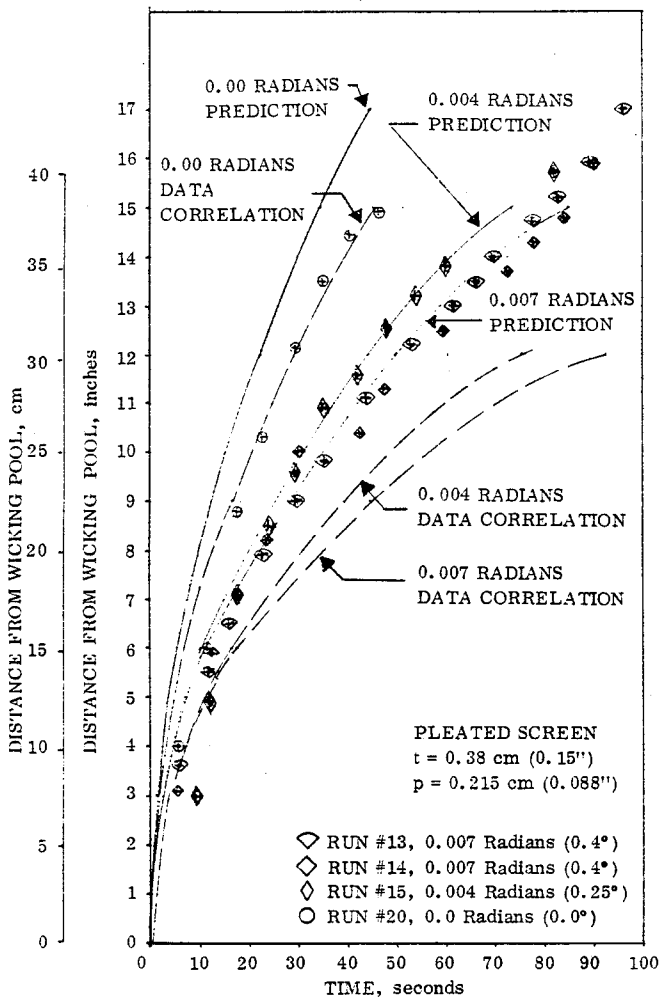
Figure 2-12.   Pleated Screen Wicking
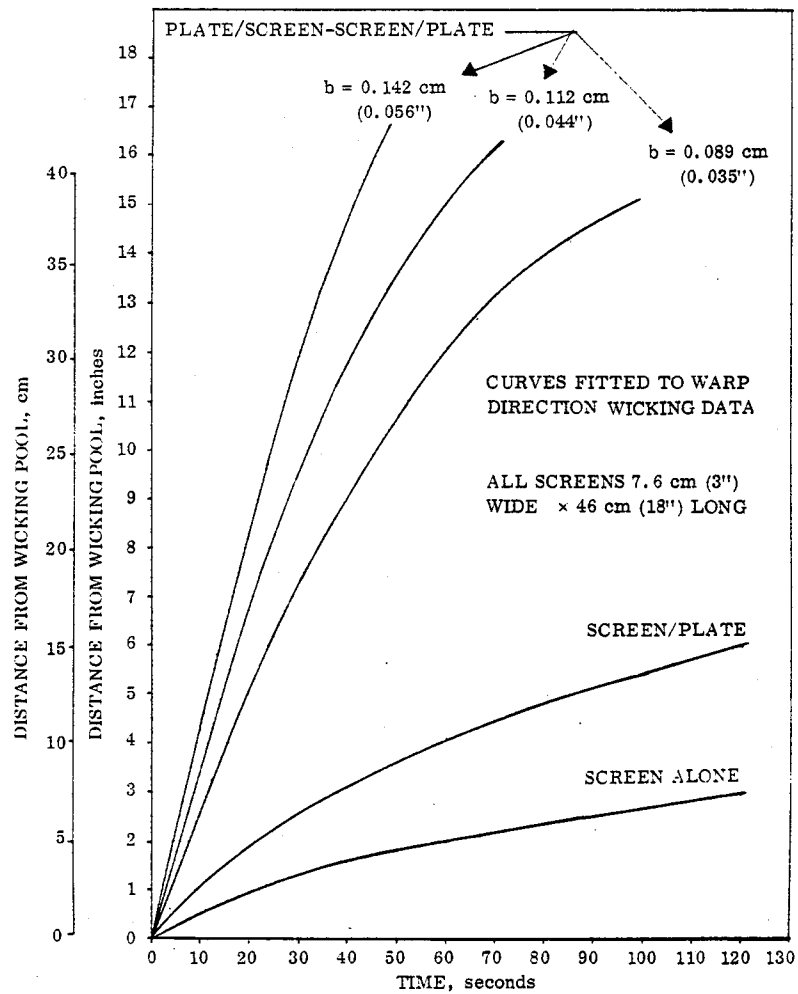
Figure 2-13.   Increased Wicking Capability for Plate/Screen-
Screen/Plate and Screen/Plate Configuration

Table 2-13. Wicking Correction Factors

Configuration	Screen	Spacing		ΔP_σ		ΔP_x		$\Delta P_{x_{mean}}$	
		cm	in.	N/m^2	psf	N/m^2	psf	N/m^2	psf
Plate/screen-screen/plate	50 × 250	.086	.034	51.7	1.08	15.8	.329	18.8	.393
		.113	.0445	39.5	.825	21.1	.44	18.8	.393
		.142	.056	31.4	.656	19.6	.41	18.8	.393
Screen/plate-plate/screen	50 × 250	.051	.02	43.8	.914	24.4	.509	26.4	.551
		.065	.0255	38.8	.811	26.8	.56	26.4	.551
		.086	.034	33.0	.69	26.3	.55	26.4	.551
		.086	.034	33.0	.69	26.8	.56	26.4	.551
		.086	.034	33.0	.69	28.0	.585	26.4	.551
Plate/screen-plate/screen	50 × 250	.065	.0255	25.4	.53	5.3	.11	8.8	.183
		.086	.034	20.6	.43	12.3	.258	8.8	.183
		.113	.0445	16.8	.35	8.7	.181	8.8	.183
Pleated screen	50 × 250	p = .224 t = .381	.088 .15	46.4	.97	16.3	.34	16.3	.34
Plate/screen-screen/plate	200 × 1400	.113	.0445	39.5	.825	18.4	.384	19.0	.397
		.142	.056	31.4	.656	19.6	.41	19.0	.397

pretest wicking correlations for several configurations are shown in Figure 2-14, 2-15, and 2-16 along with test data and post test correlation equations. ΔP_x mean is used for all correlations for each configuration. Ethanol properties (at room temperature) used to determine wicking predictions and correlations are given in Table 2-14.

2.3.2 CENTAUR D-1S PASSIVE COOLING ANALYSIS

The results of the wicking tests and data correlation, as summarized in Table 2-13, were used to analyze the required spacing and heat interception capability of each of the four wicking barriers for both the LO_2 and LH_2 D-1S start baskets. The wicking Equation 2-5 on pg 2-8 was modified to include the ΔP_x term and the screen flow area correction term, A_C. The ΔP_x correction term was interpreted both as an entrance loss term independent of gravity and as a head loss term directly dependent on gravity. For the low gravity environment experienced by the LO_2 and LH_2 start baskets, the more severe treatment is the entrance loss approach (ΔP_x is a constant). Both approaches were used in modifying Equation 2-5 and comparing the computed heat interception capability to the

Table 2-14. Ethanol Fluid Wicking Properties

Density	0.789 gm/cm^3	(49.2 lb/ft ^{3})
Surface Tension	22.3 dynes/cm	(1.53 × 10^{-3} lb$_f$/ft)
Viscosity	0.012 gm/(cm/sec)	(8 × 10^{-4} lb$_m$/ft sec)
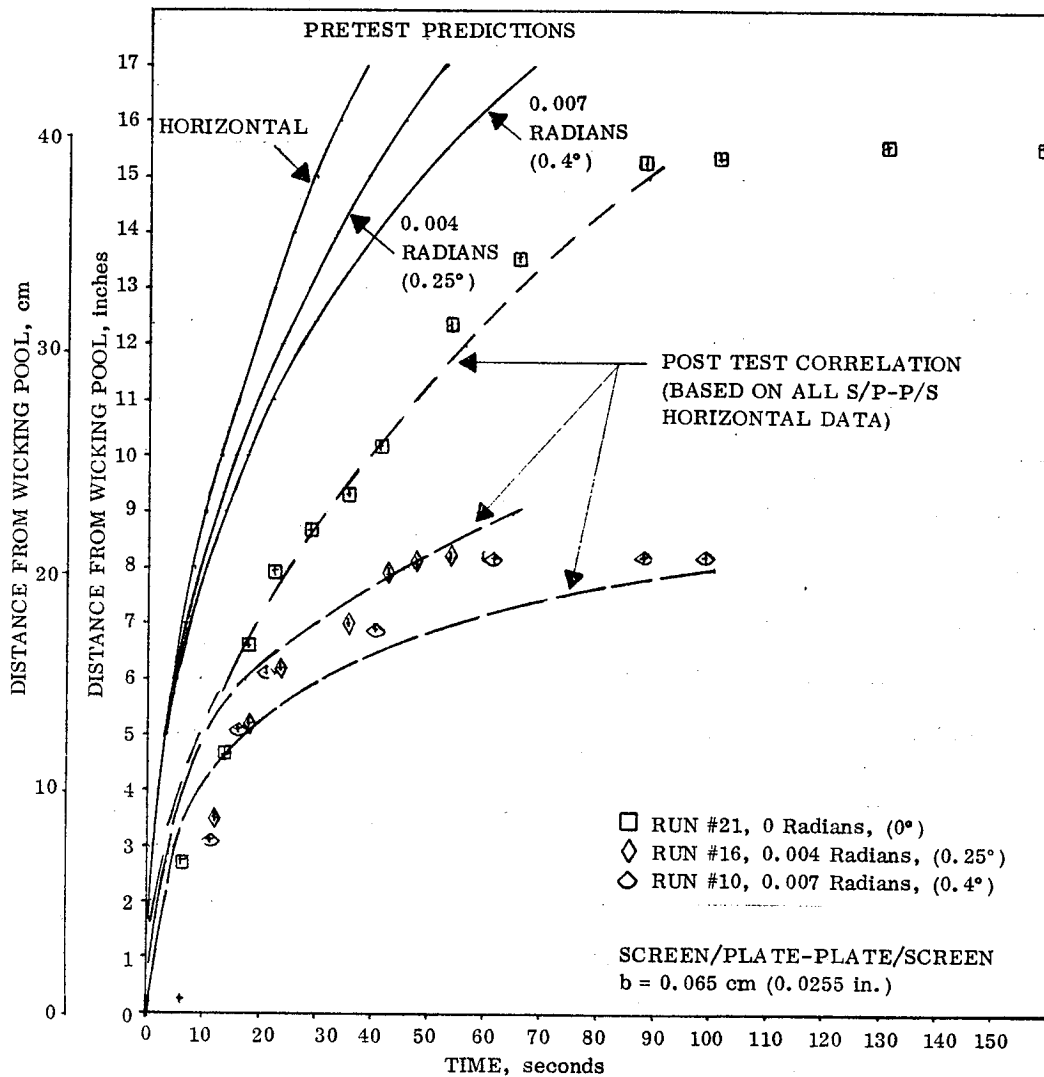
Figure 2-14. Typical Screen/Plate–Plate–Plate/Screen Data Correlation
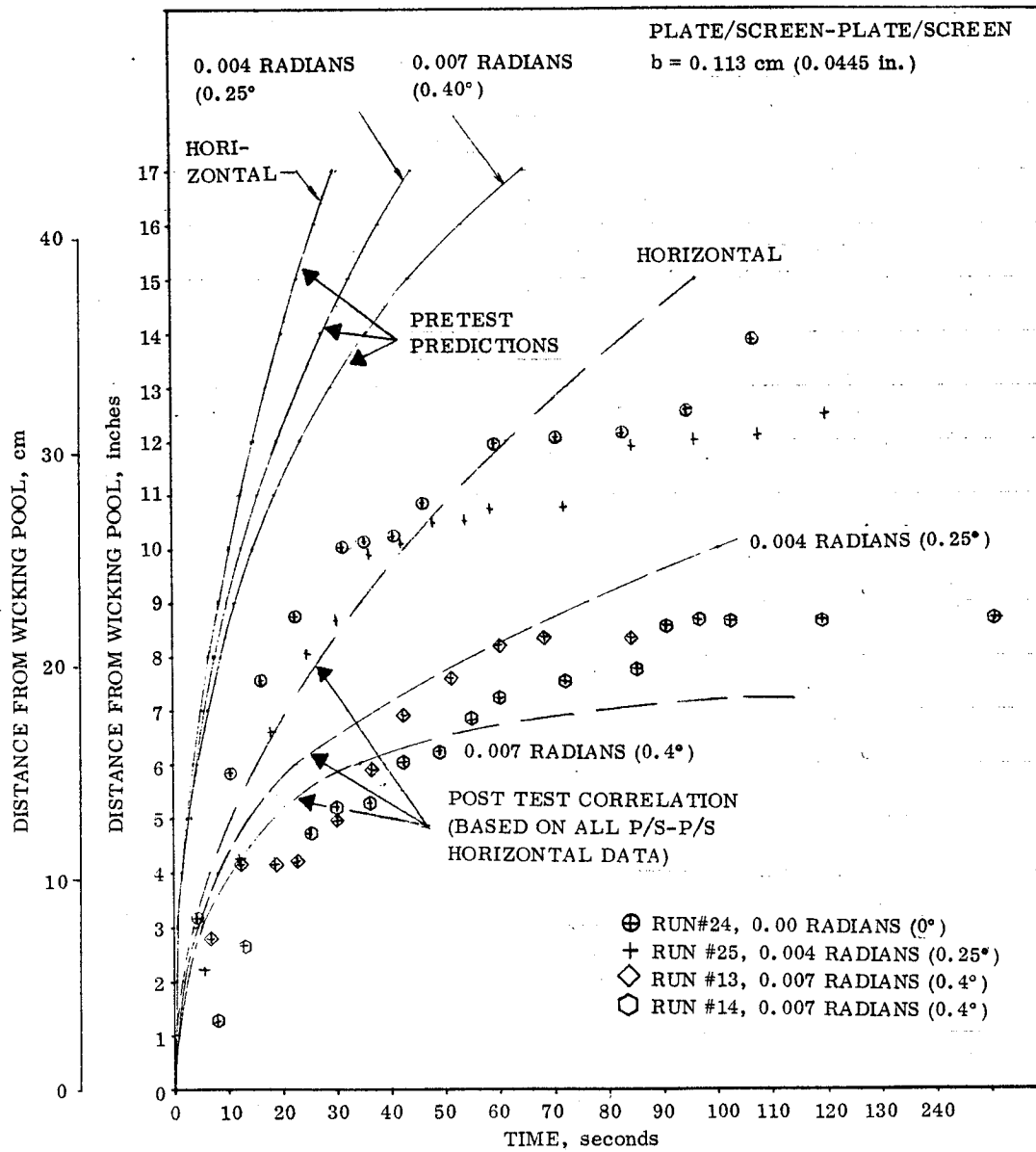
Figure 2-15. Typical Plate/Screen-Plate/Screen Data
Correlation
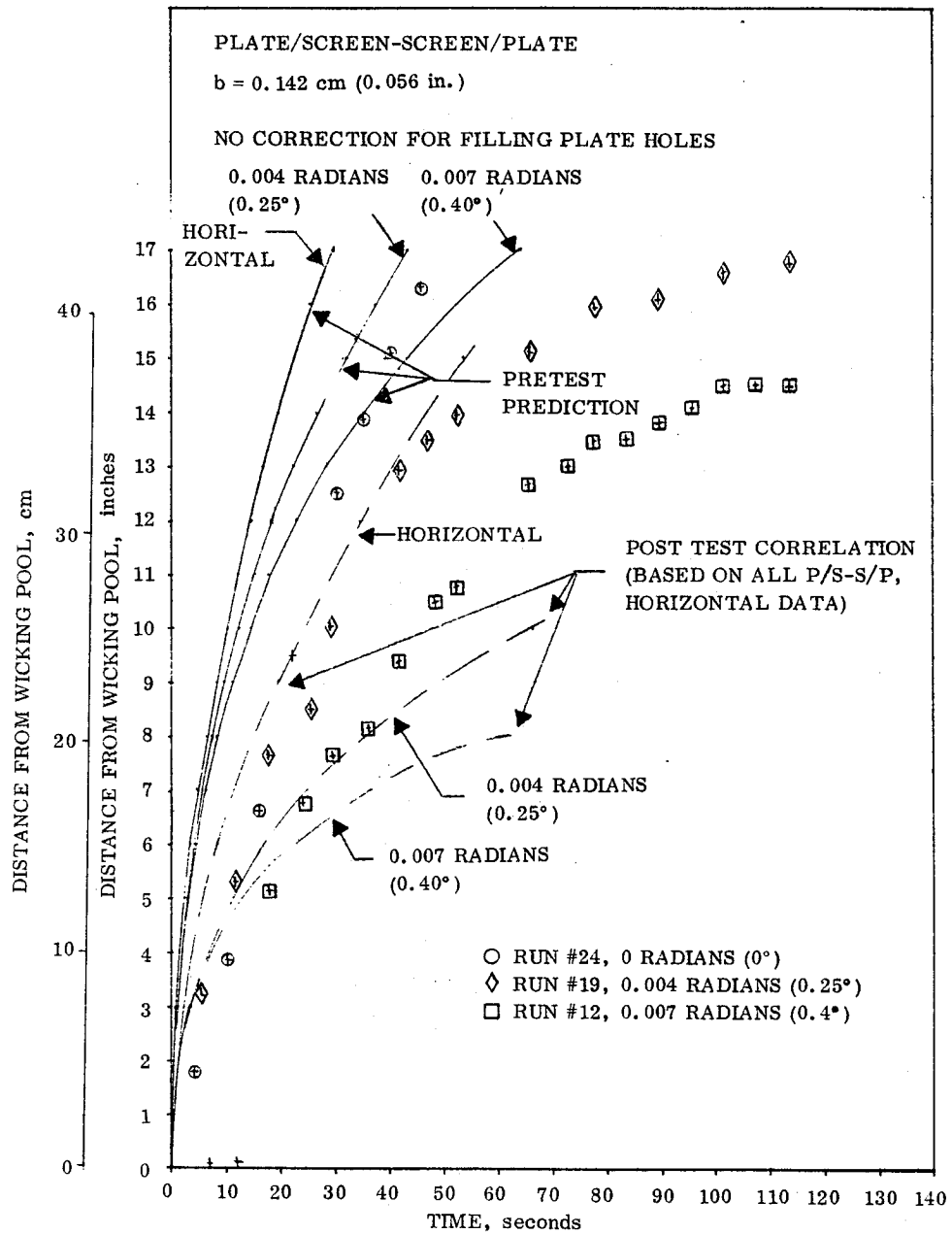
Figure 2-16. Typical Plate/Screen-Screen/Plate Data Correlation

required heat interception capability, in a manner identical to that shown in Table 2-6. Optimum minimum and maximum spacing that would best satisfy the worst case combination of heat transfer, gravity level and wicking distance from the liquid pool were computed and are shown in Table 2-15. Only one configuration is shown for the pleated screen. This is the smallest combination of pitch and depth of pleat that could be manufactured. The minimum safety factor for each configuration, as shown in Table 2-15 was determined by dividing the heat interception capability of each wick by the heat flux requirement for each condition in Table 2-6. The minimum safety factor is the smallest value of the ratio between the heat interception capability and the incident heat flux. For a configuration to be minimally acceptable this minimum safety factor must be greater than one for the optimum spacing and allow a reasonable tolerance for manufacturing error between the minimum and maximum spacing. Only plate/screen-screen/plate and plate/screen-plate/screen configurations were able to satisfy all heat interception situations for both interpretations of ΔP_x. Table 2-15 is based on worst case ΔP_x, i.e., ΔP_x does not vary with gravity. Table 2-16 gives similar information, interpreting ΔP_x to be dependent on gravity. The two configurations shown to be thermally acceptable in Table 2-15 are also acceptable from a manufacturing standpoint. Using these two configurations some additional start basket weight calculations were made.

2.3.3 CANDIDATE CONFIGURATION WEIGHTS. As indicated in the previous section, the pleated screen could not intercept the heat input to the screen with the currently manufacturable minimum pitch and pleat depth. The plate/screen-screen/plate and plate/screen-plate/screen configurations could satisfactorily intercept all heat fluxes under both correction term interpretations. The screen/plate-plate/screen could only intercept heat successfully using the less conservative gravity dependent correction term. Weight estimates were made for these three screen/plate combinations (Table 2-17) using countersunk screws to prevent dripping from the outer surfaces of the

Table 2-15. Wick Spacing Using ΔP_x Independent of Gravity

Fluid	Config.	Geometry Variable(s)	Spacing, cm (in.)					
			* Minimum Spacing	Min. Safety Factor	Optimum Spacing	Min. Safety Factor	** Maximum Spacing	Min. Safety Factor
LH$_2$	P/S-S/P	b	.041 (.016)	1	.053 (.021)	1.12	.064 (.015)	1
LH$_2$	P/S-P/S	b	-	-	.025 (.0099)	4	.046 (.018)	1
LH$_2$	S/P-P/S	b	-	-	Negative	-	-	-
LH$_2$	Pleated	t, p	-	-	.381 (.15) .022 (.088)	-	-	-
LO$_2$	P/S-S/P	b	.041 (.016)	1	.053 (.021)	15.8	.064 (.025)	1
LO$_2$	P/S-P/S	b	-	-	.048 (.018)	168	.079 (.031)	1
LO$_2$	S/P-P/S	b	-	-	Negative	-	-	-
LO$_2$	Pleated	t, p	-	-	.381 (.15) .022 (.088)	-	-	-

* Minimum spacing to yield safety factor of at least one for all cases.
** Maximum spacing to yield safety factor of at least one for all cases.

Table 2-16. Wick Spacing Using ΔP_x Dependent on Gravity

			Spacing, cm (in.)					
Fluid	Config.	Geometry Variable(s)	* Minimum Spacing	Min. Safety Factor	Optimum Spacing	Min. Safety Factor	** Maximum Spacing	Min. Safety Factor
LH_2	P/S-S/P	b	.041 (.016)	1	.066 (.026)	3.8	.081 (.032)	1
LH_2	P/S-P/S	b	–	–	.046 (.018)	6.6	.086 (.034)	1
LH_2	S/P-P/S	b	–	–	.020 (.0077)	8.6	.036 (.014)	1
LH_2	Pleated	t, p	–	–	.381 (.15) .223 (.088)	–	–	–
LO_2	P/S-S/P	b	.041 (.016)	1	.16 (.061)	708	.22 (.088)	1
LO_2	P/S-P/S	b	–	–	.132 (.052)	952	.20 (.080)	1
LO_2	S/P-P/S	b	–	–	.127 (.05)	1380	.19 (.076)	1
LO_2	Pleated	t, p	–	–	.381 (.15) .223 (.088)	270	–	–

* Minimum spacing to yield safety factor of at least one for all cases.
** Maximum spacing to yield safety factor of at least one for all cases.

Table 2-17. Bolted Passively Cooled Start Basket Weight Penalties
(Aluminum Screen and Plate)

	LO_2 Start Basket Weight, kg (lb_m)	LH_2 Start Basket Weight, kg (lb_m)	LO_2 + LH_2 Weight kg (lb_m)
Plate/Screen – Screen/Plate	17.3 (38.1)	72.8 (160.4)	90.2 (198.5)
Plate/Screen – Plate/Screen	17.3 (38.1)	72.8 (160.4)	90.2 (198.5)
Screen/Plate – Plate/Screen	17.3 (38.1)	72.8 (160.4)	90.2 (198.5)

LO_2 and LH_2 baskets. Using aluminum rivets instead of screws, nuts and washers will yield essentially identical weights to those estimated for all welded construction given in Table 2-8. As shown in Table 2-8, active cooling system hardware weight totals 148 kg (327.5 lb_m). In addition, as shown in Table 6-3 of Reference 2-1, a payload penalty of 189.9 kg (418 lb_m) results from dumping vent fluid overboard for actively cooled capillary devices for the five burn mission.

Some design work was done in identifying conceptual designs for wicking around the corners of the start basket. The two principal configurations identified, shown in Figures 2-17 and 2-18, are representative of a dripless configuration and a simpler approach that might induce some dripping. Manufacturing studies were initiated to determine if the dripless configuration could be successfully joined. Some preliminary soldering work indicates that the corner joints can successfully be made, permitting fabrication of the dripless configuration if a fine wire is inserted into the corner joint to promote sealing and soluble stopoff material is used to inhibit solder from wicking into the screens.
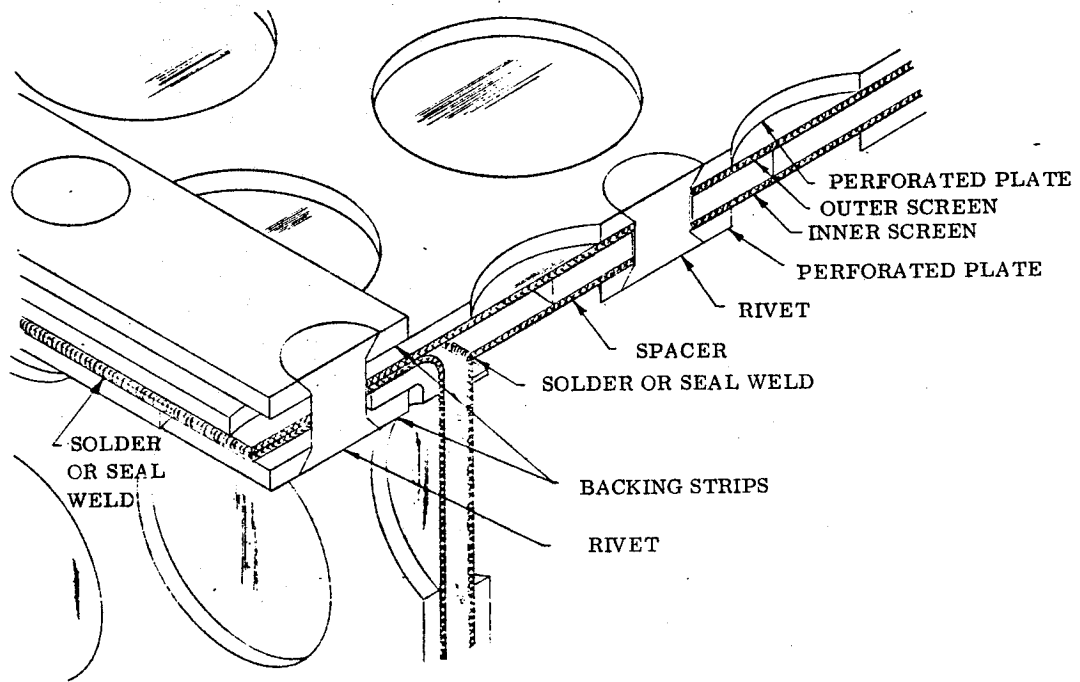
Figure 2-17. Typical Simple Corner Joint Construction Layout
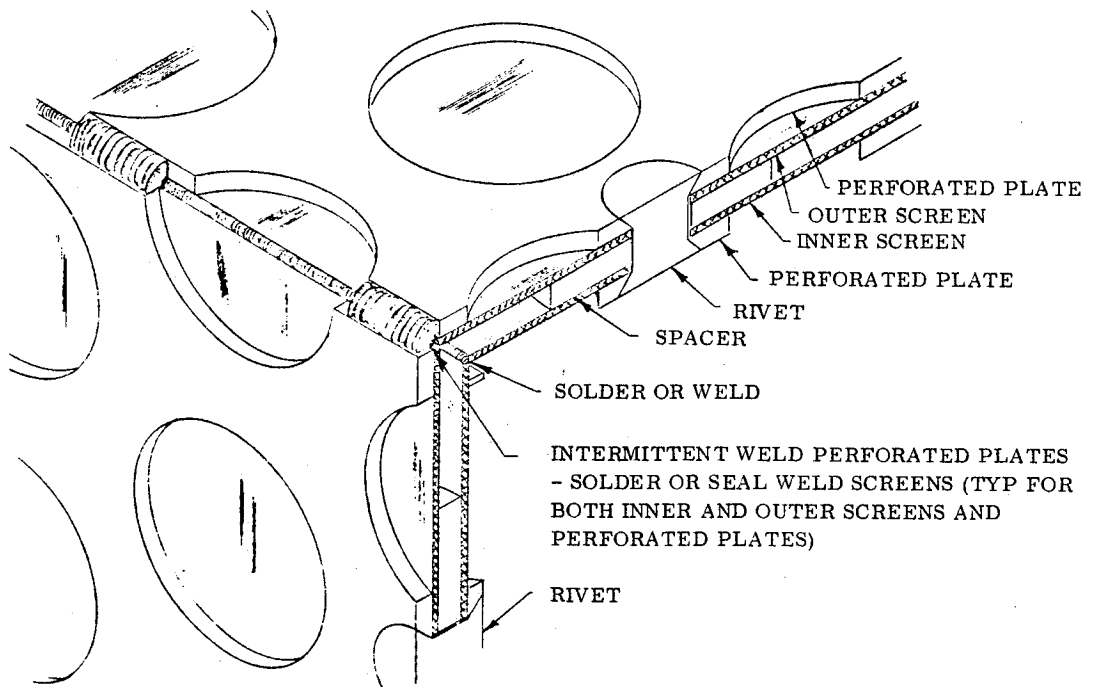
Figure 2-18. Typical Dripless Corner Joint Construction Layout

2-43

3
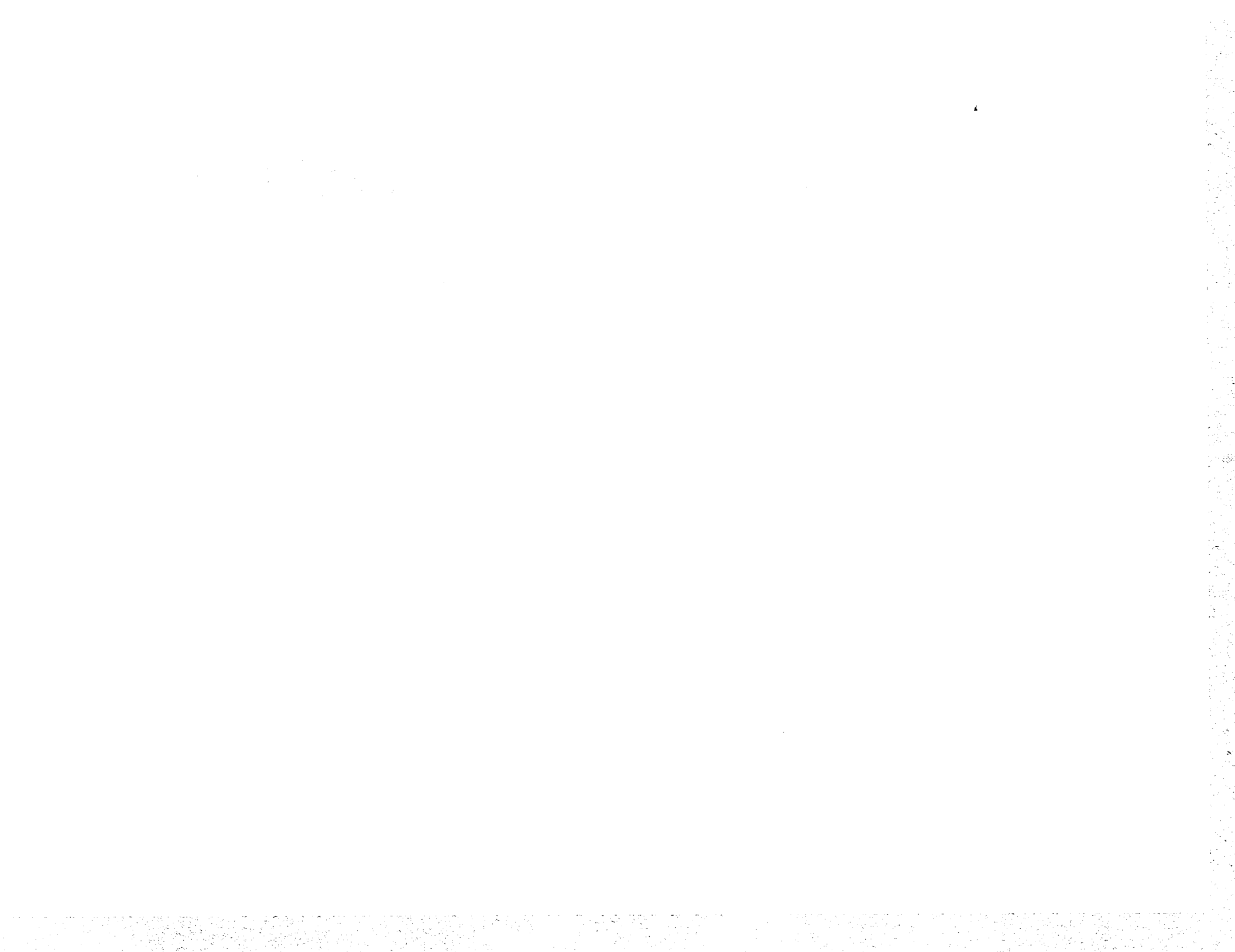
THERMAL SUBCOOLER COMPARATIVE ANALYSIS

The objective of the thermal subcooler comparative analysis was to relate system weight to the NPSP requirement of the Centaur main engines for both liquid hydrogen and liquid oxygen. The analysis was to include both the start sequence and the steady firing of the main engines. NPSP levels to be investigated were to range from near zero to the current baseline vehicle requirements. The following three system concepts were to be studied:

1. Current baseline vehicle employing propulsive settling, warm gas pressurization and boost pumps.

2. A system of thermal subcoolers with propulsive settling.

3. A system of thermal subcoolers, passively cooled screen acquisition devices and continuously cooled propellant ducts.

3.1 STUDY GROUNDRULES

The following section discusses the groundrules used in the study and includes engine system selection, engine NPSP requirements, propellant line pressure losses, engine inlet pressure requirements and tank pressure profiles to meet the engine inlet pressure requirements.

3.1.1 <u>ENGINES AND PROPELLANT SUPPLY LINES</u>. The subcooler study objective was to compare system concepts having net positive suction pressure (NPSP) levels at the main engine pump inlets ranging from near zero NPSP to the current baseline vehicle requirements. Three realistic engine configurations having NPSP levels covering the desired range were selected for comparison. The first is the baseline D-1S engine, the RL10A-3-3 engine. The other two are Pratt and Whitney engines with lower NPSP requirements, the RL10A-3-3A and RL10 Category I engines. The former was built and tested for use in a pressure-fed Centaur without boost pumps. The latter is the same engine but with reduced chilldown, NPSP and inlet pressure requirements.

The RL10A-3-3 engine was used with a pressurization system and boost pumps in the current baseline system (System 1). For Systems 2 and 3, no boost pumps or main tank pressurization systems were used. Systems 2 and 3 were sized for the RL10A-3-3, the RL10A-3-3A and the RL10 Category I engines in order to obtain parameteric information as a function of engine NPSP.

Propellant supply lines for the engines without boost pumps are larger in diameter and thus have lower pressure losses than those for the baseline RL10A-3-3 engine. For this study the LH_2 line was assumed to have the same dimensions as the duct tested with the RL10A-3-3A engine in Reference 3-1; i.e., a 12.7 cm (5.0 in.) dia. common section with each leg having an 8.9 cm (3.5 in.) dia. The baseline LH_2 sump was replaced with a simplified tank outlet. The LO_2 line was assumed to be similar in shape to the baseline duct but with a larger diameter matching the LH_2 duct. The LO_2 sump was taken to be that shown in Reference 3-2 (shallow spherical segment) but with a single outlet at the bottom instead of two. The lines are all insulated with three layers of radiation shielding over a layer of foam.

3.1.2 NPSP REQUIREMENTS. Engine NPSP requirements are shown in Table 3-1. NPSP requirements for the RL10A-3-3 engine are taken from Reference 3-3. NPSP requirements for the RL10A-3-3A engine are taken from Reference 3-4 with an adjustment in LO_2 steady state NPSP to account for a possible mixture ratio shift to 5.7:1. NPSP requirements for the RL10 Category I engine are taken from Reference 3-3 with increases in both LH_2 and LO_2 steady state NPSP to account for possible mixture ratio shifts to 5.5:1 and 6.5:1 respectively. These adjustments account for worst case NPSP requirements for all of the three engines.

Additional NPSP must be provided by the subcoolers to make up for propellant supply line pressure losses during both the start transient and steady state operation. Line pressure losses used in this study are taken from static firing measured data and are shown in Table 3-1. During the start transient, both acceleration and friction losses occur but at different times. The acceleration loss was used since it is larger.

3.1.3 ENGINE INLET PRESSURE REQUIREMENTS AND TANK PRESSURE PROFILES. Each of the three engines has a minimum inlet pressure requirement during the start transient and a lower pressure requirement during steady state operation (see Table 3-2). To determine required corresponding tank pressures, propellant supply line pressure losses and estimated subcooler losses during start and steady state operation were added to the engine inlet requirements. The results are shown in Table 3-2. Tank pressure histories were then generated for the 1-burn, 2-burn and 5-burn baseline missions, assuming minimum space heating conditions (Figures 3-1 through 3-3). The pressure history levels are high enough so that both the start and steady state tank pressure requirements of Table 3-2 are met for all burns. From these pressure histories the minimum tank pressures during engine operation were selected as the subcooler design condition for each engine and are shown in Table 3-3. For each engine, the design condition occurred at the end of the burn in the 1-burn mission pressure profile shown in Figure 3-1. Maximum tank pressures determined the tank skin weight penalty for each mission and engine are shown in Figure 3-3 for the five burn mission. Tank pressures generated for the two burn mission are shown in Figure 3-2.

Table 3-1. Engine System Inlet NPSP Requirements, kN/m^2 (psi)

	Start Transient		Steady State	
	Engine Req.	Line Loss	Engine Req.	Line Loss
1. RL10A-3-3				
LH$_2$	28 (4.0)	13 (1.9)	28 (4.0)	10 (1.5)
LO$_2$	55 (8.0)	37 (5.4)	55 (8.0)	17 (2.5)
2. RL10A-3-3A				
LH$_2$	14 (2.0)	13 (1.9)	14 (2.0)	4 (0.6)
LO$_2$	28 (4.0)	37 (5.4)	34 (4.95)	6 (0.8)
3. RL10 Category I				
LH$_2$	2 (0.3)	13 (1.9)	4 (0.55)	4 (0.6)
LO$_2$	23 (3.4)	37 (5.4)	30 (4.35)	6 (0.8)

3.2 START SEQUENCE

Main engine start sequences for the system concepts of (1) thermal subcoolers with propulsive settling, and (2) thermal subcoolers with screen acquisition and wet propellant ducts will differ from the baseline D-1S start sequence.

Table 3-2. Required Engine Inlet Pressures and Corresponding Tank
Pressures, kN/m^2 (psi)

	Start Transient		Steady State	
	Engine Inlet Requirement	Tank Pressure	Engine Inlet Requirement	Tank Pressure
1. RL10A-3-3				
LH_2	207 (30)	257 (37.3)	121 (17.5)	154 (22.4)
LO_2	310 (45)	373 (54.2)	165 (24)	209 (30.3)
2. RL10A-3-3A				
LH_2	193 (28)	246 (35.7)	121 (17.5)	147 (21.4)
LO_2	262 (38)	325 (47.2)	165 (24)	197 (28.6)
3. RL10 Category I				
LH_2	152 (22)	196 (28.5)	76 (11)	103 (14.9)
LO_2	152 (22)	215 (31.2)	103 (15)	135 (19.6)

Table 3-3. Minimum Tank Operating Pressures Used as Subcooler Design
Condition, kN/m^2 (psi)

	RL10A-3-3	RL10A-3-3A	Category I
LH_2	154 (22.4)	147 (21.4)	118 (17.1)
LO_2	299 (43.4)	260 (37.8)	172 (25.0)
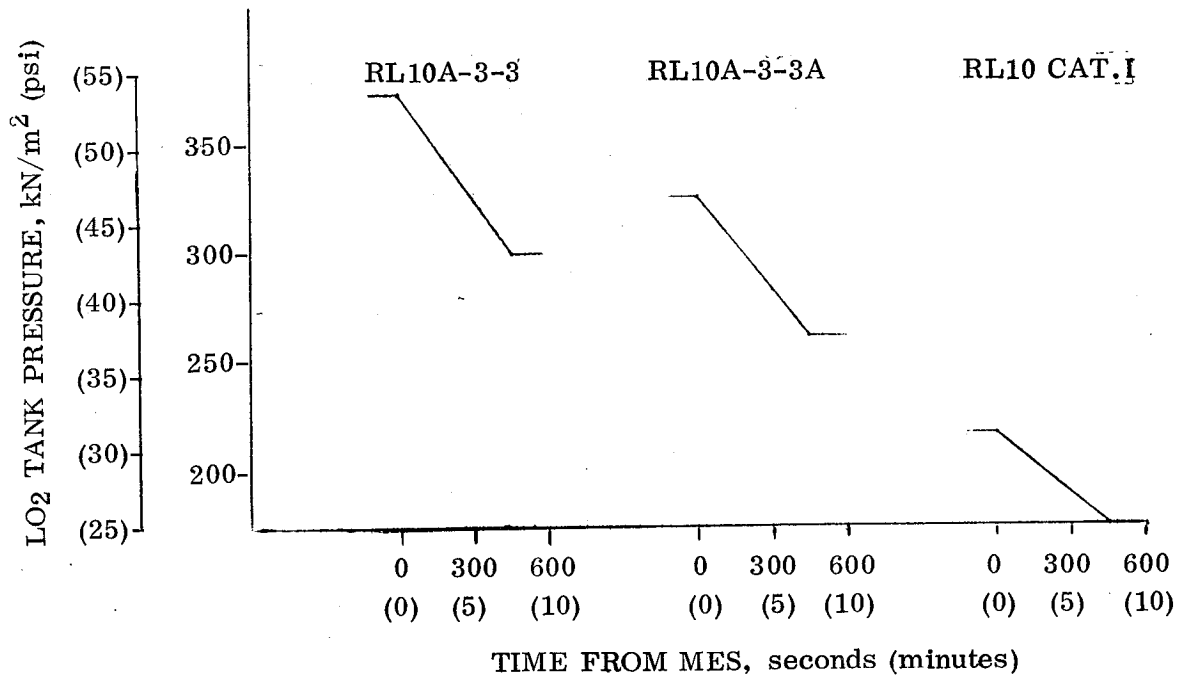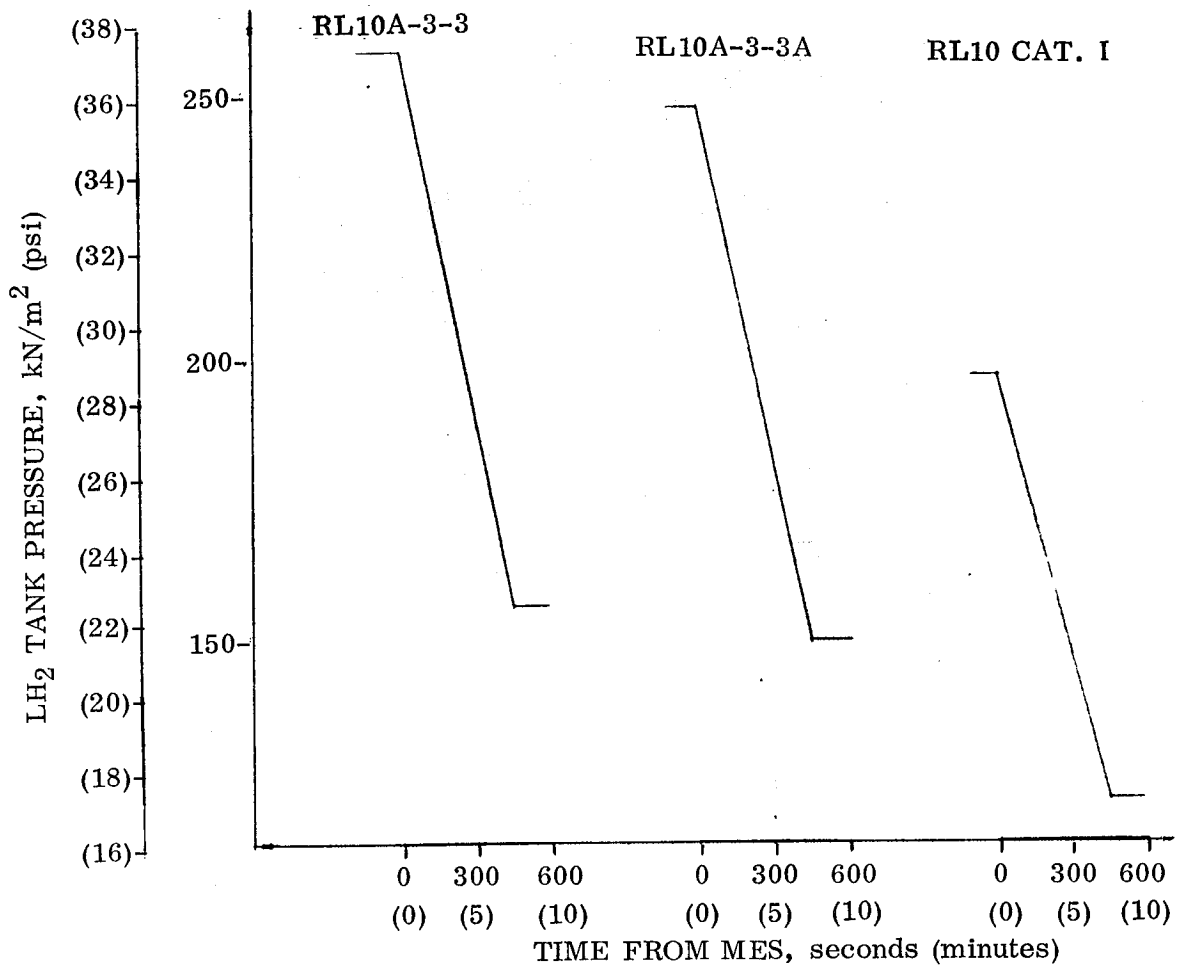
Figure 3-1. Planetary Mission (One-Burn) Pressure History
for Minimum Space Heating Conditions

3-5
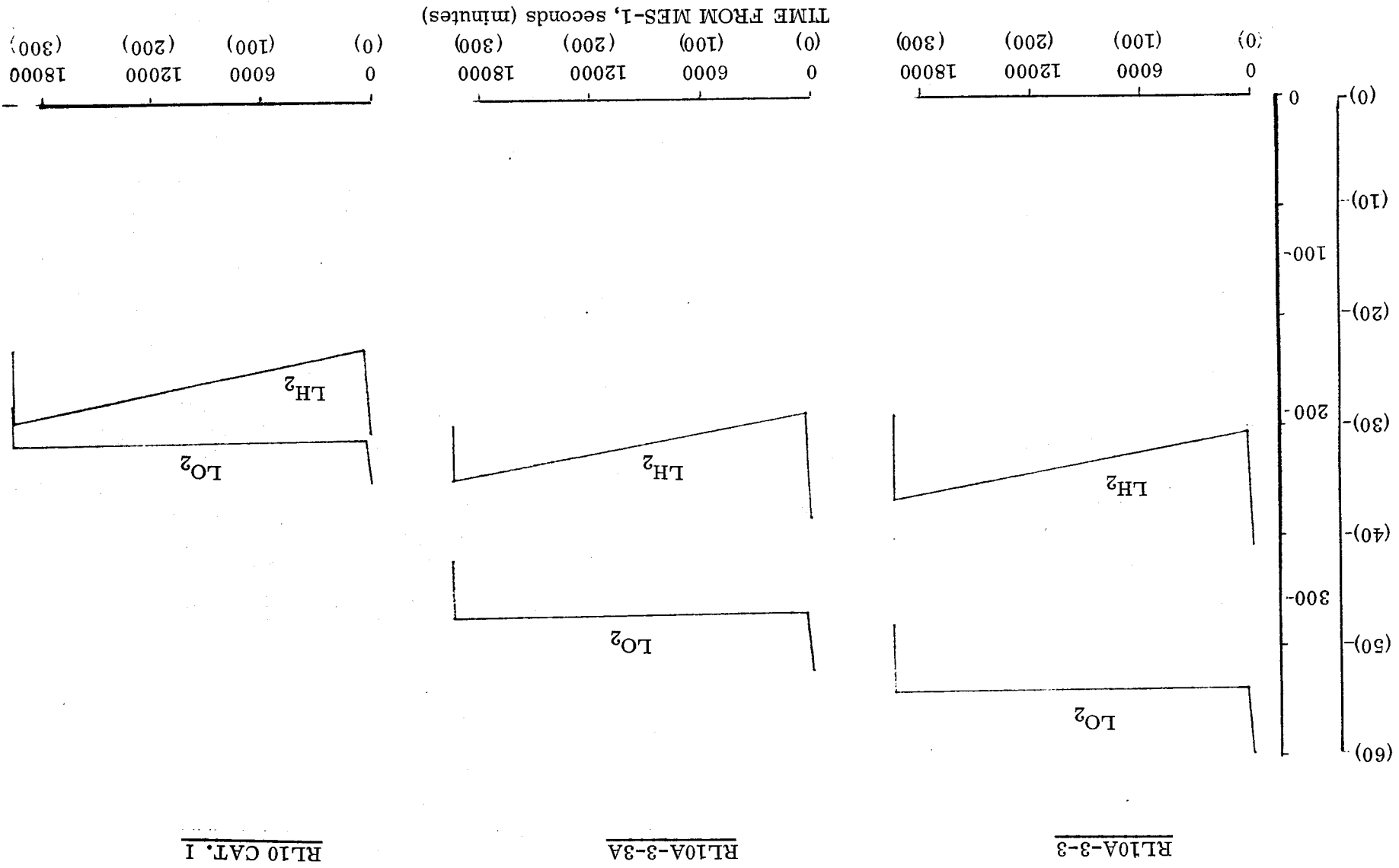
Figure 3-2. Synchronous Equatorial Mission (Two Burn) Pressure History for Minimum Space
Heating Conditions

3-6
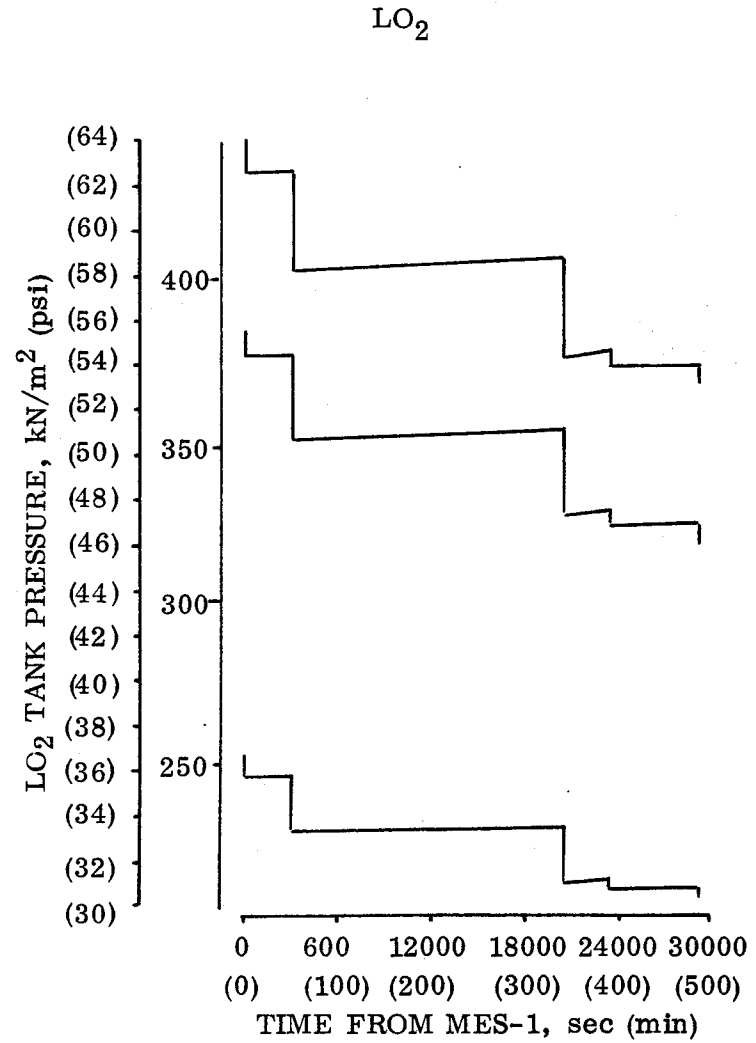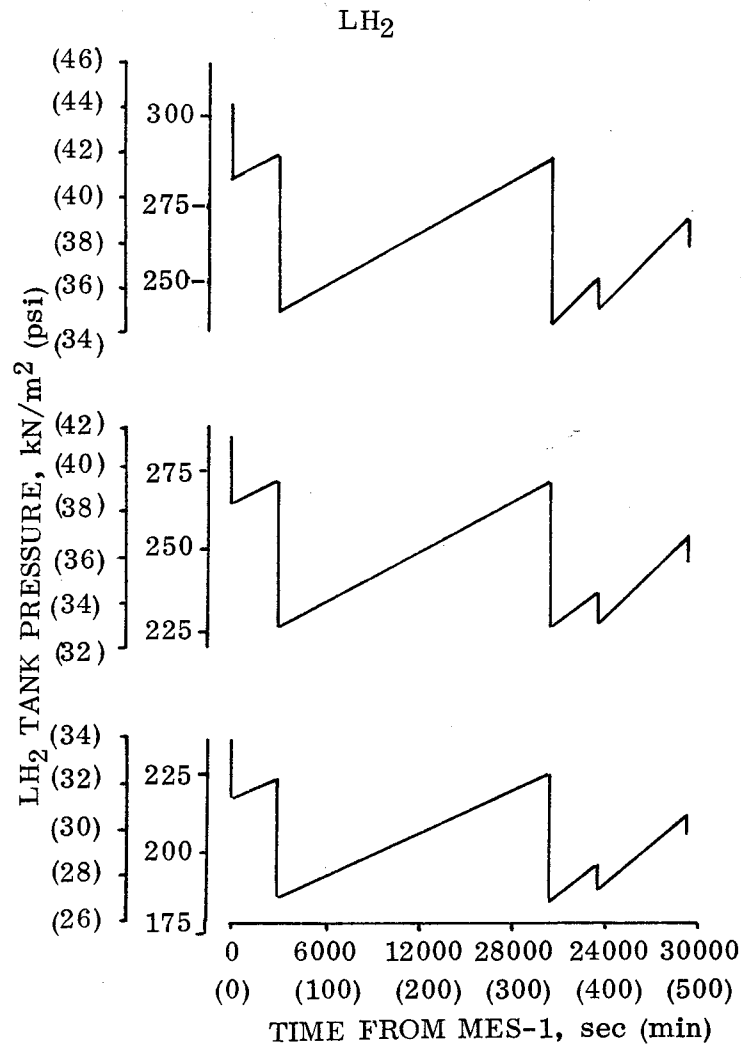
Figure 3-3. Low Earth Orbit Mission (5-Burn) Propellant Tank Pressure History for Minimum Space Heating Conditions

3.2.1 <u>BASELINE D-1S.</u> In the baseline D-1S start sequence, main tank propellants are first settled by operating small settling thrusters for a length of time which is dependent on main tank propellant levels. After propellant settling, tanks are pressurized, and the boost pumps are brought up to idle speed to condition the supply ducts by circulating propellants through the ducts and back to the tanks via a recirculation line. Engine shutoff valves are then opened to permit the propellants (under boost pump idle pressure) to pass through and condition the engine turbopumps.

Engine cooldown times and propellant consumption are a complex function of engine temperature, inlet pressure, engine NPSP and flow control valve area. Current plans are to shield the engine turbopumps with three-layer perforated radiation shielding (similar to that now used on the Centaur D-1T propellant supply ducts) and to use split chilldown to condition the turbopumps, both of which reduce chilldown propellants. Engine cooldown propellant consumption for shielded D-1S engines having split chilldown is taken from Reference 3-5. For the first start with the engines at 289°K (520°R), 3 kg (6 lb) of LO_2 and 13 kg (28 lb) of LH_2 are required (for both engines). For the other starts with the engines at a maximum of 142°K (256°R), 0.5 kg (1 lb) of LO_2 and 4 kg (9 lb) of LH_2 are required.

There is no propellant consumption penalty for baseline D-1S supply duct chilldown because the propellants are recirculated back into the tank. The initial duct conditioning vaporizes the propellants but they are recondensed by the main propellants upon re-entering the tanks.

3.2.2 THERMAL SUBCOOLERS WITH PROPULSIVE SETTLING. For the system concept of thermal subcoolers with propulsive settling, the lines and subcooler will be allowed to empty between burns. The start sequence is initiated by firing settling thrusters to settle main tank propellants. With propellant surrounding the subcooler, valves are opened permitting throttled flow through the subcooler cold side which chills down the subcooler. The engine inlet valve is then opened and propellant (under tank pressure) flows through the prechilled subcooler, through the propellant supply ducts and finally through the engine where it is vented overboard. Sufficient propellant is passed through the system prior to ignition to chill first the duct and then the engine.

Duct cooldown propellant requirements are a function of duct mass and temperature. Cooldown propellant consumption weights given in Reference 3-5 for the ducts used with the RL10A-3-3 engine,are shown in Table 3-4. Also shown in Table 3-4 are the corresponding propellant consumption weights for the larger diameter ducts used with the RL10A-3-3A and RL10 Category I engines.

Engine chilldown using only tank pressure requires a longer time period than chilldown under boost pump idle pressure. The engine interstage cooldown valve bleed area is set to achieve the desired flow rate. The most efficient propellant use occurs with very long chilldown times (over 100 seconds). However, since settling thrusters

Table 3-4. Propellant Supply Duct Cooldown Propellant Weights, kg (lb)

	RL10A-3-3 Ducts		RL10A-3-3A and RL10 Cat. I Ducts	
	LO_2	LH_2	LO_2	LH_2
First Start (Ducts at 500°R)	3.6 (8)	3.2 (7)	5.0 (11)	5.4 (12)
Other Starts (LO$_2$ Duct at 260°R LH$_2$ Duct at 240°R)	2.3 (5)	1.4 (3)	3.2 (7)	2.3 (5)

are firing during this time, thruster propellant consumption goes up with longer chilldown times. The sum of chilldown and thruster propellant used is nearly constant for chilldown times between 90 and 210 seconds (Reference 3-6, Figure 5.2.4-17.). For this study, the engine chilldown propellant consumption with flow under tank pressure only is assumed equal to that shown previously for the baseline D-1S; i.e., 16 kg (34 lb) for the first start and 4.5 kg (10 lb) for the other starts. Since all D-1S starts occur at orbital conditions, no payload penalty due to vehicle gravity loss occurs as a result of the longer chilldown times.

3.2.3 THERMAL SUBCOOLERS WITH SCREEN ACQUISITION AND WET FEEDLINES.
For the system concept of thermal subcoolers with screen acquisition and wet propellant ducts, both the subcooler and ducts remain full between burns. The start sequence is initiated by opening valves and flowing throttled propellant through the subcooler cold side. Next, the engine inlet valve is opened and propellants from the filled line and subcooler flow through and condition the engine turbopumps. The engine chilldown propellant requirement is assumed to be equal to that for the baseline D-1S.

3.2.3.1 Comparison of Engine Chilldown Requirement with Amount of Unsubcooled Propellant in Feedline and Subcooler.
The propellant in the line prior to each start is not subcooled and therefore cannot be used to start the engine. Likewise, because of the thermal inertia of the hot side propellant, the first propellant out of the subcooler is not yet adequately subcooled. An analysis was therefore performed to determine whether engine chilldown uses all the insufficiently subcooled propellant or if additional propellant must be consumed before properly subcooled liquid enters the engine (resulting in a weight penalty).

The weights of LH_2 required for turbopump chilldown (2 engines) are 13 kg (28 lb) for the first start and 4 kg (9 lb) for the other starts. The RL10A-3-3 engine ducts hold only 1.1 kg (2.5 lb) and the RL10A-3-3A and Category I engine ducts hold only 1.5 kg (3.4 lb) of LH_2. Therefore, all unsubcooled LH_2 in the lines is used before chilldown is complete.

The LH_2 passing through the subcooler hot side during engine chilldown was analyzed for transient cooldown from tank saturation temperature. The quantity of LH_2 that

leaves the subcooler before it is sufficiently subcooled to meet the engine start-up NPSP requirement was computed to be 0.5 kg (1 lb) for the Category I engine, 0.9 kg (2 lb) for the RL10A-3-3A engine, and 1.8 kg (4 lb) for the RL10A-3-3 engine. It is therefore seen that the LH_2 turbopump chilldown uses all the insufficiently subcooled LH_2 in the line and subcooler and that no further start sequence weight penalty is incurred.

The weights of LO_2 required for turbopump chilldown (2 engines) are 3 kg (6 lb) for the first start and 0.5 kg (1 lb) for the other starts. The RL10A-3-3 duct and sump hold 25 kg (56 lb) and the RL10A-3-3A and Category I engine duct and sump hold 27 kg (60 lb) of LO_2. The quantity of LO_2 leaving the subcooler before it is sufficiently sub-cooled was calculated to be 15 kg (32 lb) for the Category I engine, 16 kg (36 lb) for the RL10A-3-3A engine and 24 kg (52 lb) for the RL10A-3-3 engine. It is therefore seen that essentially all the unsubcooled LO_2 in the line plus the above quantities of LO_2 leaving the subcooler must be taken as a weight penalty for each start.

3.2.3.2 Thermal Analysis of Cooling Tubes to Keep Propellant Supply Ducts Filled.
To keep the propellant supply lines and subcooler filled between burns, the ducts and the tank skin adjacent to the subcoolers are wrapped with cooling coils through which flows throttled two-phase fluid. The method used to attach cooling tubes to duct or tank skin must provide good thermal contact. (Dip brazing is a primary candidate.) The cooling tubes must intercept heating through the duct and tank insulation and along the duct from the engine. Analysis was performed to determine the required tube spacing, required coolant flow rate and pressure drop in the cooling tubes.

The most severe heating environment occurs in the cargo bay prior to first burn. It is assumed that the liquid head will keep the lines full prior to launch and during powered boost. Cargo bay heating rates were taken from the D-1S thermal analysis in NAS3-16786, Reference 3-7, and are shown below.

	LO_2 w/m^2 (Btu/hr-ft^2)		LH_2 w/m^2 (Btu/hr-ft^2)	
Propellant Lines	140	(44.3)	67.5	(21.4)
Sump	492	(156)	—	
Tank Wall at Subcooler	198	(62.7)	7.73	(2.45)

The large difference between LO_2 and LH_2 tank wall heat flux is due to the many penetrations for equipment, struts, etc., on the LO_2 aft bulkhead.

Heating from the engines by duct wall conduction, gas conduction and radiation tunnelling was calculated using a maximum engine temperature of 216°K (388°R) (Reference 3-8) for both LO_2 and LH_2 ducts. Conical copper screens were assumed to be located in the ducts 4 inches upstream of the engine inlet flange to maintain a liquid interface which will not vaporize from engine heating. Screen meshes of 50 × 250 for the LO_2

duct and 200 × 600 for the LH$_2$ duct are sufficient to hold the required head. The screens were analyzed on the Thermal Analyzer program of Reference 3-9 to determine if the screen center could warm up above the duct liquid saturation temperature. The entire screen was found to remain well below saturation temperature by holding the outer edge near the cooling fluid temperature with close wrapping of the cooling coils. Vent lines are required between the tank screen and engine inlet flange to prevent overpressure and forcing of vapor across the conical screens.

Required cooling tube spacing is calculated using Equation 3-1 from Reference 3-10 which relates tube spacing to $T_{(a/2)}$, the maximum temperature at the midpoint between tubes.

$$\cosh (N\, a/2) = \frac{T_H - T_C}{T_H - T_{(a/2)}} \qquad\qquad (3\text{-}1)$$

where:

$$N = \sqrt{h/K_w\, t_e}$$

K_w = duct wall or tank skin thermal conductivity

t_e = duct wall or tank skin thickness

h = effective heat transfer coefficient determined by dividing the heat flux by the temperature difference between insulation outer surface and mean duct wall temperature.

T_H = heating environment temperature, assumed equal to the insulation outer surface temperature.

T_C = skin temperature where cooling is tube attached, assumed equal to the coolant temperature.

$a/2$ = half the distance between cooling tubes

$T_{(a/2)}$ was set at .6°K (1°R) below the liquid saturation temperature. Resulting required cooling tube spacing along the ducts, over the LO$_2$ sump and over the tank wall adjacent to the subcooler is shown in Table 3-5. Also shown is the corresponding total length of cooling tube.

Required coolant flow rates are given by Equation 3-2.

$$\dot{m} = Q/\Delta h \qquad\qquad (3\text{-}2)$$

where

Q = rate of heat absorbed by coolant

Δh = enthalpy difference between fluid entering and leaving the cooling tubes

Table 3-5. Cooling Tube Spacing and Lengths for Maintaining Filled
Propellant Ducts and Subcooler Between Burns

Engine Option and Cooling Tube Location	LO$_2$		LH$_2$	
	Spacing cm (in)	Length cm (in)	Spacing cm (in)	Length cm (in)
Category I				
Duct	5.1 (2.)	1275 (502)	1.3 (0.5)	8248 (3247
Sump	5.6 (2.2)	556 (219)	–	–
Tank Skin	7.6 (3.0)	1328 (523)	5.3 (2.1)	897 (353)
RL10A-3-3A				
Duct	5.8 (2.3)	1118 (440)	1.3 (0.5)	5057 (1991)
Sump	6.4 (2.5)	490 (193)	–	–
Tank Skin	8.6 (3.4)	191 (75)	6.1 (2.4)	1042 (410)
RL10A-3-3				
Duct	6.1 (2.4)	495 (195)	1.3 (0.5)	3589 (1413)
Sump	6.6 (2.6)	470 (185)	–	–
Tank Skin	9.1 (3.6)	472 (186)	6.4 (2.5)	2561 (1008)

Calculated coolant flow rates are given below:

Engine Option	LO$_2$ kg/hr	(lb/hr)	LH$_2$ kg/hr	lb/hr)
Category I	12.6	(27.8)	0.78	(1.74)
RL10A-3-3A	8.0	(17.6)	0.80	(1.78)
RL10A-3-3	9.6	(21.2)	0.96	(2.10)

The minimum permissible cooling tube diameter is set by the pressure drop in the tube. Because of the geometry of the propellant ducts, two sets of tubes (one for each engine) were assumed for each propellant. Pressure loss in the flowing two-phase coolant was calculated as a function of tube diameter using one-half of the tube lengths shown in Table 3-5, the above flow rates and the Martinelli-Nelson two-phase pressure loss correlations. This method described in detail in Appendix D-1, Reference 3-11, computes the pressure loss for two-phase turbulent flow using experimentally derived parameters dependent upon the fluid vapor-to-liquid density ratio, liquid-to-vapor viscosity ratio, and fluid quality. The experimental coefficients are used to convert the single-phase pressure loss with either liquid or vapor to the two-phase pressure loss. A computer program, written for the HP 9100 calculator, was used to compute pressure loss for both LH$_2$ and LO$_2$ configurations. Resulting minimum tube diameters are shown below.

Engine Option	LO$_2$, cm	(in.)	LH$_2$, cm	(in.)
Category I	1.27	(.50)	1.27	(.50)
RL10A-3-3A	0.95	(.375)	1.27	(.50)
RL10A-3-3	1.27	(.50)	1.27	(.50)

3.3 LO$_2$ SUBCOOLER SIZING

LO$_2$ subcooler analysis was performed to determine the size of subcooler required to meet the NPSP requirements of the RL10A-3-3, RL10A-3-3A and RL10 Category I engines. As the heat exchanger size is increased to provide more heat removal, the pressure losses in the subcooler also increase. Thus, an iterative solution was required to determine final LO$_2$ subcooler sizes. LO$_2$ subcooler configuration is basically that of NAS3-17802 (Reference 3-12) with the diameter increased and stacks added to achieve the larger sizes.

3.3.1 <u>HEAT REMOVAL REQUIREMENTS.</u> The equation giving subcooler heat removal required to achieve a given engine inlet NPSP is

$$\dot{Q}_r = \dot{m}C_p \ \Delta T / \Delta P \ (\text{NPSP} + \text{losses}) \qquad (3\text{-}3)$$

where

$\dot{Q}_r$ = required rate of heat removal

$\dot{m}$ = flow rate of liquid to turbopump

C_p = liquid propellant specific heat

$\Delta T / \Delta P$ = ratio of temperature change to pressure change

NPSP = required engine inlet net positive suction pressure

losses = pressure drop in subcooler and propellant supply ducts

Operating pressure affects both the heat removal requirement and the heat removal performance. The slope of the LO_2 saturation temperature-pressure curve, $\Delta T / \Delta P$, decreases with increasing pressure, as shown in Figure 3-4. Hence to achieve a given NPSP, less heat needs to be removed at higher pressures. The design condition LO_2 $\Delta T / \Delta P$ values for this study are .0413K/kN/m^2 (0.512R/psi) for the RL10A-3-3 at 299 kN/m^2 (43.4 psi), .0449K/kN/m^2 (0.557R/psi) for the RL10A-3-3A at 260 kN/m^2 (37.8 psi) and .0625K/kN/m^2 (0.775R/psi) for the RL10 Category I at 172 kN/m^2 (25.0 psi).

Higher pressures also increase subcooler performance by providing a higher fluid temperature on the hot side. Subcooler hot side inlet temperatures (saturation temperatures corresponding to the design operating pressures of Table 3-3) for this study are 102.0°K (183.6°R), 100.3°K (180.5°R), and 95.6°K (172.0°R).

The pressure "losses" in Equation 3-3 include both propellant supply duct and subcooler pressure losses. Supply duct losses are defined in Table 3-1.

3.3.2 HEAT TRANSFER EQUATIONS. The following heat transfer equations were used in the thermal analysis to determine the heat removed from the LO_2 as a function of subcooler size.

Fins are located on the subcooler hot side to increase heat transfer. Fin effectiveness is given by

$$\mu = \frac{1}{mL} \ \tanh \ (mL), \text{where } m = \sqrt{\frac{2h}{kw}} \qquad (3\text{-}4)$$

where:

μ = ratio of actual heat transferred to heat transferred if entire fin were at root temperature

L = fin length, root-to-tip
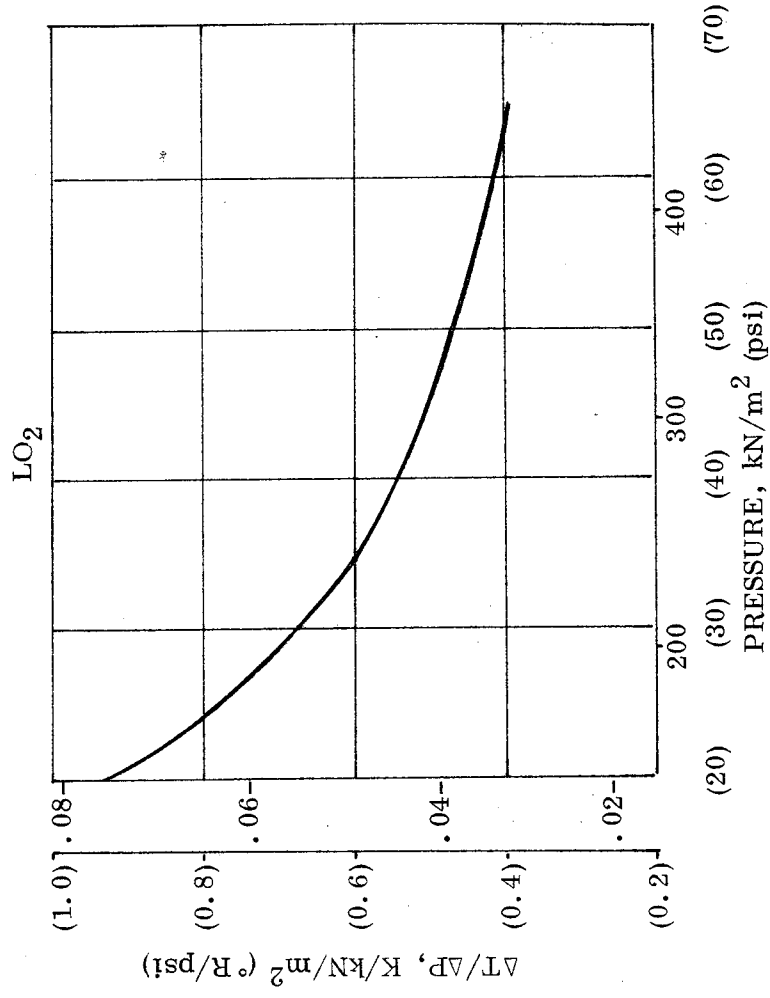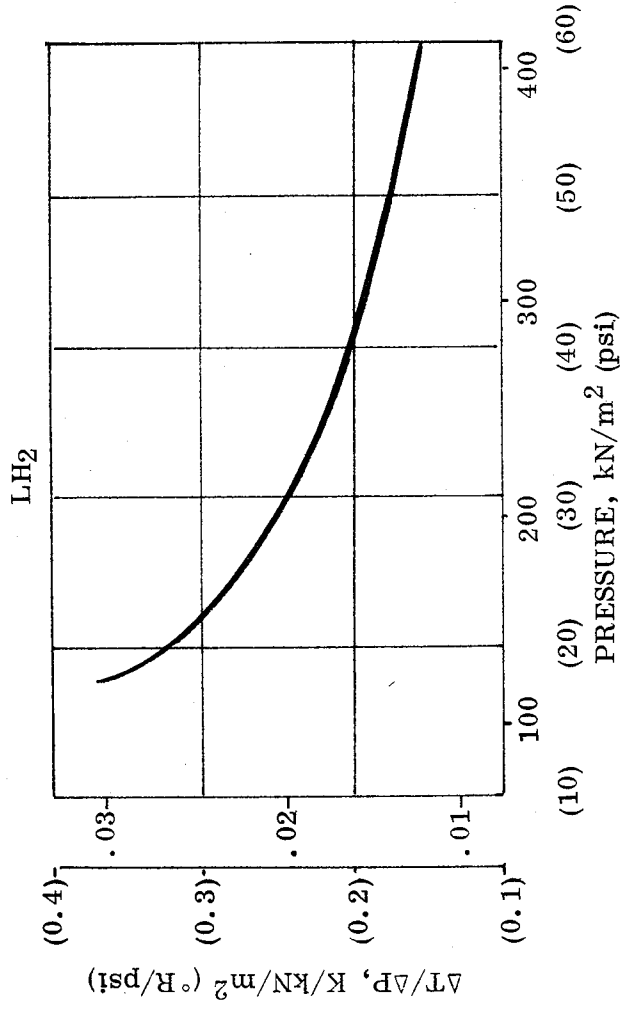
Figure 3-4. Slope of Saturation Temperature-Pressure Curve Versus Pressure for LH$_2$ and LO$_2$

3-15

h = convective heat transfer coefficient

k = fin thermal conductivity

w = fin thickness

Fin effectiveness is shown in Figure 3-5 as a function of heat transfer coefficient for several plate spacings.

On the hot side, forced convection laminar and turbulent heat transfer equations for flow over a flat plate were used. For forced convection laminar flow, the correlation used was

$$N_{Nu_L} = 0.664 \, N_{Re_L}^{1/2} \, N_{Pr}^{1/3} \tag{3-5}$$

For forced convection, turbulent flow, the correlation used was

$$N_{Nu_L} = 0.036 \, (N_{Pr})^{1/3} \left[N_{Re_L}^{0.8} - N_{Re_{CR}}^{0.8} + 18.44 \left(N_{Re_{CR}} \right)^{1/2} \right] \tag{3-6}$$

where

N_{Nu_L} is the Nusselt number, hL/k

N_{Re_L} is the Reynolds number, $\rho VL/\mu$

N_{Pr_L} is the Prandtl number, $\mu C_p/k$

$N_{Re_{CR}}$ is the transition Reynolds number (400,000)

    h is the heat transfer coefficient

    L is the characteristic length

    V is the fluid velocity

    μ is the viscosity

    k is the thermal conductivity

    C_p is the specific heat at constant pressure
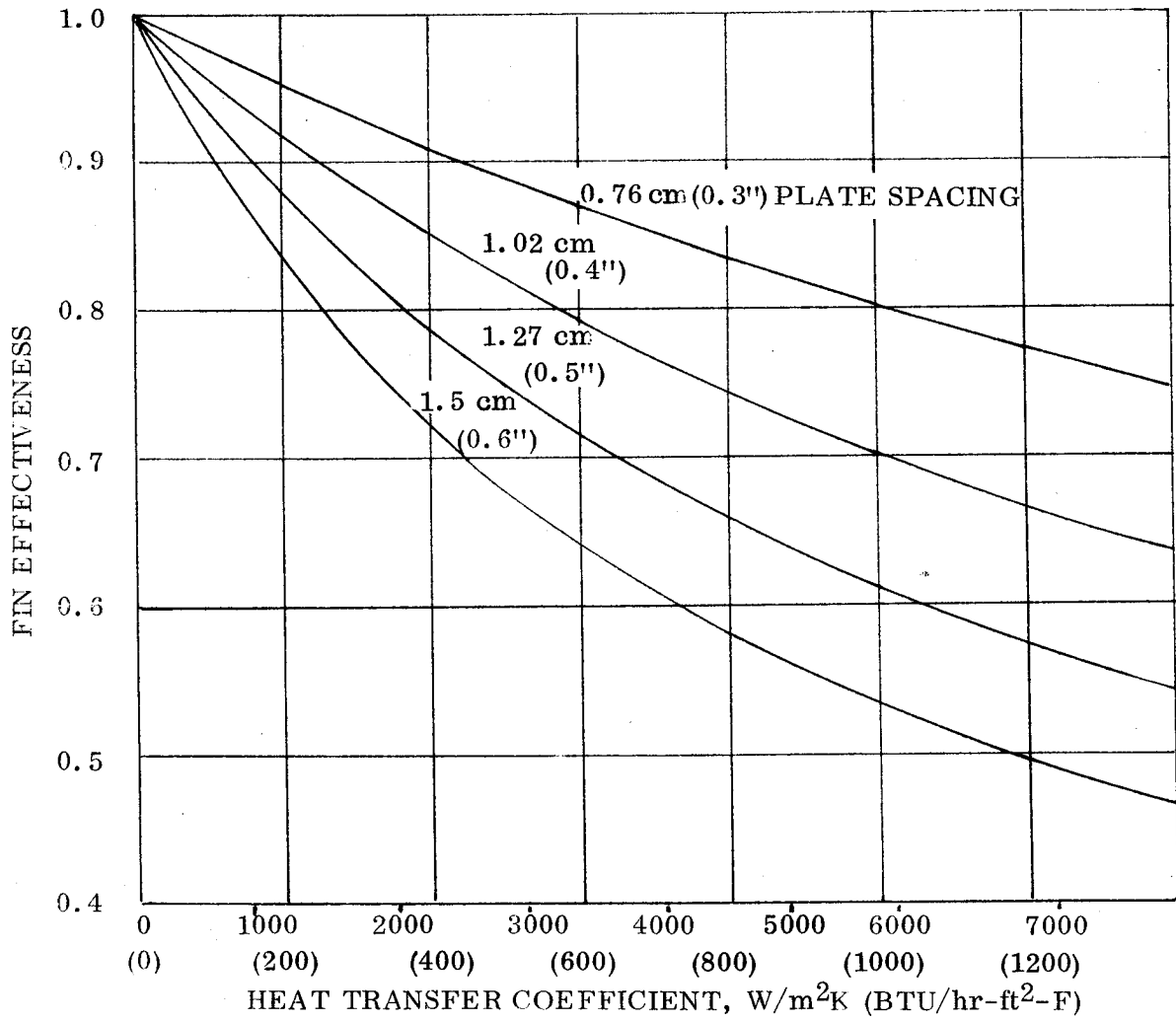
Figure 3-5. LO$_2$ Subcooler Hot Side Fin Effectiveness Versus
Plate Spacing and Heat Transfer Coefficient

Hot side heat transfer coefficients were computed from Equations 3-5 and 3-6. Typical plots of heat transfer coefficients for inward directed and outward directed flow are shown in Figures 3-6 and 3-7, respectively. In each pass the flow starts out laminar and becomes turbulent. The three passes of Figure 3-6 have different heat transfer coefficients because the inlet to each pass occurs at a different radius (and velocity).

On the cold side, for fluid quality less than 0.9, Kutateladze nucleate boiling heat transfer coefficients given by Equation 3-7 (Reference 3-11) were assumed.

$$\frac{\dot{Q}}{A_{SC}\,[0.555\,(\Delta T_{WC})]^{2.5}} = 1.547 \times 10^{-7} \left[\frac{112.3\,C_{P\ell C}}{(h_{sV} - h_{s\ell})\rho_{VC}}\right]^{1.5} \times$$

$$\left[\frac{0.0173 k_{\ell C}\,(0.01603\rho_{\ell C})^{1.282}\,(6.894\times 10^4\,P_{Ci})^{1.75}}{(\sigma_{\ell C})^{0.906}\,(14.88\mu_{\ell C})^{0.626}}\right] \quad (3\text{-}7)$$

where

A_{SC} = total cold side heat transfer surface area

$C_{P\ell C}$ = cold side liquid specific heat

$\dot{Q}$ = heat transfer rate

$k_{\ell C}$ = cold side liquid thermal conductivity

P_{Ci} = cold side inlet pressure

ΔT_{WC} = temperature difference between wall and cold side fluid

h_{sV} = specific enthalpy of saturated vapor on cold side

$h_{s\ell}$ = specific enthalpy of saturated liquid on cold side

$\rho_{\ell C}$ = cold side liquid density

$\sigma_{\ell C}$ = surface tension of cold side liquid

$\mu_{\ell C}$ = cold side liquid viscosity

In the foregoing equation, the following units apply:

$\dot{Q}$, Btu/hr	$C_{P\ell C}$, Btu/lb-°R	P_{Ci}, lb/in.^{2}	$\mu_{\ell C}$, lb/ft-sec
A_{SC}, ft^2	$k_{\ell C}$, Btu/hr-ft-°R	$(h_{sV} - h_{s\ell})$, Btu/lb	
ΔT_{WC}, °R	$\rho_{\ell C}$, lb/ft^3	$\sigma_{\ell C}$, dynes/cm	
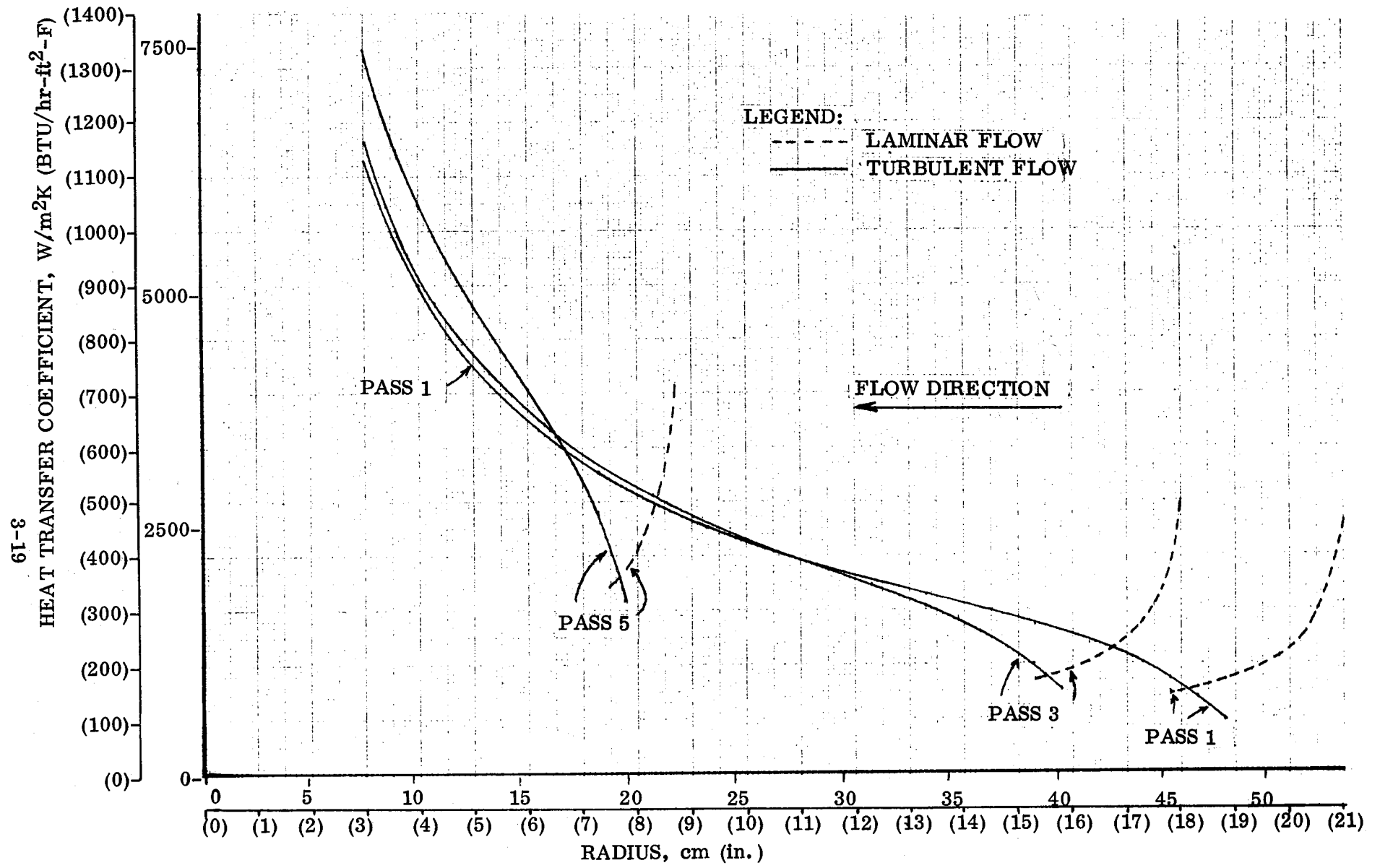
Figure 3-6. LO$_2$ 6-Pass Subcooler, Passes Flowing Toward Center, Hot Side Heat Transfer Coefficients

Figure 3-7. LO$_2$ 6-Pass Subcooler, Passes Flowing Away From Center, Hot Side Heat Transfer Coefficients
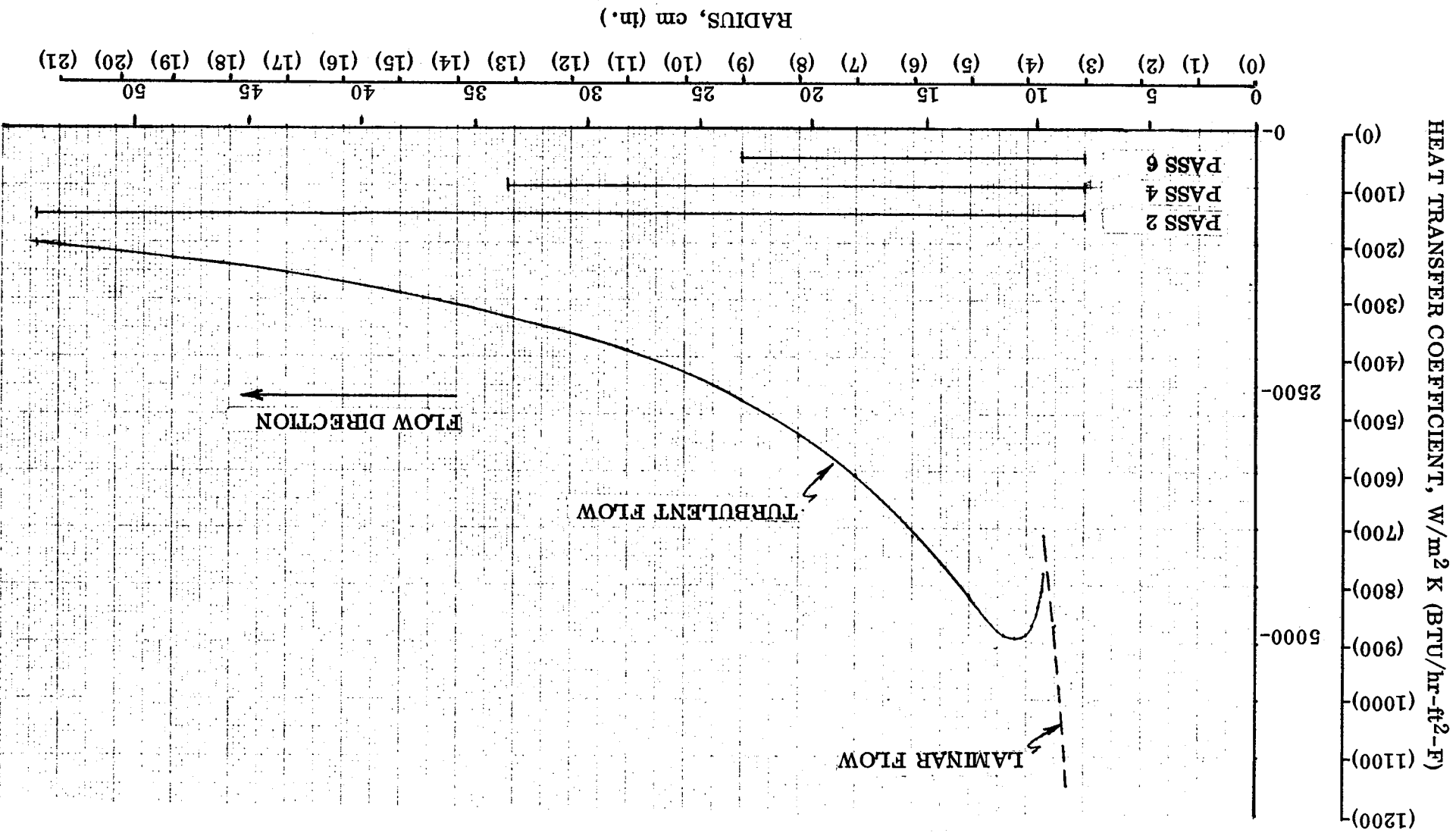
Heat transfer from the hot side LO_2 was determined using the following heat balance,

$$Q_{transferred} = h_H A (T_H - T_W) = h_C A (T_W - T_C) \tag{3-8}$$

where,

$T_H - T_C$ is known and $(T_H - T_W) + (T_W - T_C) = T_H - T_C$

T_H is the hot side temperature

T_C is the cold side temperature

h_H is the hot side heat transfer coefficient

h_C is the cold side heat transfer coefficient

A is the heat transfer area (hot side area includes fin area times fin effectiveness)

T_W is the wall or plate temperature

Hot side and cold side heat transfer were cross plotted to find T_W and thus $\dot{Q}$ transferred.

3.3.3 HOT SIDE PRESSURE LOSS. Pressure losses in the LO_2 subcooler hot side were determined using existing correlations. For pressure loss in screens at the inlet to the subcooler, Reference 3-13 was used. For frictional pressure loss, expansion, contraction and bend losses, equations and graphs similar to those in Reference 3-14 were used.

Screen pressure loss was determined by

$$\Delta P_S = A \mu V + B \rho V^2$$

where

A and B are empirical constants

μ is the fluid viscosity

ρ is the fluid density

V is the free stream velocity upstream of the screen

Pressure loss in bends were found from

$$\Delta P_b = KEC (\rho V^2 / 2g_c)$$

where

K is a pressure loss coefficient depending upon the radius ratio of the bend and the aspect ratio of the duct or passage cross section.

E is an aspect ratio factor also depending upon the aspect ratio.

C is a correction factor for other than 90° angle turns.

V is the velocity in the duct or passage.

Frictional pressure loss was found from

$$\Delta P_f = (fL/D_H)(\rho V^2/2g_c)$$

where

L is the length of the section.

D_H is the hydraulic diameter of the section.

f is the friction factor determined from a Moody diagram, such as found in Reference 3-15.

Expansion losses were found from

$$\Delta P_e = K_e (\rho V_1^2/2g_c)$$

where

V_1 is the velocity before the expansion and $K_e = [1 - (A_1/A_2)]^2$

where A_1 and A_2 are the areas before and after the expansion, respectively.

Contraction losses were found from

$$\Delta P_c = K_c C_c (\rho V_2^2/2g_c)$$

where

V_2 is the exit velocity

K_c is a function of the area ratio A_1/A_2 between the entrance and exit

C_c is a function of the entrance rounding

3.3.4 PLATE SPACING OPTIMIZATION. The heat transfer equations of Section 3.3.2 and pressure loss equations of Section 3.3.3 were used to determine an optimum plate separation distance. Heat transfer and pressure loss were computed for two

53 cm (21 in.) radius passes (inward and outward) for plate spacings of .76 cm (.3 in.) to 1.78 cm (.7 in.). To determine the best spacing, the pressure loss was converted to an equivalent heat removal loss using Equation 3-3, and subtracted from the heat removed. The results are presented in Figure 3-8 which shows a relatively flat curve with the optimum spacing at about 1.3 cm (.5 in.).

3.3.5 SUBCOOLER SIZING AND ANALYSIS ON THERMAL ANALYZER. The size of LO_2 subcooler necessary to meet the heat removal requirements given in Equation 3-3 for the three NPSP levels was determined using the equations of Sections 3.3.2 and 3.3.3 at the optimum plate spacing distance of 1.3 cm (0.5 in.). Sketches of the three subcoolers sized are shown in Figure 3-9. The subcooler for the Category I engine is the largest, requiring six hot side passes and a maximum radius of 54.9 cm (21.6 in.), even though its NPSP requirement is the lowest. The reason for this is that its operating design pressure is also the lowest which increases the heat removal requirement (Equation 3-3) and decreases the performance. The subcooler for the RL10A-3-3A engine is the smallest, requiring five hot side passes and a maximum radius of 34.3 cm (13.5 in.). The subcooler for the RL10A-3-3 engine requires five hot side passes with a maximum radius of 45.2 cm (17.8 in.).

A pie-shaped section of each of the subcoolers was modeled on the Thermal Analyzer program (Reference 3-9) to more accurately determine its performance. The largest subcooler of Figure 3-9 was subdivided into 52 nodes and 94 interconnecting resistances for computer analysis. In each case, the heat removal determined by computer was within 10% of the previously calculated value. Adjustment of the throttled cold side fluid to slightly different pressures (within the range of 26.2 kN/m^2 (3.8 psi) to 34.5 kN/m^2 (5.0 psi))allowed "fine tuning" of the subcooler to closely match the heat removal requirement.

The Thermal Analyzer program was also used to determine total heat transferred as a function of tank pressure for each LO_2 subcooler. Results are shown in Figure 3-10. Note that since heat removal can be related to an NPSP requirement at a given tank pressure, the data in Figure 3-10 will be used in Section 3.5 with calculated subcooler weights to show subcooler weight versus NPSP at given tank pressures.

The largest subcooler was also analyzed at LO_2 flow rates of 2.3 kg/sec (5 lb/sec) and 9.1 kg/sec (20 lb/sec) to determine performance during the start transient. Steady state flow rate is 25.6 kg/sec (56.4 lb/sec). The computed heat removal exceeded the requirement in both cases. The heat removal requirement during the start transient included the propellant duct inertia loss which drops to zero as the propellant comes up to speed.

A summary of subcooler requirements and computed performance during the start transient and steady state operation is shown in Table 3-6. The calculated heat removal is seen to exceed the heat removal requirement in every case; indicating satisfactory accomplishment of the required engine inlet NPSP levels.
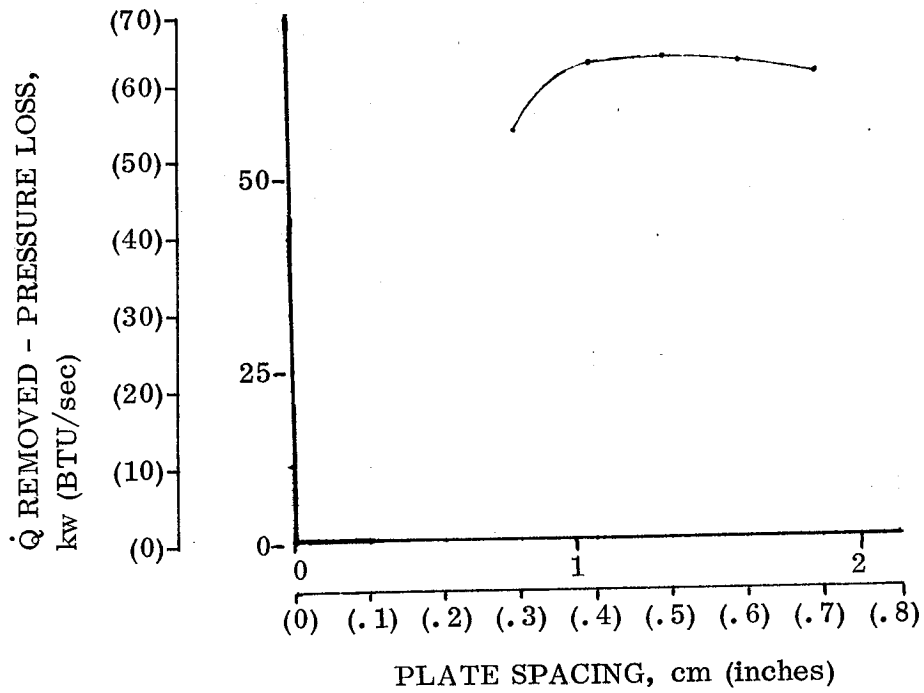
Figure 3-8. LO$_2$ Plate Spacing Optimization Analysis
Results - Net Heat Removed in Two 53.3 cm
(21-in) Rad. Passes

RL10 Cat. I: 6-Pass, Max Rad = 54.9 cm (21.6 in)

Inlet Screen
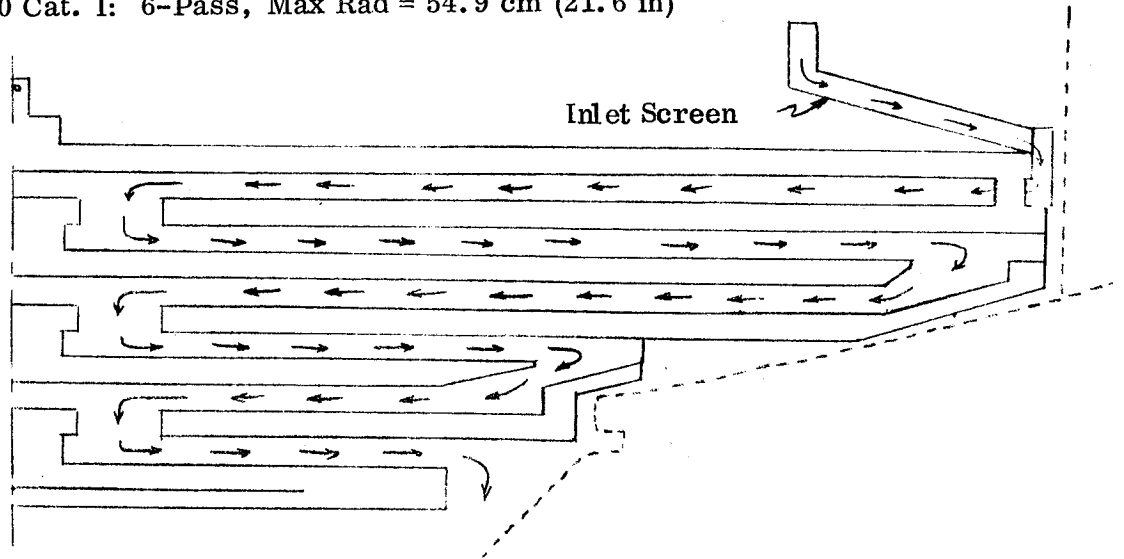
RL10A-3-3A: 5-Pass, Max Rad = 34.3 cm (13.5 in)
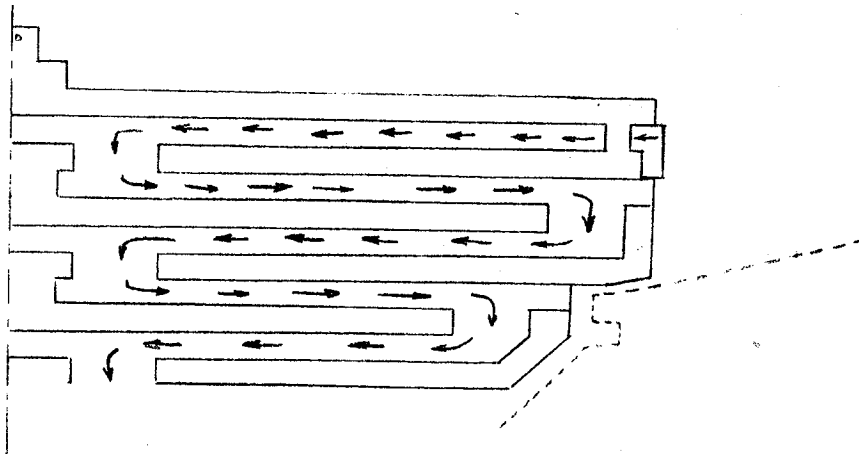
RL10A-3-3: 5-Pass, Max Rad = 45.2 cm (17.8 in)

Hot Side Flow Path
Illustrated with Arrows
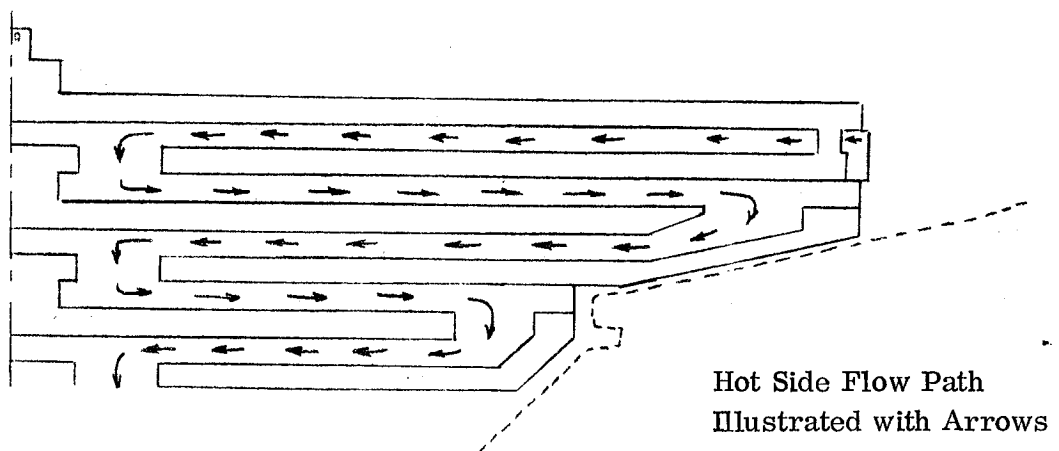
Figure 3-9. Sketches of LO$_2$ Subcoolers Sized to Meet NPSP Requirements of RL 10 Category I, RL10A-3-3A and RL-10A-3-3 Engines
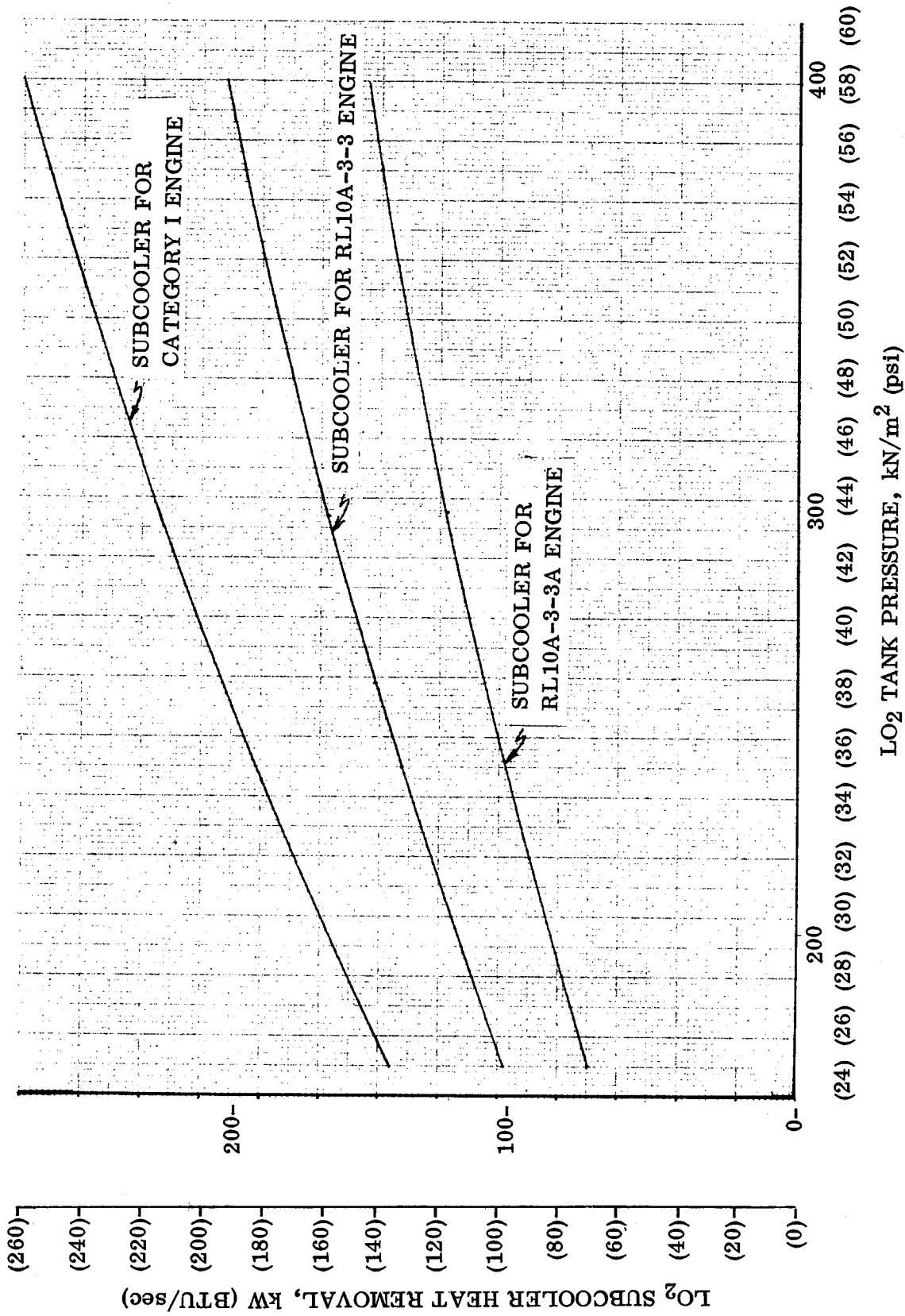
Figure 3-10. LO₂ Subcooler Heat Removal Versus LO₂ Tank Pressure

Table 3-6. Summary of LO$_2$ Subcooler Requirements and Performance

Engine	Required Subcooler NPSP Output* kN/m^2 (psi)	Required Heat Removal Kilowatts (Btu/sec)	Subcooler Size (See Figure 3-9)	Calculated Heat Removal Kilowatts (Btu/sec)
Steady State Operation (25.6 kg/sec (56.4 lb/sec))				
1. RL10 Cat. I	35.5 (5.15)	141 (134)	6 - Pass, Max radius = 54.9 cm (21.6 in)	143 (136)
2. RL10A-3-3A	39.6 (5.75)	106 (101)	5 - Pass, Max radius = 34.3 cm (13.5 in)	110 (104)
3. RL10A-3-3	72.3 (10.5)	159 (151)	5 - Pass, Max radius = 45.2 cm (17.8 in)	165 (157)
Start Transient				
1. RL10 Cat. I at 2.3 kg/sec (5.0 lb/sec) flow	60.6 (8.8)	15 (14)	Same as above	26 (25)
2. RL10 Cat. I at 9.1 kg/sec (20 lb/sec) flow	60.6 (8.8)	61 (58)	Same as above	66 (63)

* Engine NPSP requirement + line loss

3.3.6 <u>SUBCOOLER COLD SIDE FLOW</u>. Required cold side flow rates and resulting payload penalties were computed for the LO_2 subcoolers using Equation 3-2. These flow rates are based on several restricting assumptions. The design of the heat exchangers is fixed based upon the worst case NPSP conditions. The cold side outlet enthalpy is restricted to a quality of 0.9 in order to confine cold side heat transfer to the nucleate boiling range. Because of these assumptions maximum cold side flow rate occurs when the subcooler is transferring the most heat; i.e.; when tank pressure and thus hot side liquid temperature, is the highest. The design conditions for cold side flow will occur at the start of the first burn in all three missions at the pressures shown in Figures 3-1 through 3-3. Corresponding subcooler heat transfer is seen in Figure 3-10.

The LO_2 subcoolers were sized assuming nucleate boiling heat transfer on the cold side over the entire flow length. According to Reference 3-11, the heat transfer coefficient in a flowing boiling fluid decreases as the fluid quality exceeds 0.90 until, at 100% vaporization, the coefficient reaches that of a pure vapor. Therefore, for the subcooler sizes shown in Figure 3-9, the cold side flow rate must be great enough that the two-phase fluid quality does not exceed 0.90. If the exit quality were allowed to increase to 1.0, the cold side enthalpy change (Δh) would be greater, permitting a slightly reduced cold side flow rate, but the already large heat exchangers would have to be increased in size because of lower heat transfer. Continuing, if the cold side fluid were allowed to be totally vaporized and then superheated, the cold side flow rate could be reduced further, but the heat exchanger would have to be even larger. Vented cold side fluid quantities and corresponding payload penalties were computed (using the Reference 3-7 payload sensitivity factors) for a 0.90 exit quality, a 1.0 exit quality and a 5°R superheat exit condition. For this analysis it was assumed that the cold side flow could not be varied during a flight but could be adjusted for a given mission. Cold side vented fluid payload penalties for 1-burn, 2-burn and 5-burn missions are shown in Table 3-7. The vented fluid payload penalty reduction achieved by cold side heating above a 0.90 quality would be overshadowed by the requirement to enlarge the subcoolers to an unwieldy size.

The excessively high vented fluid payload penalties shown in Table 3-7 indicate the desirability of returning the cold side LO_2 back into the tank. This would also reduce the tank pressure drop during firing which reduces the required high lift-off LO_2 tank pressure and associated tank skin weight and LO_2 density penalties. Weight calculations for a battery, pump and surge tank required to recirculate the LO_2 indicate a weight of less than 23 kg (50 lb).

Cold side pressure drop in the largest LO_2 subcooler was computed to be approximately 7 kN/m^2 (1 psi) using the calculated flow rates and the Martinelli-Nelson two phase pressure loss correlations cited in Reference 3-11.

3.4 LH_2 SUBCOOLER SIZING

Liquid hydrogen subcoolers were sized to meet the NPSP requirements of the RL10A-3-3, RL10A-3-3A and RL10 Category I engines (see Section 3.1.2). LH_2 subcooler configuration is basically that of NAS3-17802 (Reference 3-12); i.e., a rectangular channel located adjacent to the tank circumference and divided by fins into a number of

Table 3-7. LO$_2$ Subcooler Cold Side Vented Fluid Payload Penalties, kg (lb$_m$)

	1-Burn Mission		2-Burn Mission		5-Burn Mission	
1. RL10 Category I Subcooler						
0.90 Exit Quality	511	(1127)	493	(1087)	458	(1009)
1.0 Exit Quality	455	(1003)	438	(965)	407	(898)
2.8K (5R) Superheat	443	(977)	426	(940)	397	(875)
2. RL10A-3-3A Subcooler						
0.90 Exit Quality	417	(920)	382	(843)	358	(790)
1.0 Exit Quality	366	(806)	332	(733)	313	(690)
2.8K (5R) Superheat	354	(781)	321	(708)	301	(664)
3. RL10A-3-3 Subcooler						
0.90 Exit Quality	657	(1448)	567	(1251)	520	(1146)
1.0 Exit Quality	570	(1256)	491	(1083)	451	(994)
2.8K (5R) Superheat	549	(1210)	472	(1041)	432	(953)

passages with cold side flow on both sides of the rectangle. To achieve the larger
sizes for this study, the flow area was enlarged and the length increased. Heat trans-
fer equations of Section 3.3.2 and pressure loss equations of Section 3.3.3 were used
to analyze the subcoolers.

3.4.1 HEAT REMOVAL REQUIREMENTS. Heat removal required to achieve a given
engine inlet NPSP is given by Equation 3-3. The LH_2 subcooler design tank pressures
(minimum operating pressures) from Figure 3-1 are 118 kN/m^2 (17.1 psi) for the
Category I engine, 147 kN/m^2 (21.4 psi) for the RL10A-3-3A engine and 154 kN/m^2
(22.4 psi) for the RL10A-3-3 engine. At the above pressures the $\Delta T/\Delta P$ values for
Equation 3-3 are 0.0308 $K/kN/m^2$ (0.382 R/psi), 0.0252 $K/kN/m^2$ (0.312 R/psi) and
0.0242 $K/kN/m^2$ (0.300 R/psi), respectively. NPSP values for Equation 3-3 are given
in Table 3-1.

3.4.2 PLATE/FIN OPTIMIZATION AND SUBCOOLER SIZING ANALYSIS. The plate/
fin spacing optimization and subcooler sizing analysis were performed simultaneously
for the Category I engine subcooler as follows. The subcooler height was held to
34.4 cm (13.6 in.) which is equal to the subcooler inlet screen channel maximum
height determined in Reference 3-12 and corresponds to 13 stacked hot side passages
at 2.54 cm (1.0 in.) inside height per passage. For the spacing optimization, the
number of passages was held at 13 and the hot side flow width was varied from 2.5 cm
(1.0 in.) to 4.6 cm (1.8 in.) in increments of 0.25 cm (0.10 in.). Increasing the width
increases the total flow area which shortens the required subcooler length but also in-
creases the fin length which increases the subcooler weight per unit length.

Subcoolers with the above hot side dimensions were modeled for analysis on the Therm-
al Analyzer computer program (Reference 3-9). Heat transfer coefficients and fin effec-
tiveness values were computed as described in Section 3.3.2 and were input to the pro-
gram. A hot side inlet temperature of 20.8 K (37.4 R) for the Category I subcooler de-
sign case, and a cold side temperature of 17.1 K (30.8 R) corresponding to a throttled
pressure of 34.5 kN/m^2 (5.0 psi) were used as boundary conditions. Output from the
program was the heat transferred from the hot side LH_2 as a function of subcooler
length.

Subcooler lengths which met the heat removal requirement for each hot side flow
width were determined and are shown in Figure 3-11. At the narrower widths ana-
lyzed, the required subcooler length is reduced with increasing width because of lower
pressure drop at lower velocities and because the corresponding lower heat transfer
coefficient tends to increase fin effectiveness. At widths above 4.3 cm (1.7 in.), the
reduced heat transfer due to greater fin lengths and lower heat transfer coefficients
begins to predominate and a longer subcooler is needed. Comparative weight penal-
ties for each of the above subcoolers were taken to be the sum of subcooler skin weight,
LH_2 not tanked into the hot side volume, and cold side residuals, with appropriate pay-
load penalty factors for a 1-burn mission. Payload weight penalties are shown in
Figure 3-11. The weight penalty is seen to be nearly constant over widths from 3.6
cm (1.4 in.) to 4.6 cm (1.8 in.). For the RL10 Category I subcooler, a width of

NOTE: SUBCOOLER SIZED FOR
CATEGORY I ENGINE NPSP
REQUIREMENTS.
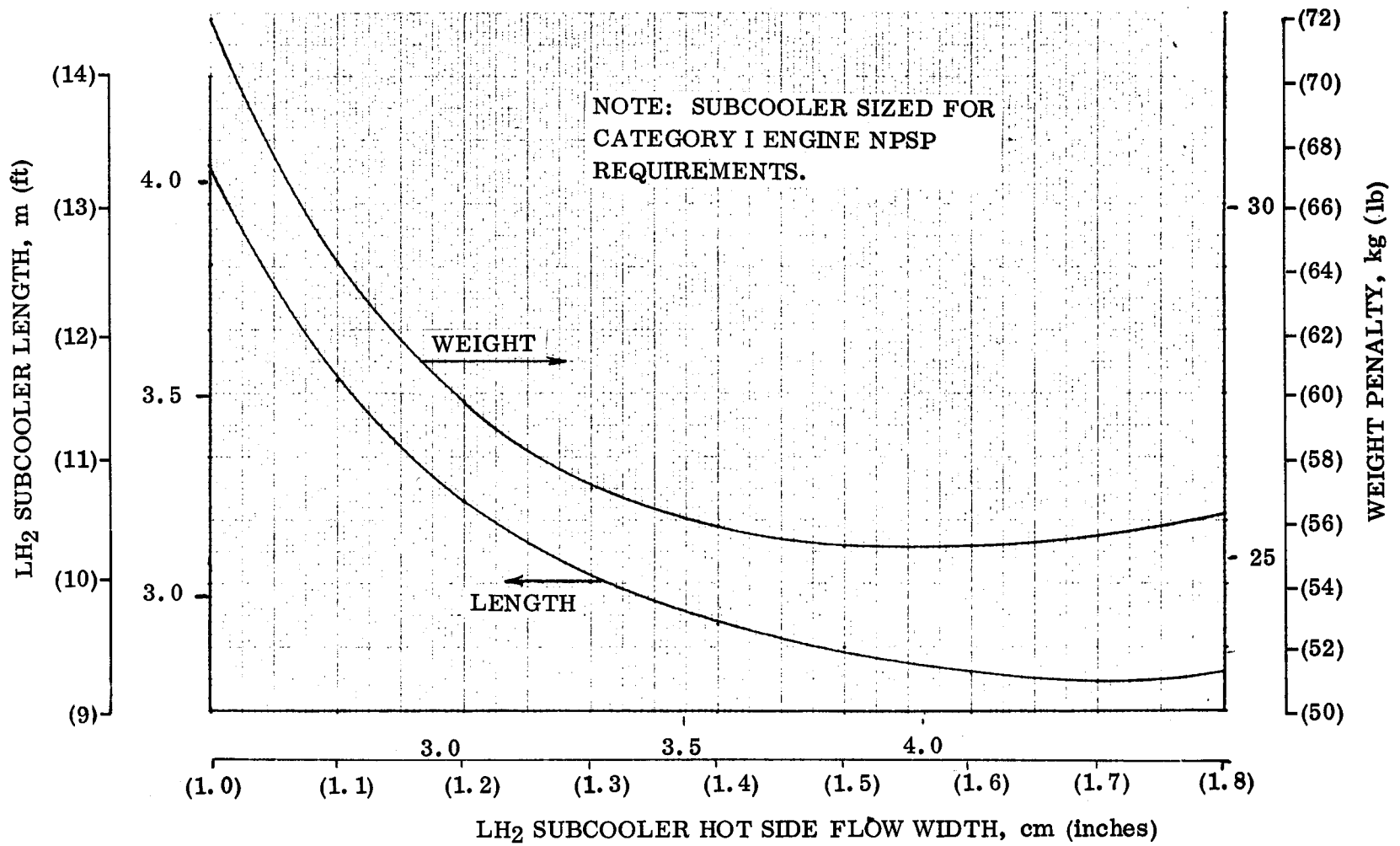
Figure 3-11. LH$_2$ Subcooler Plate Spacing Optimization Results

3.8 cm (1.5 in.) was selected as optimum with a corresponding required length of 2.9 m (9.5 ft).

The above optimized subcooler cross section was then used to calculate the subcooler lengths required for the RL10A-3-3A and RL10A-3-3 engines. A length of 3.84 m (12.6 ft) was found to meet the NPSP requirements of the RL10A-3-3A engine. However, the length around the tank circumference available for the LH_2 subcooler, was not sufficient for the RL10A-3-3 requirement (approximately 9.2 m (30 ft), less 3.4 m (11 ft) for screen channel inlet, tank outlet and fill and drain valve).

The number of fins in the RL10A-3-3 subcooler was increased to increase performance at the expense of adding weight. An optimum vertical spacing was sought in which the added fin heat removal less the increased pressure drop due to a smaller flow area would maximize the heat removal. Subcoolers with the same outside dimensions but with 16, 18, 20, 22 and 24 fins (baseline is 14 fins) were analyzed. The best performance came from the 18-fin configuration which had 17 stacked passages of 3.81 cm (1.5 in.) width by 1.92 cm (0.755 in.) height. However, subcooler performance at the full available length was still not sufficient for the RL10A-3-3 requirements. Additional passages of the same dimensions were added vertically until the required performance was achieved. The resulting LH_2 subcooler configuration for the RL10A-3-3 engine is 5.64 m (18.5 ft) long and has 30 stacked passages of 3.81 cm (1.5 in.) width by 1.92 cm (0.755 in.) height inside dimensions.

The Thermal Analyzer program was used to determine the total heat transferred as a function of tank pressure for each LH_2 subcooler. Results are shown in Figure 3-12. Note that since heat removal can be related to an NPSP requirement at a given tank pressure, the data in Figure 3-12 will be used in Section 3.5 with calculated subcooler weights to show subcooler weight versus NPSP at given tank pressures.

The Category I and RL10A-3-3 subcoolers were also analyzed at flow rates of 0.91 kg/sec (2.0 lb/sec) and 2.3 kg/sec (5.0 lb/sec) to determine performance during the start transient. The steady state flow rate is 5.1 kg/sec (11.2 lb/sec). The computed heat removal exceeded the requirement in all cases. The heat removal requirement during the start transient included the propellant duct inertia loss which drops to zero as the propellant comes up to speed.

A summary of subcooler requirements and computed performance during the start transient and steady state operation is shown in Table 3-8. The calculated heat removal is seen to meet or exceed the most severe heat removal requirement in every case, indicating satisfactory accomplishment of the required engine inlet NPSP levels.

3.4.3 LH_2 SUBCOOLER COLD SIDE FLOW. Required cold side flow rates and resulting payload penalties were computed for the LH_2 subcoolers using Equation 3-2. As discussed earlier for the LO_2 subcoolers, the maximum required cold side flow rate occurs when the subcooler is transferring the most heat (at highest tank pressures).
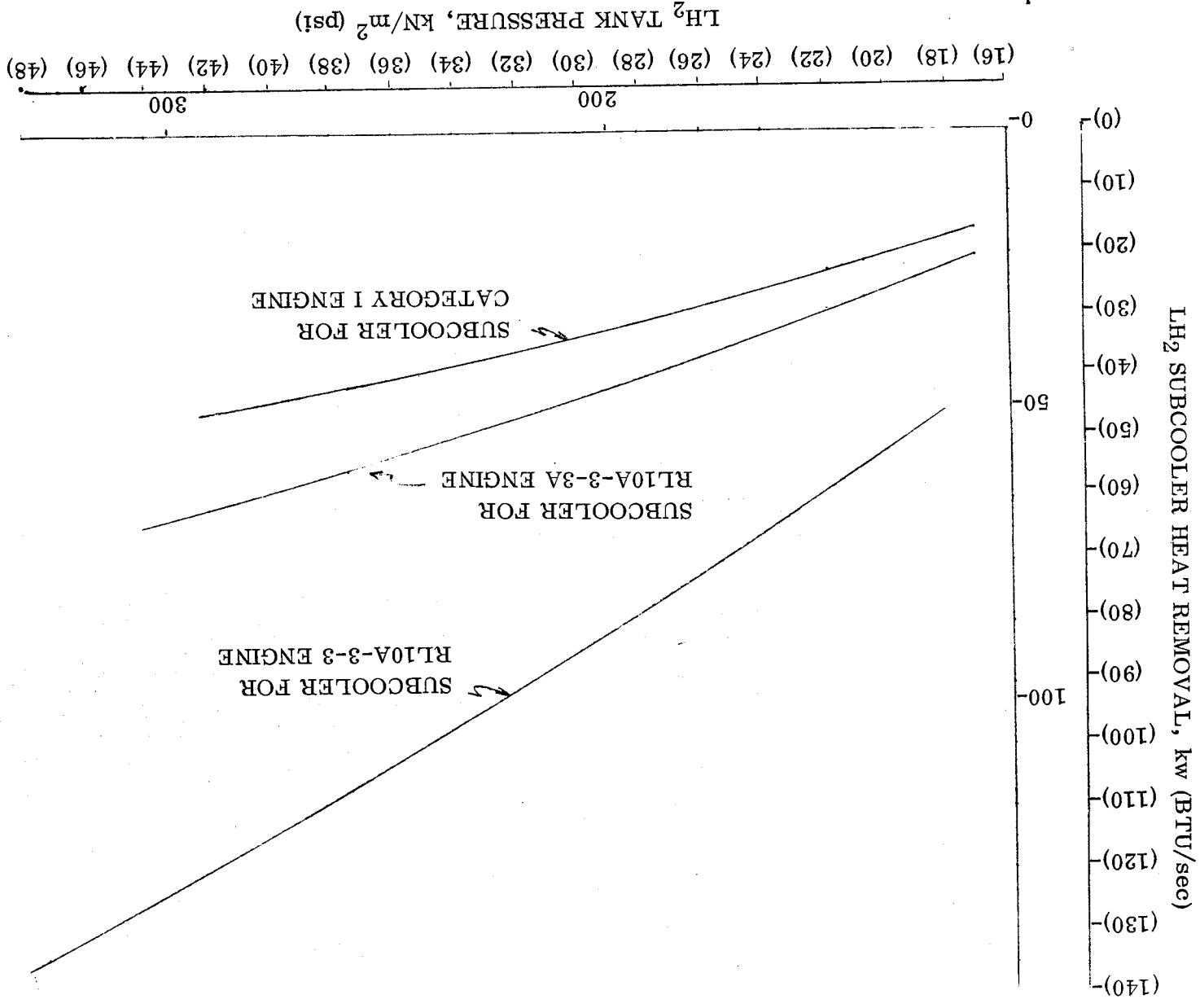
Figure 3-12. LH2 Subcooler Heat Removal vs LH2 Tank Pressure

LH2 TANK PRESSURE, kN/m² (psi)

(16) (18) (20) (22) (24) (26) (28) (30) (32) (34) (36) (38) (40) (42) (44) (46) (48)

300   200

SUBCOOLER FOR
CATEGORY I ENGINE

SUBCOOLER FOR
RL10A-3-3A ENGINE

SUBCOOLER FOR
RL10A-3-3 ENGINE

LH₂ SUBCOOLER HEAT REMOVAL, kw (BTU/sec)

(0) (10) (20) (30) (40) (50) (60) (70) (80) (90) (100) (110) (120) (130) (140)

0   50   100

Table 3-8. Summary of LH$_2$ Subcooler Requirements and Performance

Engine	Required Subcooler NPSP Output* kN/m^2 (psi)		Required Heat Removal Kilowatts (Btu/sec)		Subcooler Size	Calculated Heat Removal Kilowatts (Btu/sec)	
Steady State Operation (5.1 kg/sec (11.2 lb/sec))							
1. RL10 Cat. I	7.23	(1.05)	17.0	(16.1)	13 passages at 3.8 cm (1.5 in) × 2.5 cm (1.0 in). Length = 2.90 cm (9.5 ft)	17.0	(16.1)
2. RL10A-3-3A	17.2	(3.5)	28.7	(27.2)	13 passages at 3.8 cm (1.5 in) × 2.5 cm (1.0 in). Length = 3.84 m (12.6 ft)	28.7	(27.2)
3. RL10A-3-3	37.9	(5.5)	61.6	(58.4)	30 passages at 3.8 cm (1.5 in) × 1.92 cm (.755 in). Length = 5.64 m (18.5 ft)	61.6	(58.4)
Start Transient							
1. RL10 Cat. I at 0.9 kg/sec (2.0 lb/sec) flow	15.2	(2.2)	4.4	(4.2)	13 passages at 3.8 cm (1.5) in × 2.5 cm (1.0 in). Length = 2.90 cm (9.5)	7.4	(7.0)
2. RL10 Cat. I at 2.3 kg/sec (5.0 lb/sec) flow	15.2	(2.2)	11.4	(10.8)	13 passages at 3.8 cm (1.5 in) × 2.5 cm (1.0 in). Length = 2.90 cm (9.5 ft)	11.6	(11.0)
3. RL10A-3-3 at 0.9 kg/sec (2.0 lb/sec) flow	40.7	(5.9)	9.6	(9.1)	30 passages at 3.8 cm (1.5 in) × 1.92 cm (.755 in). Length = 5.64 m (18.5 ft)	26.0	(24.7)
4. RL10A-3-3 at 2.3 kg/sec (5.0 lb/sec) flow	40.7	(5.9)	24.2	(23.0)	30 passages at 3.8 cm (1.5 in) × 1.92 cm (.755 in). Length = 5.64 m (18.5 ft)	41.8	(39.7)

* Engine NPSP requirement + line loss

The design conditions for cold side flow will occur at the start of the first burn in all three missions at the pressures shown in Figures 3-1 through 3-3. Corresponding subcooler heat transfer is seen in Figure 3-12. Since the LH_2 subcooler cold side has such a large skin area exposed to the LH_2 in the tank, the heat addition by natural convection from the LH_2 in the tank was computed and added to the heat transferred from the subcooler hot side (this increased heating by 7%). Cold side vented flow rates and resulting payload penalties for 1-burn, 2-burn, and 5-burn missions were computed and are shown in Table 3-9. As with the LO_2 subcoolers, the vented fluid payload penalty reduction achieved by cold side heating above a 0.90 quality seen in Table 3-9 is overshadowed by the corresponding added penalty of going to a much larger subcooler. The payload penalties, although not as high as those for LO_2, indicate the desirability of returning cold side LH_2 back into the tank. Also, at the higher tank pressures, the calculated ΔT between subcooler skin and boiling cold side fluid exceeds that for critical nucleate boiling heat flux given in Reference 3-16 (approximately 3K or 5R). Returning cold side fluid back into the tank reduces the tank pressure drop during firing which permits lower initial pressures (and hot side temperatures) and a lower heat flux across the subcooler. An alternate solution would be to throttle the LH_2 to a higher cold side pressure. However, this would increase the required subcooler size unless a controllable throttling system were used.

LH_2 subcooler cold side pressure drop was computed using the calculated flow rates and the Martinelli-Nelson two phase flow pressure loss correlations. Staggered fins were assumed to be located in the cold side passages as in NAS3-17802, Reference 3-12, to promote wall wetting annular flow. The throttled cold side inlet pressure is 34.5 kN/m^2 (5.0 psi). The cold side pressure must not drop below the triple point of LH_2, 6.9 kN/m^2 (1.0 psi). The calculated pressure drop (caused primarily by the many flow turns around the fins) was found to be excessive. The cold side flow length was therefore cut in half by using two throttling valves to flow half the fluid down each side instead of flowing all the fluid down one side and back the other as in NAS3-17802, Reference 3-12. This reduced the pressure drop to an acceptable 4.3 kN/m^2 (0.62 psi) for the Category I subcooler and 14.1 kN/m^2 (2.0 psi) for the RL10A-3-3A subcooler. However, the RL10A-3-3 subcooler pressure drop was still excessive. It was necessary to increase the cold side flow width from 2.5 cm (1.0 in.) to 3.2 cm (1.25 in.) for the RL10A-3-3 subcooler in order to reduce the pressure loss to an acceptable 22.2 kN/m^2 (3.2 psi).

3.5 LO_2 AND LH_2 SYSTEM WEIGHT VERSUS NPSP

Subcooler heat removal required to achieve a given engine inlet NPSP at a given operating pressure is shown in Equation 3-3 and is repeated here.

Table 3-9. LH$_2$ Subcooler Cold Side Vented Fluid Payload Penalties, kg (lbs)

	1-Burn Mission		2-Burn Mission		5-Burn Mission	
1. RL10 Category I Subcooler						
0.90 Exit Quality	54	(118)	47	(104)	37	(80.8)
1.0 Exit Quality	47	(104)	42	(92.4)	37	(80.8)
2.8K (5R) Superheat	44	(96.6)	39	(85.5)	34	(74.7)
2. RL10A-3-3A Subcooler						
0.90 Exit Quality	88	(194)	77	(170)	64	(142)
1.0 Exit Quality	78	(171)	68	(150)	57	(125)
2.8K (5R) Superheat	72	(158)	63	(138)	53	(116)
3. RL10A-3-3 Subcooler						
0.90 Exit Quality	188	(414)	179	(394)	144	(318)
1.0 Exit Quality	166	(366)	157	(347)	127	(279)
2.8K (5R) Superheat	153	(338)	145	(320)	117	(257)

$$\dot{Q}_r = \dot{m} \, C_p \, \Delta T / \Delta P \; (\text{NPSP} + \text{losses})$$

or

$$\text{NPSP} = \frac{\dot{Q}_r}{\dot{m} \, C_p \, \Delta T / \Delta P} - \text{losses} \qquad (3\text{-}9)$$

Curves of subcooler heat removal versus pressure are presented in Figures 3-10 (LO_2) and 3-12 (LH_2). The $\Delta T / \Delta P$ term for each pressure is determined from Figure 3-4. Duct and subcooler pressure losses have been defined or calculated in the analysis. From the above, it was possible to calculate the NPSP delivered to the engine inlet for each of the design condition subcooler operating pressures given in Table 3-3 for each subcooler configuration.

For example, if the Category I LH_2 subcooler, which was sized to deliver an NPSP of 4 kN/m^2 (0.55 psi) at a tank pressure of 118 kN/m^2 (17.1 psi) were to operate at a tank pressure of 147 kN/m^2 (21.4 psi), then the NPSP delivered to the engine would be given by Equation 3-9

$$\text{NPSP} = \frac{22.1 \; \text{Btu/sec}}{11.2 \; \text{lb/sec} \times 2.5 \; \text{Btu/lb-}^\circ\text{R} \times .312 ^\circ\text{R/psi}} - .5 \; \text{psi} - .52 \; \text{psi}$$

$$= 10.4 \; \text{kN/m}^2 \; (1.51 \; \text{psi})$$

LO_2 and LH_2 system weights were tabulated for three NPSP levels at each of three tank pressures using the weights determined in Section 3.6. The one-burn weight penalties for the system concept of subcoolers with settling were used. LO_2 and LH_2 system weight versus NPSP are shown in Figures 3-13 and 3-14, respectively. LH_2 weight penalties are for dumping cold side subcooler flow overboard. LO_2 penalties are for pumping subcooler cold side fluid back into the tank. Each curve represents the performance of three different subcooler configurations at the pressure noted.

3.6 WEIGHT COMPARISONS

Hardware weights and fluid weight penalties were generated for weight comparisons of the system concepts of (1) baseline D-1S, (2) subcoolers with propulsive settling, and (3) subcoolers with screen acquisition device and wet feedlines. In each of the latter two system concepts, weights were generated for the three engine systems studied. In all three system concepts, weights were generated for one-burn, two-burn and five-burn missions. Weight breakdowns for the three system concepts are shown in Tables 3-10, 3-11 and 3-12. Weights which are common to all configurations and missions are not included. Sources of the weights of Tables 3-10, 3-11 and 3-12 are discussed in 3.6.1 and 3.6.2.
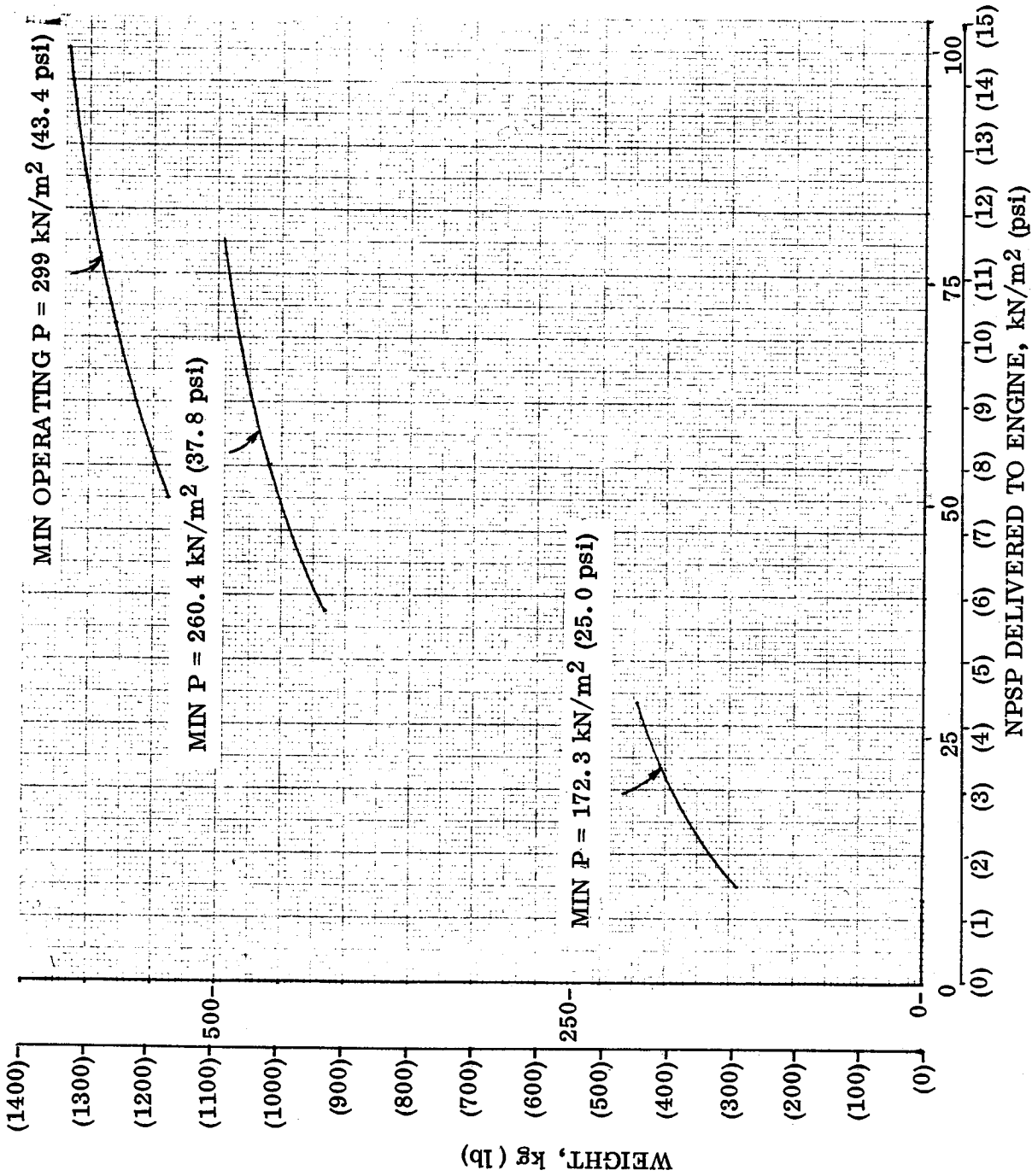
Figure 3-13. LO$_2$ System Weight Vs NPSP Delivered to Engine (Propulsive Settling, One-Burn Mission)
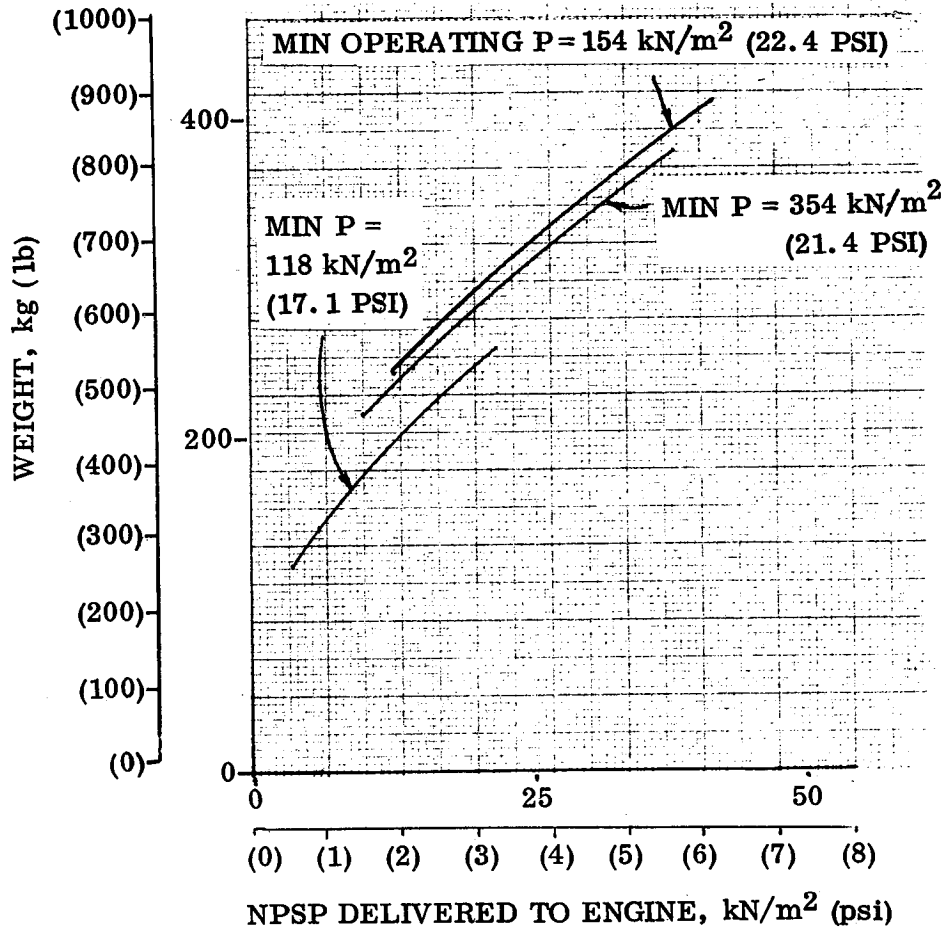
Figure 3-14. LH$_2$ System Weight Vs NPSP Delivered to Engine (Propulsive Settling, 1-Burn Mission)

3.6.1 <u>HARDWARE WEIGHTS.</u> The high tank pressures required to meet engine inlet pressure requirements (Figures 3-1 through 3-3) are in excess of current Centaur tank pressure levels. Tank weight increases as a function of tank pressures were generated for this study by the analysis of Reference 3-17.

Subcooler weights were calculated based on skin thicknesses and materials used in NAS3-17802, Reference 3-12, and the dimensions given in Section 3.3 and 3.4.

Weights shown in Tables 3-10, 3-11 and 3-12 assume that subcooler cold side flow is dumped overboard. This is the main option considered as stated in the work statement of the contract.

Some additional work was done to determine the possible advantage of pumping subcooler coolant back into the tank. This system uses a surge tank or accumulator to collect the cold side fluid and a compressor to condense the cold side vapor and pump it back into the tank. Rough estimates indicate that this system will have a total weight penalty of approximately $23 \, kg_m (50 \, lb_m)$ for both LO_2 and LH_2. Substantial reductions are also possible in tank skin weights since returning subcooler flow to the tank stabilizes tank pressure during outflow. This will allow reduced initial tank pressures. Also reduced will be subcooler size since this is based upon conditions at the end of the first burn for the one burn mission. (This pressure will increase if coolant is pumped back into the tank.) Approximate weight penalties were generated for two additional options using subcooler coolant recompression and return to the tank. These are; subcoolers, with peroxide settling, coolant return, and dry feedlines. and subcoolers with passively cooled capillary acquisition, coolant return and dry feedlines. Inspection of Tables 3-10, 3-11 and 3-12 indicated the superiority of the Category I engine. Tables 3-13, 3-14 and 3-15 give the weight comparisons for Category I engine and the 1, 2 and 5 burn mission respectively. These tables indicate that, for the five burn mission, weight advantages of approximately 91 kg (200 lbs) (subcooler weights will be reduced from those shown in the table) are possible using thermal subcooling with coolant pumped back into the tank, capillary acquisition and dry feedlines. Results of NAS3-17802, Reference 3-12, showed a weight advantage of 107 kg (238 lbs) for a passively cooled capillary device using boost pumps for providing engine NPSP and thermal subcoolers for providing boost pump NPSP with subcooler coolant pumped back into the tank, compared to the baseline Centaur D-1S system.

Baseline D-1S system weight details (boost pumps, propellant supply lines, etc.) were obtained from current Centaur Weight Group tabulations. Propulsive settling system and pressurization system weights were taken from Reference 3-12.

3.6.2 <u>FLUID WEIGHT PENALTIES.</u> The fluid weight penalties are, in general, more severe than the hardware weight penalties for the subcooler system concepts, as seen in Tables 3-11 and 3-12. Table 1-4 payload partials were used.

Table 3-10. Baseline D-1S Payload Weight Penalties for System Concept Comparison, kg (lb)

	1-Burn	2-Burn	5-Burn
1. Tank skin Δ weight over baseline: LH$_2$	-	-	-
LO$_2$	-	-	-
2. Subcooler: LH$_2$	-	-	-
LO$_2$	-	-	-
3. Propellant supply ducts: LH$_2$	13 (28)	13 (28)	13 (28)
LO$_2$	11 (25)	11 (25)	11 (25)
4. Hardware to keep supply ducts wet: LH$_2$	-	-	-
LO$_2$	-	-	-
5. Passive screen acquisition device LH$_2$	-	-	-
LO$_2$	-	-	-
6. Boost Pump: LH$_2$	39 (85)	39 (85)	39 (85)
LO$_2$	29 (64)	29 (64)	29 (64)
7. Sump assembly: LH$_2$	6 (14)	6 (14)	6 (14)
LO$_2$	8 (17)	8 (17)	8 (17)
8. Settling system incl. H$_2$O$_2$ penalty	40 (89)	49 (109)	75 (165)
9. Pressurization system	119 (262)	140 (308)	196 (431)
10. H$_2$O$_2$ usage - boost pumps	9 (20)	6 (14)	8 (18)
11. Subcooler volume tanking penalty: LH$_2$	-	-	-
LO$_2$	-	-	-
12. Subcooler cold side propellant loss: LH$_2$	-	-	-
LO$_2$	-	-	-
13. Engine chilldown propellants: LH$_2$	8 (18)	11 (25)	11 (24)
LO$_2$	2 (4)	2 (5)	3 (7)
14. Duct chilldown propellants: LH$_2$			
LO$_2$			
15. Fluid to keep ducts wet: LH$_2$	-	-	-
LO$_2$	-	-	-
16. Excess LO$_2$ in line over chilldown	-	-	-
17. Lower tanking density penalty: LH$_2$	-	-	-
LO$_2$	-	-	-
18. Residual left in subcooler cold side: LH$_2$	-	-	-
LO$_2$	-	-	-
TOTALS	284 (626)	314 (694)	399 (878)

Table 3-11. Subcoolers With Settling, Payload Weight Penalties For System Concept Comparison, kg (lb)

	Category I Engine			RL10A-3-3A Engine			RL10A-3-3 Engine		
	1-Burn	2-Burn	5-Burn	1-Burn	2-Burn	5-Burn	1-Burn	2-Burn	5-Burn
1. Tank skin Δweight over baseline: LH_2	3 (7)	3 (7)	28 (62)	42 (93)	55 (122)	70 (154)	55 (122)	72 (158)	97 (213)
LO_2	5 (10)	9 (20)	9 (20)	27 (59)	31 (69)	36 (79)	36 (79)	40 (89)	49 (109)
2. Subcooler: LH_2	14 (30)	14 (30)	14 (30)	18 (40)	18 (40)	18 (40)	49 (107)	49 (107)	49 (107)
LO_2	27 (60)	27 (60)	27 (60)	13 (29)	13 (29)	13 (29)	20 (43)	20 (43)	20 (43)
3. Propellant supply ducts: LH_2	18 (40)	18 (40)	18 (40)	18 (40)	18 (40)	18 (40)	10 (23)	10 (23)	10 (23)
LO_2	14 (31)	14 (31)	14 (31)	14 (31)	14 (31)	14 (31)	10 (23)	10 (23)	10 (23)
4. Hardware to keep supply ducts wet: LH_2	-	-	-	-	-	-	-	-	-
LO_2	-	-	-	-	-	-	-	-	-
5. Passive screen acquisition device: LH_2	-	-	-	-	-	-	-	-	-
LO_2	-	-	-	-	-	-	-	-	-
6. Boost pump: LH_2	-	-	-	-	-	-	-	-	-
LO_2	-	-	-	-	-	-	-	-	-
7. Sump assembly: LH_2	3 (7)	3 (7)	3 (7)	3 (7)	3 (7)	3 (7)	3 (7)	3 (7)	3 (7)
LO_2	7 (15)	7 (15)	7 (15)	7 (15)	7 (15)	7 (15)	7 (15)	7 (15)	7 (15)
8. Settling system incl H_2O_2 penalty	40 (89)	49 (109)	75 (165)	40 (89)	49 (109)	75 (165)	40 (89)	49 (109)	75 (165)
9. Pressurization system	-	-	-	-	-	-	-	-	-
10. H_2O_2 usage – boost pumps	-	-	-	-	-	-	-	-	-
11. Subcooler volume tanking penalty: LH_2	2 (5)	2 (4)	1 (3)	3 (6)	3 (6)	2 (4)	10 (21)	9 (19)	6 (14)
LO_2	7 (16)	6 (14)	5 (10)	4 (8)	3 (7)	2 (5)	5 (11)	5 (10)	3 (7)
12. Subcooler cold side propellant loss: LH_2	54 (118)	47 (104)	41 (91)	88 (194)	77 (170)	64 (142)	188 (414)	179 (394)	144 (318)
LO_2	512 (1127)	493 (1087)	458 (1009)	418 (920)	383 (843)	359 (790)	657 (1448)	568 (1251)	520 (1146)
13. Engine chilldown propellant: LH_2	8 (18)	11 (25)	11 (24)	8 (18)	11 (25)	11 (24)	8 (18)	11 (25)	11 (24)
LO_2	2 (4)	2 (5)	3 (7)	2 (4)	2 (5)	3 (7)	2 (4)	2 (5)	3 (7)
14. Duct chilldown propellants: LH_2	4 (8)	5 (12)	11 (25)	4 (8)	5 (12)	11 (25)	2 (5)	3 (7)	6 (14)
LO_2	3 (7)	6 (13)	15 (32)	3 (7)	6 (13)	15 (32)	2 (5)	5 (10)	10 (23)
15. Fluid to keep ducts wet: LH_2	-	-	-	-	-	-	-	-	-
LO_2	-	-	-	-	-	-	-	-	-
16. Excess LO_2 in lines over chilldown	-	-	-	-	-	-	-	-	-
17. Lower tanking density penalty: LH_2	-	-	23 (50)	37 (82)	51 (113)	69 (151)	46 (101)	69 (151)	86 (189)
LO_2	-	67 (148)	101 (223)	270 (594)	337 (742)	387 (853)	370 (816)	438 (965)	505 (1113)
18. Residual left in subcooler coldside: LH_2	5 (12)	5 (12)	5 (11)	7 (16)	7 (16)	6 (14)	24 (53)	23 (51)	21 (46)
LO_2	98 (216)	94 (207)	84 (184)	45 (99)	43 (95)	38 (84)	80 (176)	61 (135)	54 (119)
TOTALS	826 (1820)	882 (1950)	953 (2099)	1071 (2359)	1136 (2509)	1221 (2691)	1624 (3580)	1633 (3597)	1689 (3725)

Table 3-12. Subcooler With Screen Acquisition and Wet Feedlines, Payload Weight Penalties for System Concept Comparisons, kg (lb)

3-43

	Category I Engine			RL10A-3-3A Engine			RL10A-3-3 Engine		
	1-Burn	2-Burn	5-Burn	1-Burn	2-Burn	5-Burn	1-Burn	2-Burn	5-Burn
1. Tank skin Δ weight over baseline: LH_2	3 (7)	3 (7)	28 (62)	42 (93)	55 (122)	70 (154)	55 (122)	72 (158)	97 (213)
LO_2	5 (10)	9 (20)	9 (20)	27 (59)	31 (69)	36 (79)	36 (79)	40 (89)	49 (109)
2. Subcooler: LH_2	14 (30)	14 (30)	14 (30)	18 (40)	18 (40)	18 (40)	49 (107)	49 (107)	49 (107)
LO_2	27 (60)	27 (60)	27 (60)	13 (29)	13 (29)	13 (29)	20 (43)	20 (43)	20 (43)
3. Propellant supply ducts: LH_2	18 (40)	18 (40)	18 (40)	18 (40)	18 (40)	18 (40)	10 (23)	10 (23)	10 (23)
LO_2	14 (31)	14 (31)	14 (31)	14 (31)	14 (31)	14 (31)	10 (23)	10 (23)	10 (23)
4. Hardware to keep supply ducts wet: LH_2	16 (35)	16 (35)	16 (35)	16 (36)	16 (36)	16 (36)	16 (36)	16 (36)	16 (36)
LO_2	9 (19)	9 (19)	9 (19)	4 (9)	4 (9)	4 (9)	5 (12)	5 (12)	5 (12)
5. Passive screen acquisition device: LH_2	55 (121)	55 (121)	55 (121)	55 (121)	55 (121)	55 (121)	55 (121)	55 (121)	55 (121)
LO_2	15 (32)	15 (32)	15 (32)	15 (32)	15 (32)	15 (32)	15 (32)	15 (32)	15 (32)
6. Boost Pump: LH_2	-	-	-	-	-	-	-	-	-
LO_2	-	-	-	-	-	-	-	-	-
7. Sump Assembly: LH_2	3 (7)	3 (7)	3 (7)	3 (7)	3 (7)	3 (7)	3 (7)	3 (7)	3 (7)
LO_2	7 (15)	7 (15)	7 (15)	7 (15)	7 (15)	7 (15)	7 (15)	7 (15)	7 (15)
8. Settling system incl H_2O_2 penalty	-	-	-	-	-	-	-	-	-
9. Pressurization system	-	-	-	-	-	-	-	-	-
10. H_2O_2 usage - boost pumps	-	-	-	-	-	-	-	-	-
11. Subcooler volume tanking penalty: LH_2	2 (5)	2 (4)	1 (3)	3 (6)	3 (6)	2 (4)	10 (21)	9 (19)	6 (14)
LO_2	7 (16)	6 (14)	5 (10)	4 (8)	3 (7)	2 (5)	5 (11)	5 (10)	3 (7)
12. Subcooler cold side propellant loss: LH_2	54 (118)	47 (104)	41 (91)	88 (194)	77 (170)	64 (142)	188 (414)	179 (394)	144 (318)
LO_2	512 (1127)	493 (1087)	458 (1009)	418 (920)	383 (843)	359 (790)	657 (1448)	568 (1251)	520 (1146)
13. Engine chilldown propellant: LH_2	8 (18)	11 (25)	11 (24)	8 (18)	11 (25)	11 (24)	8 (18)	11 (25)	11 (24)
LO_2	2 (4)	2 (5)	3 (7)	2 (4)	2 (5)	3 (7)	2 (4)	2 (5)	3 (7)
14. Duct chilldown propellants: LH_2	-	-	-	-	-	-	-	-	-
LO_2	-	-	-	-	-	-	-	-	-
15. Fluid to keep ducts wet: LH_2	Negligible	1 (1)	1 (2)	Negligible	1 (1)	1 (2)	Negligible	1 (1)	1 (2)
LO_2	Negligible	1 (1)	1 (1)	Negligible	1 (1)	1 (2)	Negligible	1 (1)	1 (2)
16. Excess LO_2 in lines over chilldown	26 (57)	64 (140)	179 (394)	28 (62)	69 (151)	194 (428)	33 (73)	80 (176)	226 (497)
17. Lower tanking density penalty: LH_2	-	-	23 (50)	37 (82)	51 (113)	69 (151)	46 (101)	69 (151)	86 (189)
LO_2	-	67 (148)	101 (223)	270 (594)	337 (742)	387 (853)	370 (816)	438 (965)	505 (1113)
18. Residual left in subcooler cold side: LH_2	5 (12)	5 (12)	5 (11)	7 (16)	7 (16)	6 (14)	24 (53)	23 (51)	21 (46)
LO_2	98 (216)	94 (207)	84 (184)	45 (99)	43 (95)	38 (84)	80 (176)	61 (135)	54 (119)
TOTALS	900 (1980)	983 (2165)	1128 (2481)	1142 (2515)	1237 (2726)	1406 (3099)	1704 (3755)	1749 (3850)	1917 (4225)

Table 3-13. Weight Comparison of Propellant Feed Options for Single Burn Mission, Payload Penalty, kg (lb)

Weight Penalty Element	Option 1		Option 2		Option 3		Option 4		Option 5	
1. Tank Skin Delta	–		8	(17)	8	(17)	8	(17*)	8	(17*)
2. Subcooler	–		41	(90)	41	(90)	41	(90)	41	(90)
3. Supply Ducts	24	(53)	32	(71)	32	(71)	32	(71)	32	(71)
4. Wet Duct Hardware	–		–		25	(54)	–		–	
5. Capillary Device	–		–		69	(153)	–		69	(153)
6. Boost Pumps	68	(149)	–		–		–		–	
7. Sumps	14	(31)	10	(22)	10	(22)	10	(22)	10	(22)
8. Peroxide Settling System	40	(89)	40	(89)	–		40	(89)	–	
9. Pressurization System	119	(262)	–		–		–		–	
10. Boost Pump Peroxide	9	(20)	–		–		–		–	
11. Subcooler Volume	–		19	(21)	10	(21)	10	(21)	10	(21)
12. Subcooler Cold Side Flow	–		565	(1245)	565	(1245)	23	(50*)	23	(50*)
13. Engine Chilldown	10	(22)	10	(22)	10	(22)	10	(22)	10	(22)
14. Duct Chilldown	–		7	(15)	–		7	(15)	7	(15)
15. Fluid to Keep Ducts Wet	–		–		–*		–		–	
16. Excess LO_2 In Lines	–		–		26	(57)	–		–	
17. Tanking Density	–		–		–		–		–	
18. Subcooler Cold Side Residual	–		104	(228)	104	(228)	104	(228)	104	(228)
TOTAL	284	(626)	827	(1820)	900	(1980)	285	(625)	314	(689)

* Approximate

Option 1   Baseline Centaur D-1S with Boost Pumps, Pressurization and Settling Rockets
Option 2   Thermal Subcooling with Settling Rockets
Option 3   Thermal Subcooling with Capillary Acquisition and Wet Feedlines
Option 4   Thermal Subcooling with Coolant Pumped Back into the Tank and Settling Rockets
Option 5   Thermal Subcooling with Coolant Pumped Back into the Tank, Capillary Acquisition and Dry Feedline

Options 2 through 5 use the Category I Engine
Option 1 uses the Existing RL10A-3-3 Engine

Table 3-14. Weight Comparison of Propellant Feed Options for Two Burn Mission, Payload Penalty, kg (lb)

Weight Penalty Element	Option				
	1	2	3	4	5
1. Tank Skin Delta	–	12 (27)	12 (27)	8 (17)	8 (17*)
2. Subcooler	–	41 (90)	41 (90)	41 (90)	41 (90)
3. Supply Ducts	24 (53)	32 (71)	32 (71)	32 (71)	32 (71)
4. Wet Duct Hardware	–	–	25 (54)	–	–
5. Capillary Device	–	–	69 (153)	–	69 (153)
6. Boost Pumps	68 (149)	–	–	–	–
7. Sumps	14 (31)	10 (22)	10 (22)	10 (22)	10 (22)
8. Peroxide Settling System	49 (109)	49 (109)	–	49 (109)	–
9. Pressurization System	140 (308)	–	–	–	–
10. Boost Pump Peroxide	6 (14)	–	–	–	–
11. Subcooler Volume	–	8 (18)	8 (18)	8 (18)	8 (18)
12. Subcooler Cold Side Flow	–	541 (1191)	541 (1191)	23 (50*)	23 (50*)
13. Engine Chilldown	14 (30)	14 (30)	14 (30)	14 (30)	14 (30)
14. Duct Chilldown	–	11 (25)	–	11 (25)	11 (25)
15. Fluid to Keep Ducts Wet	–	–	1 (2)	–	–
16. Excess LO$_2$ in Lines	–	–	64 (140)	–	–
17. Tanking Density	–	67 (148)	67 (148)	–*	–*
18. Subcooler Cold Side Residual	–	99 (219)	99 (219)	99 (219)	99 (219)
TOTAL	315 (694)	884 (1950)	983 (2165)	295 (651)	315 (695)

* Approximate

Option 1 Baseline Centaur D-1S with Boost Pumps, Pressurization and Settling Rockets
Option 2 Thermal Subcooling with Settling Rockets
Option 3 Thermal Subcooling with Capillary Acquisition and Wet Feedlines
Option 4 Thermal Subcooling with Coolant Pumped Back into the Tank and Settling Rockets
Option 5 Thermal Subcooling with Coolant Pumped Back into the Tank, Capillary Acquisition and Dry Feedline

Options 2 through 5 Use the Category I Engine
Option 1 Uses the RL 10A-3-3 Engine

Table 3-15. Weight Comparison of Propellant Feed Options for Five Burn Mission, Payload Penalty, kg (lb)

Weight Penalty Element	Option				
	1	2	3	4	5
1. Tank Skin Delta	–	37 (82)	37 (82)	8 (17*)	8 (17*)
2. Subcooler	–	41 (90)	41 (90)	41 (90)	41 (90)
3. Supply Ducts	24 (53)	32 (71)	32 (71)	32 (71)	32 (71)
4. Wet Duct Hardware	–	–	25 (54)	–	–
5. Capillary Device	–	–	69 (153)	–	69 (153)
6. Boost Pumps	68 (149)	–	–	–	–
7. Sumps	14 (31)	10 (22)	10 (22)	10 (22)	10 (22)
8. Peroxide Settling System	75 (165)	75 (165)	–	75 (165)	–
9. Pressurization System	196 (431)	–	–	–	–
10. Boost Pump Peroxide	8 (18)	–	–	–	–
11. Subcooler Volume	–	6 (13)	6 (13)	6 (13)	6 (13)
12. Subcooler Cold Side Fow	–	499 (1100)	499 (1100)	23 (50*)	23 (50*)
13. Engine Chilldown	14 (31)	14 (31)	14 (31)	14 (31)	14 (31)
14. Duct Chilldown	–	26 (57)	–	26 (57)	26 (57)
15. Fluid to Keep Ducts Wet	–	–	1 (3)	–	–
16. Excess LO_2 in Lines	–	–	179 (394)	–	–
17. Tanking Density	–	124 (273)	124 (273)	–*	–*
18. Subcooler Cold Side Residual	–	89 (195)	89 (195)	89 (195)	89 (195)
TOTAL	399 (878)	953 (2099)	1126 (2481)	324 (711)	318 (699)

*Approximate

Option 1   Baseline Centaur D-1S with Boost Pumps, Pressurization and Settling Rockets

Option 2   Thermal Subcooling with Settling Rockets

Option 3   Thermal Subcooling with Capillary Acquisition and Wet Feedlines

Option 4   Thermal Subcooling with Coolant Pumped Back into the Tank and Settling Rockets

Option 5   Thermal Subcooling with Coolant Pumped Back into the Tank, Capillary Acquisition and Dry Feedline

Option 2 through 5 use the Category I Engine

Option 1 uses the existing RL10A-3-3 Engine

The penalty for not tanking propellants because of subcooler volume is much more severe for LO_2 than for LH_2 because of its high density. The weight penalties shown are based on the assumptions that the hot sides of both subcoolers are filled during tanking and that the LO_2 subcooler cold side can be primed and filled during tanking by using the recirculation pump.

LH_2 subcooler cold side losses are those of Table 3-9. Penalties on Tables 3-10, 3-11 and 3-12 are for subcooler cold side propellant dumped overboard. Approximate weights of Tables 3-13, 3-14 and 3-15 use a system to return coolant to the tank.

Engine and duct chilldown penalties (Reference 3-5) and fluid used to keep the lines wet between burns (Section 3.2.3.2) are all seen to be quite low. However, the penalty for unsubcooled LO_2 in the line which must be removed prior to engine start (Section 3.2.3.1) is seen to be large).

One of the more severe penalties accompanying high tank pressures is the reduction in propellants tanked because of the lower liquid density at higher tanking pressures. The higher tank pressures are required because of the blowdown nature of the outflow. When subcooler coolant is pumped back into the tank, the tank pressures will be stabilized during outflow allowing the initial tank pressures to be reduced. This will considerably reduce the liquid density penalty due to higher tanking pressures. Another significant penalty of the subcooler concept is the residual propellant remaining in the cold side of the subcooler at the end of the last firing.

3.6.3 WEIGHT COMPARISON BY SYSTEM CONCEPT. Weights of all three system concepts that dump subcooler cold side fluid overboard can be compared by comparing weight totals for corresponding mission and engine columns of Tables 3-10, 3-11 and 3-12. The subcooler system employing settling is seen to be lighter than the system of screen acquisition and wet propellant ducts. One of the major wet duct penalties is the insufficiently subcooled LO_2 residing in the feedlines between burns which must be consumed or dumped prior to each start.

Weights of both subcooler concepts are seen to be higher than the baseline D-1S. The system used with the Category I engine (lowest NPSP requirement) is seen to have the lowest weight of the three engine systems and the only one which comes close to the baseline D-1S. The major weight penalties incurred by the subcooler concepts are the LH_2 subcooler cold side fluid loss, the lower tanking density penalty and the residual left in the subcooler cold side.

Pumping cold side fluid from the thermal subcooler back into the tank can provide an overall weight advantage over the baseline system if dry feedlines are used (to eliminate the dumping of unsubcooled LO_2.) The weights of the five system concepts (or options) are shown in Tables 3-13, 3-14 and 3-15 for the RL10 category I engine. Comparisons show that substantial weight advantages are possible for the 5 burn mission using

3-47

thermal subcooling to replace the boost pumps and pressurization systems, passively cooled capillary acquisition devices to replace the peroxide settling system, a subcooler recompression system to return cold side fluid to the tank, and uncooled feedlines.

More work is required to define tank pressure profiles during coolant return and engine firing. Additional work is also required to define the accumulator and compressor requirements for the coolant return system in order to make more accurate comparisons between concepts employing subcooler coolant return and the baseline Centaur D-1S system. These comparisons might allow subcoolers to be sized at higher tank pressure conditions, reducing subcooler weight and cold side residuals.

4

THERMODYNAMIC VENT MIXER ANALYSIS

Centaur/Shuttle integration studies have indicated the importance of using a thermo-dynamic vent system for controlling tank pressure while in the Shuttle cargo bay and in low gravity, particularly when the tanks are relatively full. Centaur/Tug deriva-tives require the use of thermodynamic vent systems. The thermodynamic vent/mixer analysis performed on the current study is the initial effort required to bring the vent system to a fully operational flight status. This work is preparatory to the procurement of hardware, flight qualification and flight of a noninterference LH_2 vent system on a future Centaur flight.

A thermodynamic vent system is a system for venting only vapor in low gravity, regardless of the phase of the fluid entering the system. The system, shown schematic-ally in Figure 4-1, throttles the inlet fluid to a lower temperature and pressure than the surrounding tank fluid. The hot side tank fluid is then pumped over the throttled fluid in a heat exchanger to vaporize any liquid initially present in the vent stream. The vapor is then vented overboard. The pump provides forced convection on the hot side of the heat exchanger as well as mixing flow for destratifying the tank contents. Destratification is vital if removal of fluid from the liquid pool (for venting) is to result in tank pressure reductions.

The feasibility of this concept has been demonstrated in ground testing using a compact LH_2 bulk heat exchanger (NAS8-20146, GD Convair, Ref. 4-1; NAS3-7942, LMSC, Ref. 4-2), with a compact LO_2 bulk heat exchanger (NAS8-26972, GD Convair, Ref. 4-3) and using a wall heat exchanger (NAS3-16979, LMSC, Ref. 4-4).

Results from these ground tests led to the following conclusions; (1) the thermodynamic vent concept will vent vapor only with either vapor or liquid at the vent inlet, (2) the compact heat exchanger concept is more efficient than the wall heat exchanger and (3) the effectiveness of the compact heat exchanger system could be improved with a better understanding of tank mixing and the use of less conservative mixing correlations.

Because of the importance of understanding tank mixing, effort in this study concentra-ted on reviewing existing information on mixing of fluids in order to develop an analysis that can be used to size mixers for the destratification of cryogenic liquids. The mixing correlation providing the best fit of the data was incorporated into the existing Convair computer program CHEAP (Cryogenic Heat Exchanger Analysis Program). This program was then used to size LH_2 thermodynamic vent systems for candidate Centaur and Centaur/Tug derivatives described in Section 4.1.
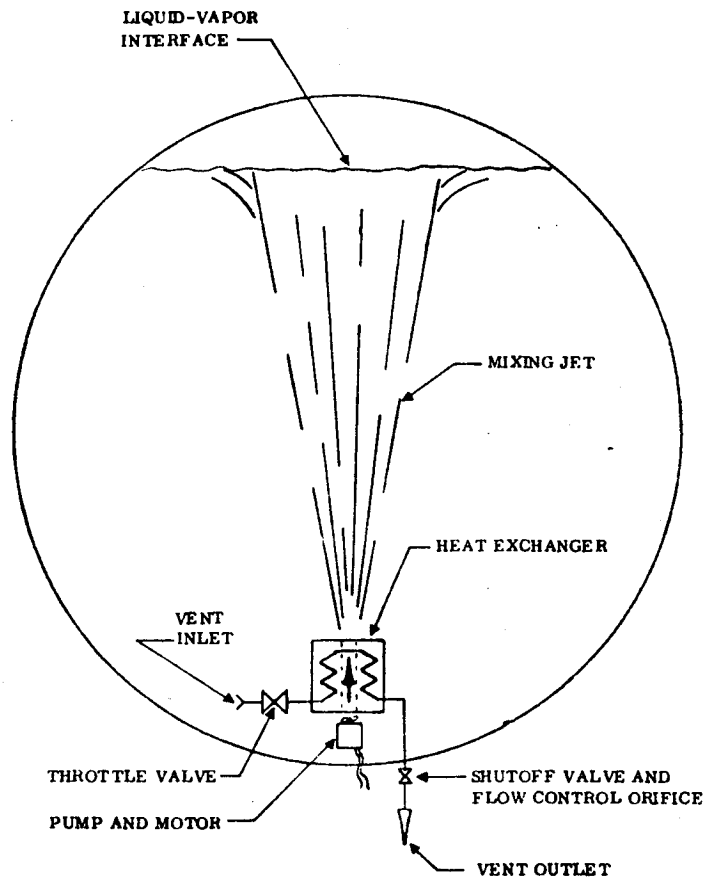
Figure 4-1. Compact Heat Exchanger Vent System Schematic

4.1 GROUND RULES

The baseline configuration for this study was the Centaur D-1S as defined in Reference 4-5. The Centaur D-1S is a minimum modification Centaur D-1T designed to be compatible with Space Shuttle.

In addition to this vehicle, all versions of Shuttle based Centaur were considered in order to define worst case thermodynamic vent/mixer design requirements. Both reusable and expendable Centaur Interim Upper Stage Vehicles were considered. Three tank sizes were defined for each expendable and reusable version (a total of six vehicles). The expendable versions are similar to the Centaur D-1S in the areas of thermal protection, fill and drain and propulsion. The reusable versions have Superfloc insulation. Vehicle conditions affecting thermodynamic vent system sizing were determined based on information developed in Reference 4-6. The baseline Space Tug

configuration (Ref. 4-7) was also included in evaluation of thermodynamic vent system design conditions.

The objective of the vehicle evaluation was to develop worst case thermodynamic design conditions. This was to allow a single vent system to be designed to meet all vehicle and mission conditions and thus eliminate the need for requalification of new hardware for a specific vehicle.

Because of this approach, Centaur D-1T conditions were also considered in designing the thermodynamic vent system. Studies performed in Reference 4-8 illustrated the desirability of using a thermodynamic vent system for extending mission performance for Centaur D-1T advanced multiburn missions.

4.2 MIXING ANALYSIS

Experiments using a jet mixing device to eliminate stratification or to blend fluids have been conducted in the aerospace and petro-chemical industry with both cryogenic and non-cryogenic fluids. Ability of the jet to penetrate the stratified layer and the time required to completely mix the tank have been the primary criteria in evaluating the mixing experiments. These are also the primary criteria required in sizing the thermodynamic zero-g vent system.

4.2.1 MIXING EXPERIMENTAL METHODS – Jet mixing experiments have taken several forms in order to provide the mixing data required by the experimenter. The primary evaluation criteria for determining the performance of the jet mixing system is mixing time. Methods used for measuring mixing time included:

      a. Chemical reaction
      b. Electrolyte addition
      c. Dye motion
      d. Residual temperature
      e. Pressure decay

Fox and Gex (Ref. 4-9) derived their mixing time equation from experimental data obtained with a visual color-disappearance (chemical reaction) technique. This technique consisted of filling a tank with a known amount of NaOH and adding phenolphthalein to give the fluid a deep red color. The same gram molecular weight of HCℓ was added to the tank and the axial jet mixer was turned on. The time interval required for all the red color to disappear was defined as the mixing time.

Fossett and Prosser (Ref. 4-10) studied mixing of an aqueous Na_2CO_3 solution in tanks by jets. A pair of electrodes was located in the tank with second pair outside the tank in a sample of Na_2CO_3 solution whose concentration was the expected final average in the tank. These two electrodes were used as arms in an a.c. bridge circuit in which a galvanometer was used to detect unbalanced bridge potential. Time

for mixing was the time for injecting the Na_2CO_3 solution, plus the time to obtain a zero galvanometer deflection indicating the tank solution was equivalent in concentration to the sample solution.

Okita and Oyama (Ref. 4-11) conducted jet mixing tests similar to those of Fossett and Prosser. Two conductivity probes were used in a Wheatstone bridge to determine the time to obtain the same conductivity at the two probe locations after injections of a pulse of $NaCl$ solution.

Poth (Ref. 4-12) ran tests in water using dye movement in an open lucite tank and tests using residual temperature difference in pressurized water in a closed tank. In the open tank testing, heaters were used to generate a stratified layer into which dye was injected. Mixing time was measured as the time of initiation of dye movement until the time the dye level reached the jet outlet. In the closed tank testing a stratified layer was developed with the use of heaters. Mixing time was measured from the time the pump was actuated until the time the residual temperature difference was ten percent of the initial stratification level. VanHook (Ref. 4-13) used the same residual temperature criteria for mixing time measurements on the large scale open tank water tests.

Lovrich (Ref. 4-14) used Freon in closed tanks of various sizes on a centrifuge at various acceleration levels greater than 1-g. Heaters were used to simulate wall heat leakage. Tank pressure and Freon temperature measurements were made primarily for the purpose of establishing stratification scaling data. An axial flow mixing jet was installed to destratify the tank upon completion of the stratification build-up. No mixing time measurements were reported.

An experimental investigation of the forced circulation pattern at zero gravity using an axial jet in Centaur configured tanks was conducted by the NASA/LeRC during the latter part of 1975. These currently unpublished test results were obtained using a 10 cm diameter tank with a 0.4 cm axial jet. The test fluid was ethanol and a dye was injected in the mixing jet. Motion pictures of several of the tests taken by a high speed camera were supplied to Convair for evaluation of mixing performance.

Cryogenic testing in LH_2 at normal gravity of a propellant tank vent/mixer unit designed for zero gravity was completed by Convair in 1967 (Ref. 4-1) and 1970 (Ref. 4-15) and by Lockheed in 1972 (Ref. 4-2). In each case, mixing performance was evaluated based on the time required to reach a predetermined value of pressure decay. The tank was considered mixed when the tank pressure reached a value equal to the vapor pressure at the bulk mixed temperature or when the pressure decay rate was equivalent to the homogeneous pressure decay rate. Cryogenic testing of an LO_2 vent system was also conducted by Convair. Mixing time evaluation of the test data (Ref. 4-3) was based on the same criteria as defined for the LH_2 tests conducted at Convair.

4.2.2 EVALUATION OF MIXING TIME DATA - Mixing time information is given in all the aforementioned experiments except for that of Lovrich (Ref. 4-14) and the

NASA/LeRC drop test program. In the data presented by Lovrich the sizing of the mixing jet was such that complete mixing of the tank was not accomplished in the cases where the heaters remained on. Only in the cases where the heaters were turned off was mixing accomplished. In addition, there was no venting of the tank so these data could not be considered in the evaluation of mixing time during venting.

Evaluation of mixing time in the NASA/LeRC tests was based on dye movement measurements made from the high speed motion picture data of several representative cases supplied by NASA/LeRC. Mixing time was defined as the time from the initiation of the jet flow until the dye layer would reach the tank bottom. Test runs had insufficient drop time to allow the dye layer to reach the tank bottom. Thus, interface velocities prior to the cessation of low gravity were used to extrapolate the time that the dye layer would reach the tank bottom.

The dye movement in general proceeded from the jet outlet, spread at approximately a 0.44 radian (25 degree) angle until it reached the surface where it spread toward the wall. Upon reaching the wall, the dye movement advanced at a fairly uniform rate until the end of the run. The velocity of the dye interface was measured as indicated in Figure 4-2. The distance that the dye interface moved is $x_2 - x_1$. The time required for this movement is $\theta_2 - \theta_1$. The dye interface velocity is $(x_2 - x_1)/(\theta_2 - \theta_1)$. The time required for the dye interface to reach the tank bottom is $[x_3/(x_2 - x_1)][\theta_2 - \theta_1] = \theta_T$. Table 4-1 presents the mixing times determined from the film data supplied by NASA/LeRC.

4.2.3 MIXING TIME CORRELATION - Correlation of the mixing time cited in Sections 4.2.1 and 4.2.2 has yielded the following three unique mixing time relationships.

Fox and Gex (Reference 4-9)

Table 4-1. Mixing Time

Run No.	Per-cent Fill	Jet Flow Rate (ml/sec)	Mixing Time (sec)
N-5-7	57	2.1	- *
N-5-3	70	3.0	- *
N-5-8	57	4.3	16.92
N-5-9	35	4.75	9.48
N-5-11	56	6.15	11.2
N-6-1	30	6.17	7.8

* Insufficient time to establish dye interface movement.

$$\theta_m = \frac{118 \, Y^{1/2} \, D_t}{(V_j D_j)^{4/6} \, g_c^{1/6}} \left[\frac{V_j D_j \, \rho}{\mu} \right]^{-1/6}$$
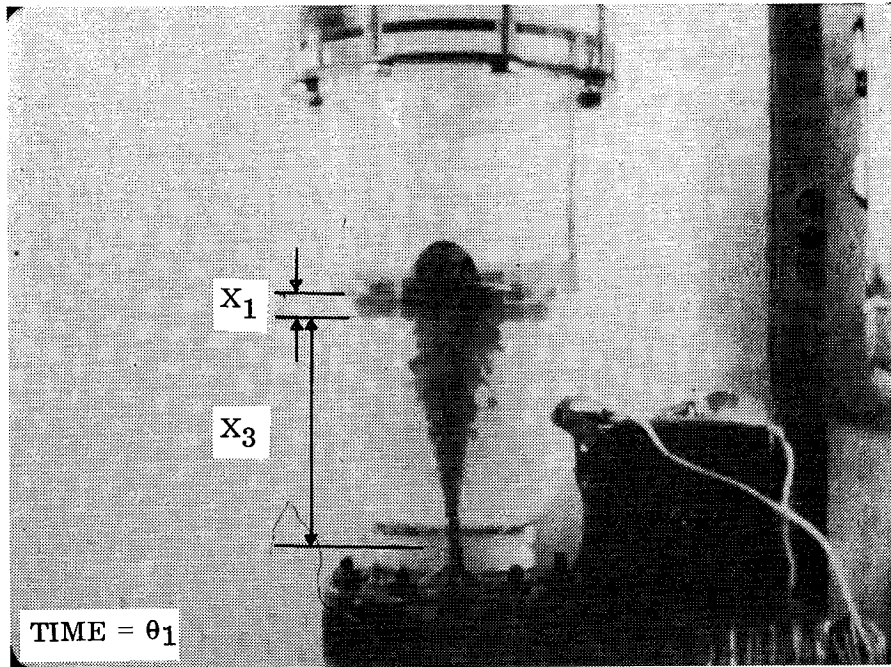
where

θ_m is the mixing time, sec

Y is the liquid height, ft

D_t is the tank diameter, ft

V_j is the jet velocity, ft/sec

D_j is the jet diameter, ft

TEST CASE
N-5-11
56% FILL
6.15 mℓ/sec
Time 3.2 sec

TIME = θ_1

Time 5.1 sec

TIME = θ_2
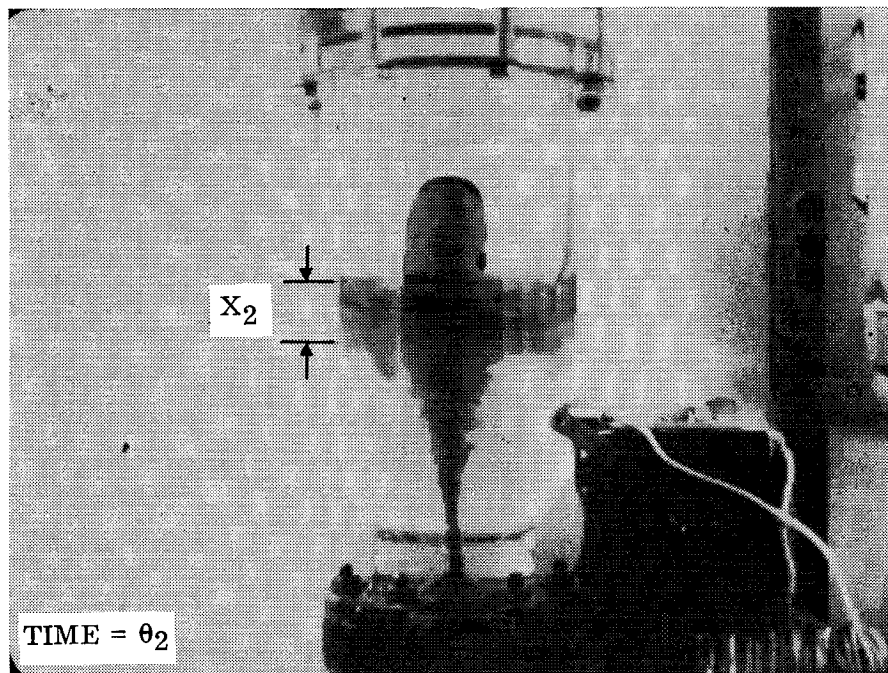
Figure 4-2.   Dye Interface Velocity Measurement

ρ is the density, lb/ft^3

μ is the dynamic viscosity, $lb/sec-ft$

g_c is a dimensional constant, $lb_m\ ft/lb_f\ sec^2$

Fossett and Prosser (Reference 4-10)

$$\theta_m = \frac{9\ D_t^2}{V_j D_j}$$

where

θ_m is the mixing time, sec

D_t is the tank diameter, ft

V_j is the jet velocity, ft/sec

D_j is the jet diameter, ft

and Okita and Oyama (Reference 4-1)

$$\theta_m = \frac{5.2\ V\ D_j}{Q\ Y^{1/2}\ D_t^{1/2}}$$

where

θ_m is the mixing time, sec

V is the tank volume, ft^3

D_t is the tank diameter, ft

Q is the jet flow rate, ft^3/sec

Y is the liquid height, ft

D_j is the jet diameter, ft

Data correlation with the Fox and Gex mixing equation is presented in Figure 4-3. A mixing time factor recommended by Fox and Gex is plotted as a function of the Reynolds number for the mixing jet, $V_j D_j \rho/\mu$. This dimensionless mixing factor is defined as

$$\theta_m = \frac{118 \, Y^{1/2} D_t}{(V_j D_j)^{4/6} g_c^{1/6}} \left[\frac{V_j D_j \, \rho}{\mu} \right]^{-1/6}$$

Legend (on plot):
- ⊙ LO_2 Vent Test
- ⊡ LH_2 Vent Test
- △ H_2O Large Scale
- ◇ H_2O Small Scale
- ⊡ Drop Tower Tests

Y-axis: MIXING FACTOR, $\dfrac{\theta_m (V_j D_j)^{4/6} g_c^{1/6}}{Y^{1/2} D_t}$

X-axis: JET REYNOLDS NUMBER, $(V_j D_j \rho)/u$
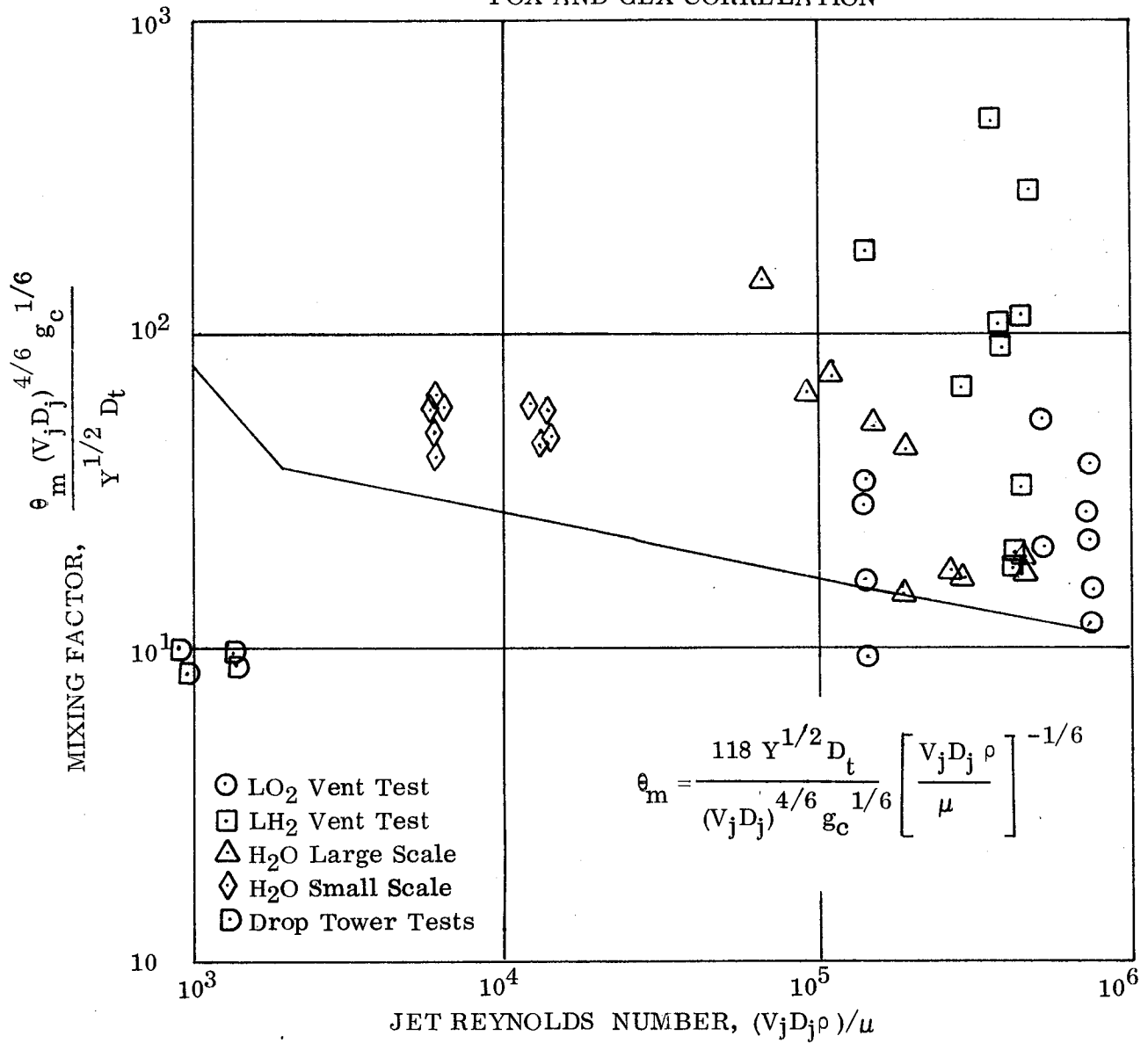
Figure 4-3. Test Data Comparison With Fox and Gex Correlation

$$P_o = \frac{\theta_m (V_j D_j)^{4/6} g_c^{1/6}}{Y^{1/2} D_t}$$

This correlation is slightly dependent upon jet Reynolds Number above 2×10^3 and represents the lower limit of anticipated mixing times. A line with slope, -4/3 represents the correlation in the laminar region and a line with a slope -1/6 denotes the turbulent region in Figure 4-3. The large amount of scatter in the data may be due to differences in definition and measurement of mixing time. In addition, it is reasonable that the effect of density variation in the one-g experiments should result in longer mixing times than those observed by Fox and Gex whose data was obtained with uniform

density fluid. The energy requirements to penetrate the stratified layer could result in longer mixing times. The existence of the stratified layer was part of each experiment reported.

Data correlation, for the mixing experiments under consideration, with the Fossett and Prosser mixing equation is presented in Figure 4-4. A mixing time factor recommended by Fossett and Prosser is plotted as a function of jet Reynolds number. This dimensionless mixing factor is defined as

$$P_o = \frac{\theta_m D_t^2}{V_j D_j}$$

Fossett and Prosser found their data to be independent of the jet Reynolds number yielding a constant mixing factor of nine. The data presented in this figure tend to support the conclusion that the mixing time is independent of the jet Reynolds number. With this correlation there continues to be considerable scatter in the data. This could be in part due to the difference in the experimental methods. In addition there is very weak geometry dependence in this correlation which does not account for considerable differences in geometries between the experiments.

A third correlation is presented by Okita and Oyama. Figure 4-5 presents the mixing data represented by the mixing factor recommended by Okita and Oyama and plotted as a function jet Reynolds number. The mixing factor is defined as

$$P_o = \frac{\theta_m Y^{1/2} D_t^{1/2} Q}{V D_j}$$

This correlation is also found to be independent of jet Reynolds number for data with a jet Reynolds number greater than 5×10^3. This correlation has a greater geometry dependence than the Fossett and Prosser equation as well as an incorporation of a volume turn-over relationship. Use of this mixing factor reduces the amount of scatter in the experimental data. Scatter continues to be a problem partially attributable to differences in experimental procedure and definition of mixing time. With regards to the LO_2 vent test data (Ref. 4-3), the Okita and Oyama correlation provides a conservative prediction of the mixing time for all data points where the jet discharge is directed toward the liquid vapor interface.

The Okita and Oyama correlation gave the best fit through the available data, defined a mixing factor with the least scatter, and gave a conservative estimate compared to recently acquired drop test data. (Table 4-2 presents a tabulation of the drop test data parameters used for mixing time correlation.) The Okita and Oyama correlation therefore was chosen as the mixing time correlation to be incorporated into the zero-g vent system sizing computer program.
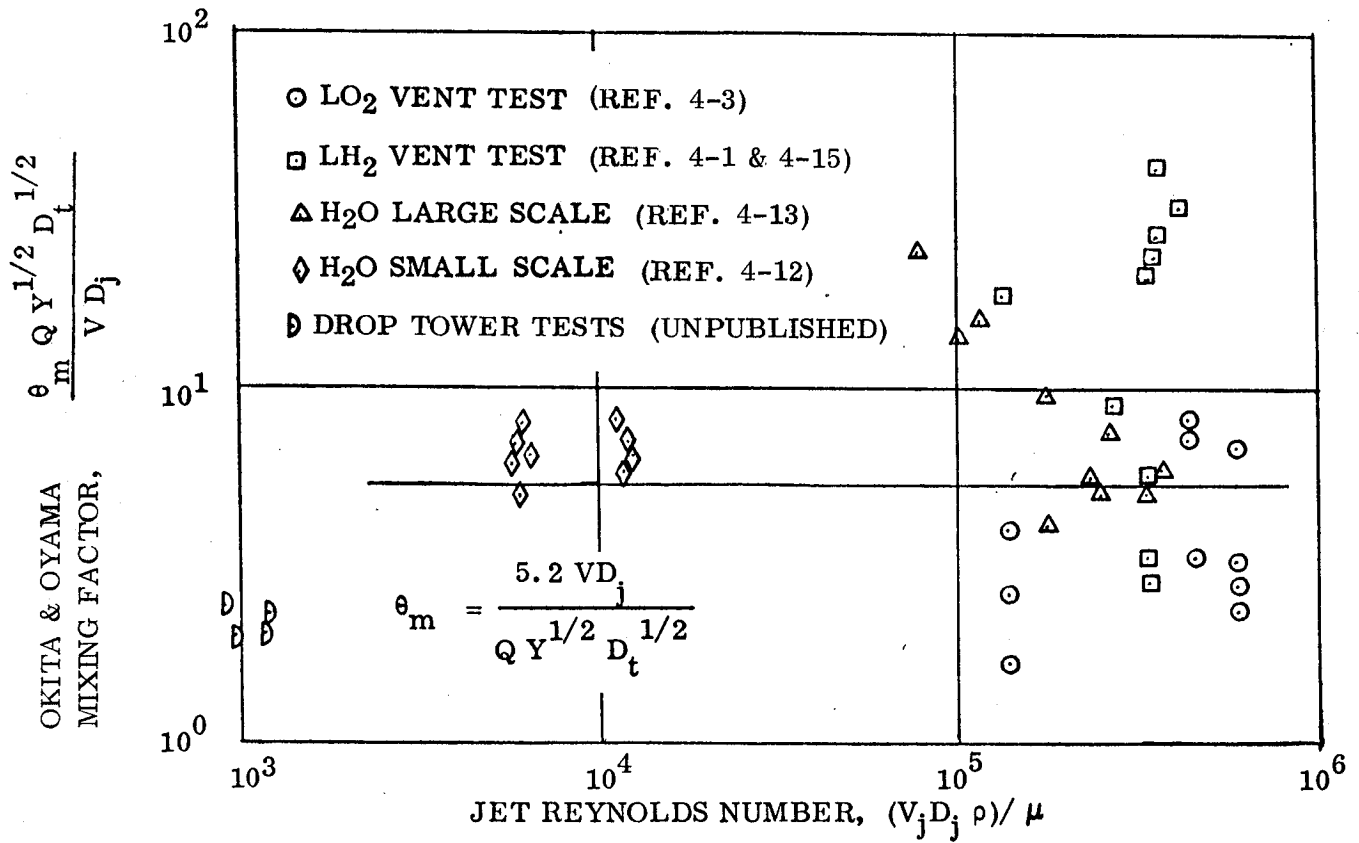
Figure 4-4. Test Data Comparison With Fosset and Prosser Correlation

Legend:
- $\odot$ LO$_2$ VENT TEST (REF. 4-3)
- $\square$ LH$_2$ VENT TEST (REF. 4-1 & 4-15)
- $\triangle$ H$_2$O LARGE SCALE (REF. 4-13)
- $\diamond$ H$_2$O SMALL SCALE (REF. 4-12)
- $\mathcal{D}$ DROP TOWER TESTS (UNPUBLISHED)

Y-axis: $\dfrac{\theta_m Q Y^{1/2} D_t^{1/2}}{V D_j}$, OKITA & OYAMA MIXING FACTOR

$$\theta_m = \frac{5.2\, V D_j}{Q\, Y^{1/2}\, D_t^{1/2}}$$

X-axis: JET REYNOLDS NUMBER, $(V_j D_j \rho)/\mu$

Y-axis: $\dfrac{\theta_m V_j D_j}{D_t^2}$, FOSSETT & PROSSER MIXING FACTOR

$$\theta_m = \frac{9\, D_t^2}{V_j\, D_j}$$

X-axis: JET REYNOLDS NUMBER, $(V_j D_j \rho)/\mu$

Figure 4-5. Test Data Comparisons With Existing Correlations

4-10

Table 4-2. LeRC Drop Tower Mixing Evaluation

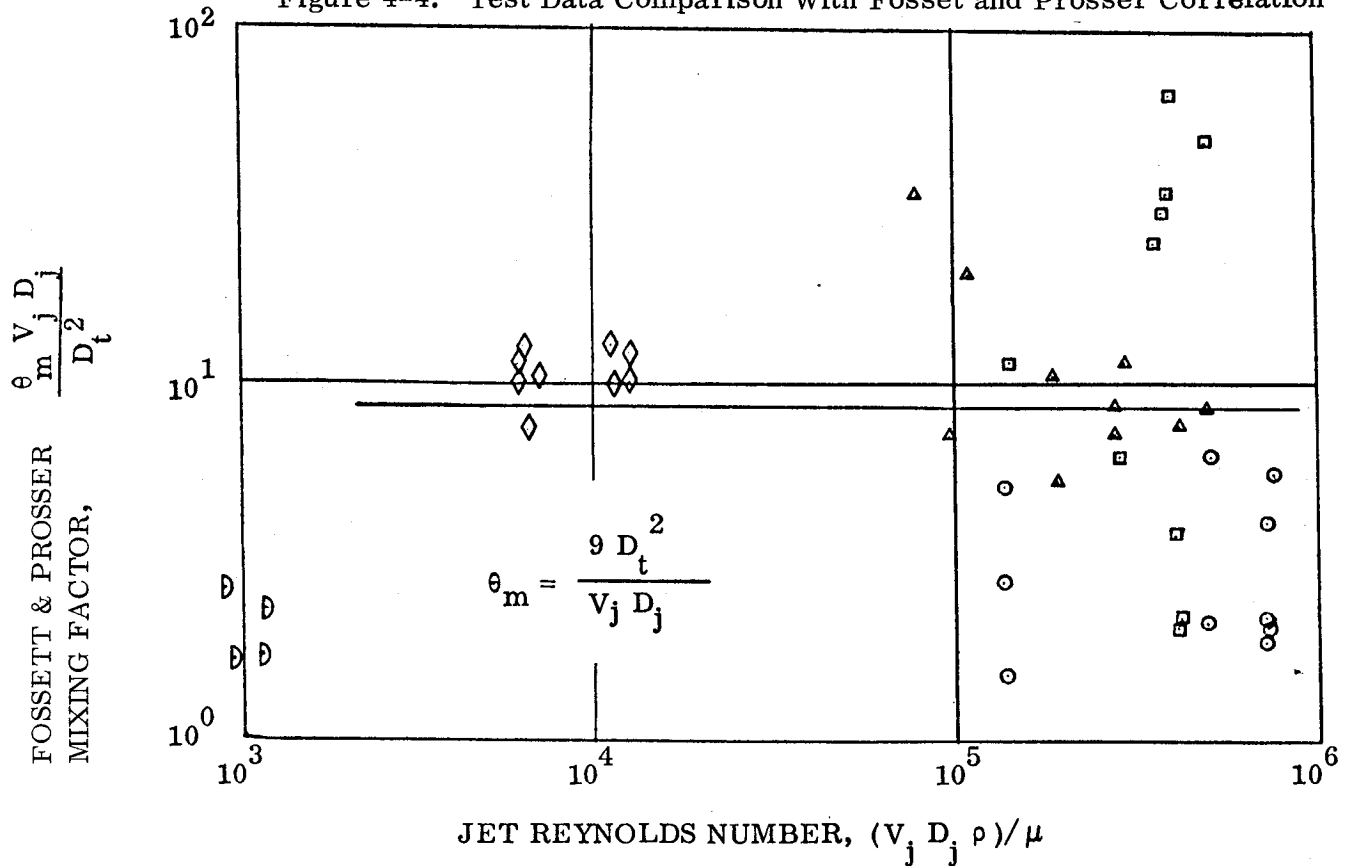| LeRC Run No.	Percent Fill	Flow Rate (ml/sec)	$V_j D_j$ cm^2/sec	Re_j	Predicted θ^*_m (sec)	Actual θ (sec)
N-5-7	57	2.1	6.88	439	74.47	–
N-5-3	70	3.0	9.55	628	56.97	–
N-5-8	57	4.3	13.69	900	35.90	16.92
N-5-9	35	4.75	15.12	994	23.03	9.48
N-5-11	56	6.15	19.57	1287	25.18	11.20
N-6-1	30	6.17	19.64	1291	18.42	7.80

* Mixing Time according to Okita and Oyama
$D_j = 0.4$ cm, $\rho = 0.789$ g/cm^3, $\mu = 1.2 \times 10^{-2}$ g/cm-sec

4.3 THERMODYNAMIC VENT SYSTEM SIZING

The zero-g thermodynamic vent system sizing for incorporation as a non-interference flight article was accomplished such that the unit would meet the requirement of all proposed Centaur D-1S, D-1T, IUS-Recoverable, IUS expendable and Space-Tug vehicles. This would provide a flight demonstration vent package that could operate successfully on any of the contemplated vehicles without modification. The following paragraphs define the vehicle descriptions, vehicle operational environment, and system optimization.

4.3.1 VEHICLE DESIGN CRITERIA - The objective of this program was to design a production prototype low-gravity thermodynamic vent system capable of exhausting only vapor to space from an all liquid or two-phase mixture of hydrogen. Design criteria are based on the vent system successfully functioning in the LH$_2$ tank of any of the following vehicles; Centaur D-1S, D-1T, IUS-recoverable, IUS-expendable and Space Tug. All Vehicles except for the Space Tug were derivatives of the Centaur.

The current Centaur D-1T is a pressure stabilized vehicle designed to be boosted on a Titan vehicle. The D-1T uses peroxide thrusting to settle the propellants for venting. The LH$_2$ tank sidewall insulation on the D-1T consists of three layers of X-850 aluminized Mylar. The inner layer is double aluminized without perforations and serves as a leakage containment membrane. The outer layers are perforated for outgassing. The forward bulkhead insulation consists of two 1.91 cm (3/4 inch) blankets of Dimplar enclosed by double aluminized Mylar face sheets. The integral LH$_2$ and LO$_2$ tanks are separated by an intermediate bulkhead. An evacuated compressed fiberglass net and coarse mesh screen are used for insulation in this area. LH$_2$ tank volume is approximately 35.9 m^3 (1270 ft^3.)

The Centaur D-1S LH$_2$ sidewall insulation has three X-850 aluminized Mylar layers similar to the D-1T. Between the inner and middle X-850 layers are two blankets,

each consisting of eleven dimpled Kapton layer pairs (one layer dimpled, one layer flat.) The forward bulkhead insulation uses the same configuration as the D-1T but replaces Mylar and Dacron material with Kapton and fiberglass. The intermediate bulkhead insulation is unchanged from the Centaur D-1T. Compared to the D-1T, system changes for the D-1S were: the reorientation and/or relocation of the fluid penetrations and umbilical connections, revision of the insulation system, modification of the fill and drain system, addition of an aft structural latch skirt, elimination of the ground helium engine chilldown, and addition of zero-g thermodynamic vent and mixer devices in both propellant tanks.

The Expendable Centaur (EC) and Reusable Centaur (RC) IUS in each of their three configurations are modifications of Centaur D-1T vehicles. The vehicles have integral tanks. The LH_2 sidewall insulation for the expendable IUS is similar to the D-1S sidewall insulation, however Schjeldahl X-966 radiation shields are used, MLI blanket face sheets are made of Schjeldahl G134600 aluminized sheets, the leakage containment membrane is made of Orcon ER 864 and a purge bag, enclosing the insulation, is fabricated from Schjeldahl X-966. Also shown in Reference 4-16, is the insulation configuration for the Reusable Centaur IUS. This also has two blankets of multilayer insulation, similar to the D-1S and EC. Instead of aluminized Dimplar blankets, aluminized Kapton Superfloc is used for the multilayer insulator. Face sheets, leakage containment membrane, radiation shields and purge bag are identical to the Expendable Centaur sidewall insulation configuration. Forward and intermediate bulkhead insulation on both EC and RC are identical to that used on the Centaur D-1S.

LH_2 tank volumes for the three versions of Expendable Centaur are 21.5 m^3 (758 ft^3) for EC-25, 35.86 m^3 (1267 ft^3) for EC-31, and 35.5 m^3 (1256 ft^3) for EC-22. EC-25 and EC-31 are 13.05 m (10 ft) in diameter. EC-22 is 4.42 m (14.5 ft) in diameter. Tank volumes are 27.2 m^3 (962 ft^3) for RC-20, 35.5 m^3 (1256 ft^3) for RC-22 and 50.4 m^3 (1782 ft^3) for RC-28. RC-22 and RC-28 versions are 4.42 m (14.5 ft) in diameter and the RC-20 is 4.32 m (14.2 ft). This data was presented in Reference 4-17.

For the baseline Space Tug (Reference 4-7) separate tanks are used. The LH_2 tank has two blankets with a total of 22 layers of double goldized Kapton Superfloc. The LH_2 tank volume is 49.3 m^3 (1748 ft^3).

Nominal heating rates to the vehicles in low earth orbit are defined in Reference 4-18 for the Centaur D-1T, Reference 4-19 for the Centaur D-1S, Reference 4-20 for the Centaur/IUS expendable and reusable versions, and Reference 4-21 for the Space Tug.

All vehicles were assumed to operate at an acceleration level of 10^{-5} g or less during venting. LH_2 tank operating pressure was assumed to be 18.0 ± 0.5 psia. A summary of the operating conditions that effect the design of the vent system are presented in Table 4-3.

Table 4-3. Summary of Thermodynamic Vent System Design Constraints

	Fluid Volume m^3 (ft^3)	Tank Diameter m (ft)	Liquid Height m (ft)	Tank Pressure kN/m^2 (psia)	Heating Rate, watts (Btu/hr)
Centaur					
D-1T	23.1 (818)	3.05 (10)	3.17 (10.4)	124 ± 3.5 (18 ± 0.5)	788 (2690)
D-1S	33.3 (1178)	3.05 (10)	4.23 (13.87)	124 ± 3.5 (18 ± 0.5)	604 (2063)
IUS					
EC 25	19.3 (682)	3.05 (10)	2.25 (7.37)	124 ± 3.5 (18 ± 0.5)	595 (2033)
EC 31	33.3 (1178)	3.05 (10)	4.23 (13.87)	124 ± 3.5 (18 ± 0.5)	604 (2063)
EC 22	34.6 (1222)	4.42 (14.5)	2.58 (8.45)	124 ± 3.5 (18 ± 0.5)	626 (2138)
RC 20	23.1 (815)	4.33 (14.2)	1.92 (6.3)	124 ± 3.5 (18 ± 0.5)	634 (2163)
RC 22	27.7 (980)	4.42 (14.5)	2.58 (8.45)	124 ± 3.5 (18 ± 0.5)	648 (2213)
RC 28	45.2 (1597)	4.42 (14.5)	3.35 (11.0)	124 ± 3.5 (18 ± 0.5)	654 (2233)
Space Tug					
MSFC Baseline	45.5 (1608)	4.18 (13.7)	4.36 (14.3)	124 ± 3.5 (18 ± 0.5)	411 (1402)

The mission used to size the vent systems was a geosynchronous mission with insertion into a 296 km (160 n.mi.) parking orbit. The first burn, for the Shuttle based vehicles occurs at the second descending node, one hour and fifty seven minutes after liftoff. After the first burn, the vehicle and payload coast for five hours and fifteen minutes on a Hohmann transfer ellipse to geosynchronous orbit. A second burn at geosynchronous altitude positions the vehicle and payload in a 19,323 n.mi. circular orbit.

All vent systems were sized for two different coast times, 1.18 hr and 5.25 hr.

4.3.2 SYSTEM SIZING - The Okita and Oyama correlation discussed in Section 4.2.3 was incorporated in the existing Cryogenic Heat Exchanger Analysis program (CHEAP) to produce a program (CHEAPMX) that will determine the size of the pump/mixer and heat exchanger combination. The required programming was accomplished so that given the vehicle operating conditions of tank side wall heat leak, fluid volume, operational pressure level, pressure dead band, fluid properties and liquid level, the program will develop a weight map of the pump-heat exchanger combination as a function of assumed vent flow rate.

CHEAPMX was used to generate size data for nine different advanced Centaur vehicle configurations. A total weight penalty for each system was used to find the proper interaction of sizing variables that would result in an optimum component combination for each configuration. The zero-g vent system sized in this study was made up of: (1) pump to provide hot side flow through a heat exchanger which becomes a mixing jet flow, (2) the heat exchanger system to ensure that the vent flow is completely vaporized (which includes a throttling regulator, flow control orifice and shutoff valve), (3) a motor to drive the pump, and (4) a power supply for the pump motor.

The three major sizing variables used in the study were the system vent down time (TVNT), the mixer jet orifice diameter (D_j) and the hot side flow rate (FH). One constraint was that the mixing must be completed within 90% of the vent down time. This meant that for every combination of the TVNT and D_j there was a minimum value of FH.

The basic approach was to minimize the total system weight penalty for each configuration and each coast time based on nominal operating conditions. The heat exchanger was sized to operate with a completely liquid inlet and to discharge vapor at a given (input) number of degrees below the tank saturation temperature.

The initial effort was spent finding a minimum weight system for each given operating condition. The nominal heat flux into the tank was used as part of the nominal operating condition.

Whenever mixing requirements were considered, the velocity-diameter product of the mixer jet was the primary term of interest. This product controls the mixing time for a given configuration. In the presence of a gravitational field there is a minimum velocity-diameter product which is required to overcome buoyancy forces and allow the mixing jet to penetrate and mix the warm layer of liquid near the liquid-vapor interface. For this study, configurations were such that the small acceleration field had no affect on mixer sizing.

There are qualitative relationships between the system weight penalty, the major sizing variables, and the computed and input sizing variables. A decreasing ventdown time (with D_j constant) causes a smaller mixing time with a corresponding larger velocity-diameter product. This would increase the jet velocity and required head. A greater

4-14

jet velocity causes greater hot side flow rate and therefore large heat exchanger pressure losses. These factors all result in a larger pump. One offsetting effect is that the increased hot side flow results in a higher hot side heat transfer coefficient and tends to allow the heat exchanger to be shorter. The amount of accumulated energy that must be removed via the vent stream stays constant with a smaller vent-down time, so the vent flow rate must increase. The larger vent flow tends to increase heat exchanger cold side heat transfer coefficients as well as required heat transfer area.

The effects of a sizing variable change are therefore complex and inter-related. Many of the effects have opposing tendencies in terms of weight.

Some of the effects of increasing hot side flow rate (beyond the minimum established by the mixing time requirement for a given vent downtime and mixer jet orifice diameter) are an increase in the hot side heat transfer coefficient which tends to decrease heat exchanger weight, an increase in hot side flow pressure loss and mixer jet head which causes a pump size increase and a greater pump input power to the tank which also causes an increase in vent flow rate. A hot side flow greater than the minimum required means that the tank fluid is being mixed more rapidly than 90% of the vent down time.

An increase in mixer jet orifice diameter (D_j) with vent down time (TVNT) constant, results in a direct increase in a heat exchanger weight. It also means an increase in the (FH) minimum hot side flow rate. These two changes in D_j and FH have opposing tendencies as far as the hot side heat transfer coefficient and hot side heat exchanger pressure drop.

The minimum fixed weight for the LH_2 vent system was determined for each vehicle and is presented in Table 4-4. The fixed weight includes; pump, motor, heat exchanger, pressure switch and throttling valve. The D-1T as the flight test vehicle, has the highest weight required due primarily to the low performance of the existing sidewall insulation. This mixer/heat exchanger configuration, while oversized for the other vehicles, will satisfactorily control tank pressure for these vehicles.

Table 4-4. LH$_2$ Vent System Sizing Results

Vehicle	Type	Vehicle Length, m (ft)		Vent System Fixed Weight, kg (lb)	
Centaur	D-1T	9.45	(31)	6.58	(14.50)
	D-1S	9.45	(31)	5.25	(11.57)
IUS	Expendable	6.71	(22)	4.97	(10.94)
	Expendable	7.62	(25)	5.23	(11.52)
	Expendable	9.45	(31)	4.74	(10.46)
	Reusable	6.10	(20)	5.43	(11.98)
	Reusable	6.71	(22)	5.13	(11.31)
	Reusable	8.53	(28)	4.96	(10.93)
Space Tug	MSFC Baseline	9.14	(30)	3.65	(8.03)

5

CONCLUSIONS AND RECOMMENDATIONS

5.1 CONCLUSIONS

Passive cooling appears to be a promising method of thermal conditioning cryogenic capillary acquisition devices. Plate/screen-screen/plate and plate/screen-plate/ screen are the two most attractive capillary pumping candidates for the Centaur D-1S. These configurations offer a payload advantage for the five burn mission over actively cooled systems that dump fluid directly overboard. Their completely passive operation provides reduced complexity and increased reliability.

Subcooler systems (for replacing Centaur boost pumps and pressurization systems) that dump coolant overboard are heavier than the baseline system. The dry feedline concept using settled fluid to refill the feedlines was lower in weight than the cooled feedline concept. For these subcooler systems, weight penalties were lowest for the RL10 Category I engine followed by the RL10A-3-3A and the baseline RL10A-3-3 engines. Subcooler systems that pump coolant back into the tank can provide an overall weight advantage over the baseline system if dry feedlines are used. Payload advantages of 81 kg (179 lb$_m$) are possible for the five burn mission using thermal subcooling with coolant pumped back into the tank, capillary acquisition and dry feedlines. Adding the coolant return pumping system to the thermal subcooler system reduces system weight and the weight dependence on the number of burns but also reduces system reliability and increases development requirements.

Low weight LH$_2$ thermodynamic vent mixers can be developed to satisfy all Centaur/ Tug derivatives. The highest weight system was the Centaur D-1T LH$_2$ thermo-dynamic vent mixer system; 6.58 kg (14.50 lb$_m$). Since this system will satisfy the venting and mixing requirements of all nine vehicles investigated, and has an increased weight of only 2.94 kg (6.47 lb$_m$) compared to the lightest weight system, future development work should concentrate on the Centaur D-1T system. This assures that a flight qualification program would only have to be accomplished once regardless of the vehicle using the thermodynamic vent system.

5.2 RECOMMENDATIONS

Passively cooled cryogenic capillary acquisition system development should be continued. Programs of primary interest are determining retention capability when the wicking barriers are subjected to vapor flow and refilling of passively cooled acquisition systems with settled fluid.

Other recommended development programs are integrated system testing including the effects of venting, heat input, feedline heating and transients and outflow requirements on prototype cryogenic capillary device thermal and fluid performance. Fabrication and checkout studies in conjunction with this integrated testing are recommended, including study of controlled screen spacing, screen repair techniques, and film bubble point checkout.

Additional thermal subcooler system development should be undertaken if multiburn missions (beyond five burns) for Centaur derivatives are anticipated. This work would include definition of tank pressure profiles during coolant return and engine firing. Additional study is also required to define accumulator and compressor requirements for the coolant return system in order to make more accurate comparisons between concepts employing subcooler coolant return and the baseline Centaur D-1S system. These comparisons may allow subcoolers to be sized at higher tank pressure conditions, reducing subcooler weight and cold side residuals. Hardware development of the subcooler coolant return system should include specification, procurement, assembly and testing of components under realistic operating conditions.

The program for flight testing an LH_2 thermodynamic vent system on a noninterference basis for a future Centaur flight should be continued. The next step would be to procure hardware. Ground testing, flight qualification, installation and flight testing would follow.

6

REFERENCES

1-1   Blatt, M. H. and Walter, M. D., "Centaur Propellant Acquisition System Study," NAS3-17802, NASA-CR-134811, CASD-NAS-75-023, June 1975.

1-2   Bock, E. H., et al, "Centaur/Shuttle Integration Study," GDCA-BNZ73-006-8, NAS3-16786, NASA CR-134488, December 1973.

1-3   Clarke, W. D., "Baseline Space Tug - Configuration Definition," MSFC 68 M00039-2, June 28, 1974.

2-1   Blatt, M.H., and Walter, M.D., "Centaur Propellant Acquisition System Study," NASA CR-134811, CASD-NAS-75-023, NAS3-17802, June 1975.

2-2   J.C. Aydelott to M.H. Blatt, Contract NAS3-19693, "Centaur Propellant Thermal Conditioning Study," (Approval to initiate Tasks V and VI) November 5, 1975.

2-3   Symons, E.P., "Wicking of Liquid in Screens," NASA TN D-7657, May 1974.

2-4   Bressler, R.G. and Wyatt, P.W., "Surface Wetting through Capillary Grooves," Transactions of the ASME, Journal of Heat Transfer, February 1970.

2-5   Blatt, M.H. and Pleasant, R.L., "Centaur Propellant Thermal Conditioning Study," Third Monthly Progress Report, 667-2-078, NAS3-19693, August 11, 1975.

3-1   "Centaur Space Vehicle Pressurized Propellant Feed System Test," NASA TN D-6876, 8 October 1972.

3-2   "Sump-LO$_2$ Tank," GD Convair Drawing 65-77201, Sheet 5.

3-3   Cuffe, J.P.B., "Design Study of RL10 Derivatives," Pratt and Whitney Aircraft Report FR-6011, Vol. I, 15 December 1973.

3-4   "RL10A-3-3A Rocket Engine Model Specification 2289," Pratt and Whitney Aircraft Col, 21 April 1969.

3-5   "Centaur Interim Upper Stage (IUS) System Study," Vol. I, Book II, Section 7, GDC Report CASD/AFS 75-004.

3-6   "Reusable Centaur Study, Data Dump," Vol. 5 – Systems, NAS8-30290, 26 September 1973.

3-7   "Centaur/Shuttle Integration Study Final Report," Vol. II – Technical, GDC Report GDCA-BNZ73-006-8, December 1973.

3-8   Worscheck, G.A., 966-3/R70/005, "Thermal Analysis of the Insulation System for Three-Burn Centaur Propellant Feedlines," 26 May 1970.

3-9   O'Neill, R.F., "Convair Thermal Analyzer Computer Program No. P4560," Report GDC-BTD69-005A, 29 May 1969.

3-10   Blatt, M.H., et al, "Low Gravity Propellant Control Using Capillary Devices in Large Scale Cryogenic Vehicles," Phase II Final Report, GDC-DDB70-008, NAS8-21465, August 1970.

3-11   Mitchell, R.C., et al, "Study of Zero-Gravity, Vapor/Liquid Separators," GDC-DDB65-009, NAS8-20146, January 1966.

3-12   Blatt, M.H. and Walter, M.D., "Centaur Propellant Acquisition System Study," NASA CR-134811, CASD-NAS-75-023, NAS3-17802, June 1975.

3-13   Cady, E.C., "Study of Thermodynamic Vent and Screen Baffle Integration for Orbital Storage and Transfer of Liquid Hydrogen," NASA CR-134482, MDC G4798, August 1973.

3-14   "SAE Aerospace Applied Thermodynamics Manual," Part 1A, Incompressible Fluid Flow, ARP 1168, Society of Automotive Engineers, Inc., 1969.

3-15   "Flow of Fluids Through Valves, Fittings and Pipe," Engineering Division of Crane Company, Technical Paper No. 410, Chicago, 1957.

3-16   Brentari, E.G. and Smith, R.V., "Nucleate and Film Pool Boiling Design Correlations for O_2, N_2, H_2 and He," Vol. 10, Sections M-U, Advances in Cryogenic Engineering, 1965.

3-17   J.E. Dyer, 671-4 to M. Blatt/R.L. Pleasant, 632-3, "Effects of Increased Pressure on Centaur Tank Weights, Convair internal memo., 15 May 1975.

4-1   Stark, J. A. and Blatt, M. H., "Cryogenic Zero-Gravity Prototype Vent System," GDC-DDB67-006, Contract NAS8-20146, October 1967.

4-2   Sterbentz, W. H., "Liquid Propellant Thermal Conditioning System," Final Report, NAS3-7942, LMSC K-07-68-2, 15 August 1968.

4-3   Erickson, R. C., "Space LOX Vent System," Final Report, NAS8-26972, CASD-NAS75-021, April 1975.

4-4   Bullard, B. R., "Wall Mounted Heat Exchanger Characterization," Final Report NAS3-16769, LMSC D465537, January 1975.

4-5   Bock, E. H., "Centaur/Shuttle Integration Study," GDCA-BNZ73-006-8, Contract NAS3-16786, NASA CR-134488, December 1973.

4-6   "Centaur Interim Upper Stage (IUS) System Study," CASD-AFS-75-003, F04701-75-C-0035, April 1975.

4-7   Clarke, W. D., "Baseline Space Tug - Configuration Definition," MSFC 68 M00039-2, June 28, 1974.

4-8   James, M. E., "Attitude Control System," PD 73-0103, Centaur Improvement Study, Task 3, October 1973.

4-9   Fox, E. A. and Gex, V. E., AIChE, 2, (1956), 539.

4-10 Fossett, H. and Prosser, I. E., Proceedings of the Institute of Mechanical Engineers (London), Vol. 160, 224, 1944.

4-11 Uhl, V. W. and Gray, J. B., Mixing Theory and Practice, Academic Press, New York, p. 245.

4-12 Poth, L. J. and VanHook, J. R., et al, "A Study of Cryogenic Propellant Stratification Reduction Techniques," GD/FW FZA-419-1, NAS8-20330, September 15, 1967.

4-13 VanHook, J. R. and Poth, L. J., "Study of Cryogenic Fluid Mixing Techniques," GD/FW FZA-450-1, NAS8-24882, 15 September 1970.

4-14 Lovrich, T. M., et al, "Development of Thermal Stratification and Destratification Scaling Concepts," MDC G4753, NAS8-23747, July 1973.

4-15 Stark, J. A., et al, "Cryogenic Propellant Control and Transfer," GDC-ERR-1538, December 1970.

4-16 O'Neill, R. F., Walburn, A. B., "Centaur IUS Insulation Analyses and Trades," IUS-75-87, February 24, 1975.

4-17 Heald, D. A., et al, "Centaur Interim Upper Stage (IUS) System Study," Volume II, Technical, CASD/AFS-75-006, Contract F04701-75-C-0035, Final Report CDRL A008, July 31, 1975.

4-18   Christensen, E. H., "Centaur D-1TR One-, Two-, and Three-Burn and Proof Flight Four-Burn Mission LH$_2$ and LO$_2$ Tank Dispersed Heat Rates (SOW M1421)," 965-4/HT71/025, 3 August 1972.

4-19   Bock, E. H., et al, "Centaur/Shuttle Integration Study - Final Report," NASA CR-134487, GDCA-BNZ73-006-8, December 1973.

4-20   Wilson, G. C., "Centaur IUS Main Propellant Tank Heating," 672-3/PD75/006, 28 March 1975.

4-21   Space Tug Systems Study," NAS8-29676, Data Dump Volume 5 - Systems, Book 3, System 3, 18 September 1973.